NTNU

Norwegian University of
Science and Technology

Stability assessment of the asphalt concrete tunnel invert of Roskrepp hydropower project

Anna Helene Mong Urdal

Geotechnology
Submission date: June 2018
Supervisor: Krishna Kanta Panthi, IGP
Co-supervisor: Bibek Neupane, IGP
Kaspar Vereide, Sira-Kvina

Norwegian University of Science and Technology
Department of Geoscience and Petroleum

NTNU
Norwegian University of
Science and Technology

Department of
Geosciences and Petroleum

Your ref.: MS/N30T43/IGB/AHUKKP

Date: 12.01.2018

TGB4930 INGGEOL/BERGMEK – MSc. THESIS

for

Eng. geo. student Anna Helene Mong Urdal

STABILITY ASSESSMENT OF THE ASFALTCONCRETE TUNNEL INVERT OF ROSKREPP HYDROPOWER PLANT

Background

The Roskrepp hydropower plant has a headrace tunnel, which is invert lined with asphalt concrete. The power plant is operated with variable load depending on the market situation and hence the headrace system is experiencing periodic fluctuation of the water pressure. More importantly, a study is being made to convert this power plant to pump storage, which will further increase the pressure variations in the headrace system. Therefore, it is of importance to investigate the potential stability challenges associated to the headrace tunnel, in particular the interaction between the invert asphalt concrete, base material and the in-situ rock mass and weakness zones.

MSc thesis task

This MSc thesis is a continuation of the project work where the candidate has carried out engineering geological field mapping and assessed the engineering geological conditions along the headrace tunnel of Roskrepp hydropower plant. Hence, the MSc thesis will have the following tasks:

- Literature review on the Norwegian power plants and design issues for unlined tunnel systems.
- Literature review of the mechanical properties of asphalt concrete and intact rock material.
- Present the engineering geological conditions along the headrace tunnel alignment.
- Carry out laboratory testing of the rock specimens collected from the case project.
- Carry out physical modelling of the conduit with asphalt concrete base and observe the pressure variation above and below the asphalt concrete.
- Discuss the findings from the physical modelling.
- Carry out stability assessment using numerical modelling.
- Discuss the findings and conclude the work.

Relevant computer software packages

Candidate shall use *roc-science package* and other relevant computer software for the master study.

Co-operating partner

Sira-Kvina is the co-operating partner. Adjunct Associate Professor Kaspar Vereide from the Department of Civil and Environmental Engineering and Project Developer at Sira-Kvina is the contact person and co-supervisor for the MSc thesis work. In addition, PhD Fellow Mr. Bibek Neupane will also co-supervise this project.

The thesis work is to start on January 12, 2018 and to be completed by June 11, 2018.

The Norwegian University of Science and Technology (NTNU)
Department of Geology and Mineral Resources Engineering

January 12, 2018

Krishna Panthi

Dr. Krishna K. Panthi
Associate Professor of geological engineering, main supervisor

ACKNOWLEDGEMENT

Thanks to my thesis advisor Associate Professor, Dr.Krishna Kanta Panthi, of the Norwegian University of Science and Technology. He steered me in the right direction whenever he thought I needed it.

A gratefully thank to PhD student, Bibek Neupane, for good guidance and help through the project- and master process. Especially thanks for the work that was done for the project during and after field mapping, and for great photographs of the Roskrepp area from field mapping. I would not be able to collect as much data from field if he would not have helped.

Accosiate Professor Dr. Kasper Vareide should also be thanked for finding relevant information from Sira-Kvina Power Plant, for good guidance of the Sira-Kvina- system at Tonstad and for arranging the visit.

Special thanks to the carpenters at Vassdragslaboratoriet, Eirik, Gisle, Morten, Frank, for their help with building the physical model. Engineer, Geir Tesaker, and senior engineer, Thai Mai, should also be thanked for their contribution to the physical model test. An appreciation to Peab Asphalt for distribtution and layering of asphalt and aggregate.

Thanks to senior engineer, Gunnar Vistnes, for help in laboratory regarding rock samples.

I would also like to my companion, Kjetil Refsland, for his support and help of this thesis.

Anna Helene Mong Urdal

Trondheim, June 2017

SUMMARY

Rebuilding a hydropower plant into a pumped-storage plant in an underground tunnel, means that the water will rapidly change directions, instead of streaming evenly in one direction. This will cause extra water pressure in the headrace tunnel and can cause stability problems that can damage the turbines. The hydropower plant, Roskrepp, is being considered to become a pumped-storage plant. During the construction of the hydropower plant, an asphalt layer was put at the floor. With rapidly change of water pressure, the asphalt can tear up and cause damage to the turbines. Investigation of the rock condition along the tunnel alignment and an assessment of the asphalt lining in conjunction with the possibilities of pumped-storage plant for Roskrepp has been done.

To evaluate the problem, literature research, field investigation, laboratory testing on rock samples, numerical analysis and physical model test has been carried out.

The stability assessment of the rock mass included literature study, field investigation, laboratory testing and numerical analysis. One of the six possible weakness zones crossing the tunnel area, appears to be more crucial regarding the stability of the tunnel. This could be of crushed rock material. If extra pressure occurs, a caving situation can happen in the ceiling. Erosion under asphalt from the crushed rock materials can also cause instabilities. With water streaming under asphalt lining, the crushed rock can erode and tear up the asphalt lining. Eventually the materials can stream down to the turbines and cause destruction.

The assessment of the asphalt lining included literature study, numerical analysis, and physical model test. If cracks are developed in the asphalt, or the contact between the asphalt layer and the rock walls are not fully sealed, water can easily stream under the lining and disturb the aggregate under it. Literature study and physical model test results shows that pressure under asphalt lining is delayed comparing with pressure over asphalt lining when mass oscillation is present. If a fine combination between trapped air and water under the lining are present, there will be a possibility of lifting the asphalt when mass oscillation is on its way down. This can cause tearing up the asphalt and destroy the turbines.

SAMMENDRAG

Ombygging av et vannkraftverk til et pumpekraftverk vil påføre hurtige forandringer av vannretning og vannhastighet i en undergrunns tunnel. Dette vil føre til ekstra vanntrykk i innløpstunnelen, som igjen kan føre til stabilitetsproblemer som kan ødelegge turbinene. Det vurderes å gjøre Roskrepp vannkraftverk om til et pumpekraftverk. Under bygningsprosessen av vannkraftet, ble det lagt et asfaltlag i innløpstunnelen. Med hurtige endringer i vanntrykk, kan asfaltlaget rives opp og påføre skader på turbinene. Undersøkelses på bergtilstanden langs innløpstunnel området og stabilitets vurderinger på asfaltlaget med hensyn på muligheten å omgjøre Roskrepp vannkraftverk om til et pumpekraftverk har blitt utført.

For å vurdere problemet, har det blitt gjort litteratur studie, felt undersøkelse, laboratorium tester på berg prøver, numeriske analyser og fysisk modell test.

Stabilitetsvurderingen på bergmassen langs tunnelen inkluderte litteratur studie, felt undersøkelse, laboratorium testing og numeriske analyser. En av seks potensielle svakhetssoner langs innløpstunnelen virker å være mer kritisk enn de andre. Denne kan være av knust bergmasse som kan forårsake ras i taket dersom ekstra vanntrykk påføres. Dette kan igjen føre til strømning av bergamateriale ned til turbinene og ødeleggelse av dem. Med vann strømning under asfaltlaget, kan grusen graves og påføre trykk på asfalten og forårsake oppriving.

Stabilitetsvurderingen på asfaltlaget inkluderte litteratur studie, numeriske analyser og fysisk modell test. Dersom det er oppstått sprekker i asfalten, eller at kontakt mellom asfalt lag og tunnelveggen ikke er helt tett, kan vann strømme lettere under laget og forstyrre gruslaget under. Litteratur studie og fysisk modell test viste at trykket under asfaltlaget henger etter, sammenlignet med trykket i innløpstunnelen når vannføringen går fra stasjonær til ikke-stasjonær. Under ikke-stasjonær vannføring, vil masse oscillasjoner oppstå i trykk-kammeret. Dersom en fin kombinasjon av luft og vann er tilstede når masse oscillasjonene beveger seg nedover, er det en mulighet for løfting av asfaltlaget. Dette kan føre til oppriving av asfalten som deretter kan ødelegge turbinene.

TABLE OF CONTENT

1 INTRODUCTION

1.1 Background

The energy consumption worldwide has increased with 1.7 % per year the last 40 years. Electricity has become a source that most people worldwide rely on (Hofstad, 2017). The markets demand of being flexible and dynamic, such as the possibilities for storage and quick response, is in rapid development. Norway is according to HydroCen in a unique position to deliver a combination of effect, storage, availability, and stability (HydroCen, 2017).

Sira-Kvina Kraftselskap is interested to store energy in an already consisting hydropower plant, Roskrepp. Rebuilding the underground hydropower plant to a pump-storage plant will involve more frequently and bigger pressure variations in the headrace tunnel, because of the switching between turbine- and pump drift. There are some uncertainties around the stability when extra pressure is applied in the tunnel. Investigations in potential stability problems with rebuilding of today's conventional hydropower plant into a pumped- storage plant will maybe give an indication of the possibilities to perform the project.

1.1.1 Sira-Kvina System

Sira-Kvina Kraftverk is a power generation company that produces renewable energy in seven hydropower plants located in Rogaland, Vest-Agder and Aust-Agder. The development of the powerplants started in 1963 and completed after six building steps in 1986. Sira-Kvina's power plants have a regulated magazine and a tunnel system.

Sira-Kvina's competitiveness is based on high standard in power plants, high level of competence and optimal use of technology. The annual production of the company is according to Sira-Kvina about 6300 GWh. This makes it a total of five percent of all power production in Norway. It covers about five percent of the electrical consumption in the country and plays an important role in the drifting of the mainline net in South-West in Norway.

The company has four owners; Lyse Produksjon AS, Statkraft Energi AS, Skagerak Kraft AS and Agder Energi Produksjon AS. The distribution of the ownership is shown below in Figure 1.

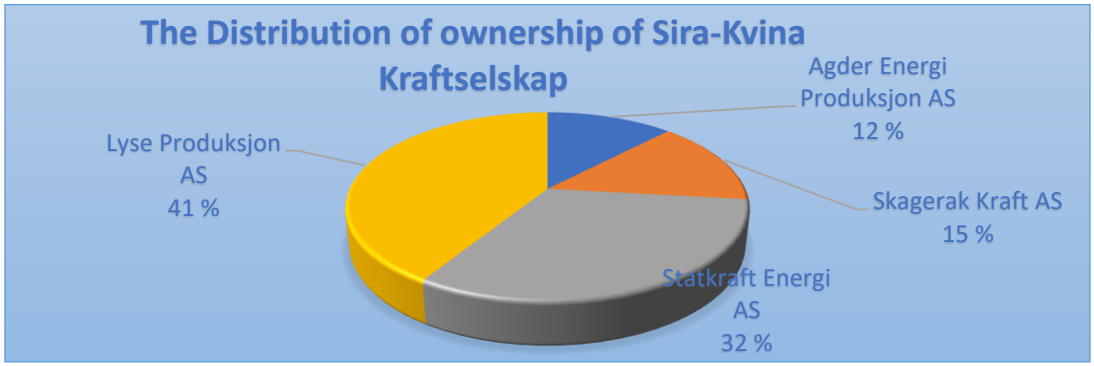

Figure 1 - Distribution of ownership of Sira-Kvina Kraftselskap

There are two watercourses of Sira-Kvina; Sira- and Kvina watercourse. An illustration of the watercourses including the hydropower plants are shown in Figure 2 and divided in Table 1.

Table 1 - Watercourses of Sira-Kvina system.

	Sira-watercourse	Kvina-watercourse
Hydropower plants	Duge Tjørhom	Roskrepp Kvinen Solholm

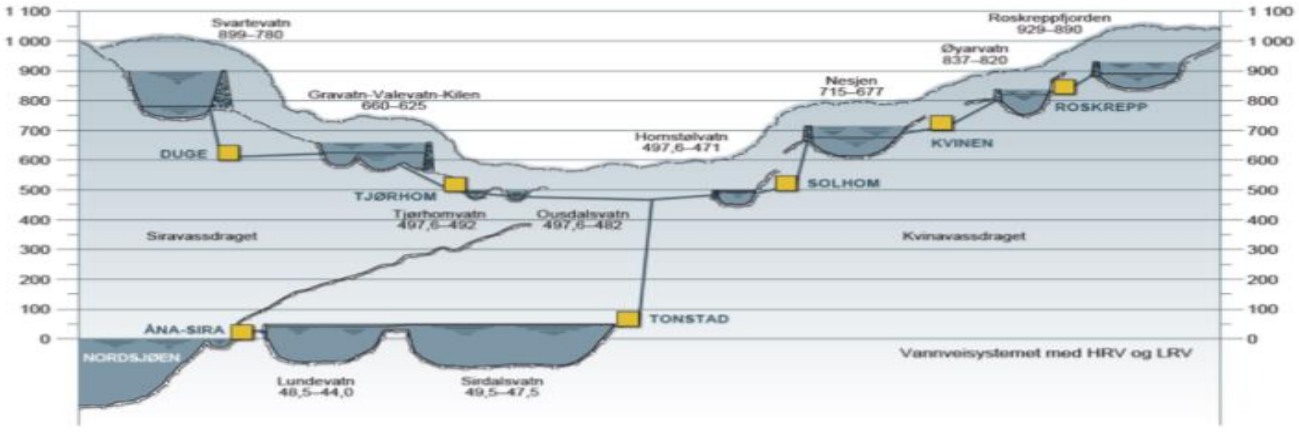

Figure 2 - Watercourses of Sira-Kvina system.

As the headquarter of Sira-Kvina and the largest of the seven power plants both in size and production, Tonstad power plant is one of the largest in production in Norway. After collecting the waterflow from the Sira- and Kvina watercourses, the water streams from Tonstad powerplant to Åna-Sira powerplant, which is the last powerplant of Sira-Kvina. This powerplant is located nearby the coastline and is close to the level of the ocean (Sira-Kvina, 2017b).

1.1.2 Roskrepp Headrace Tunnel

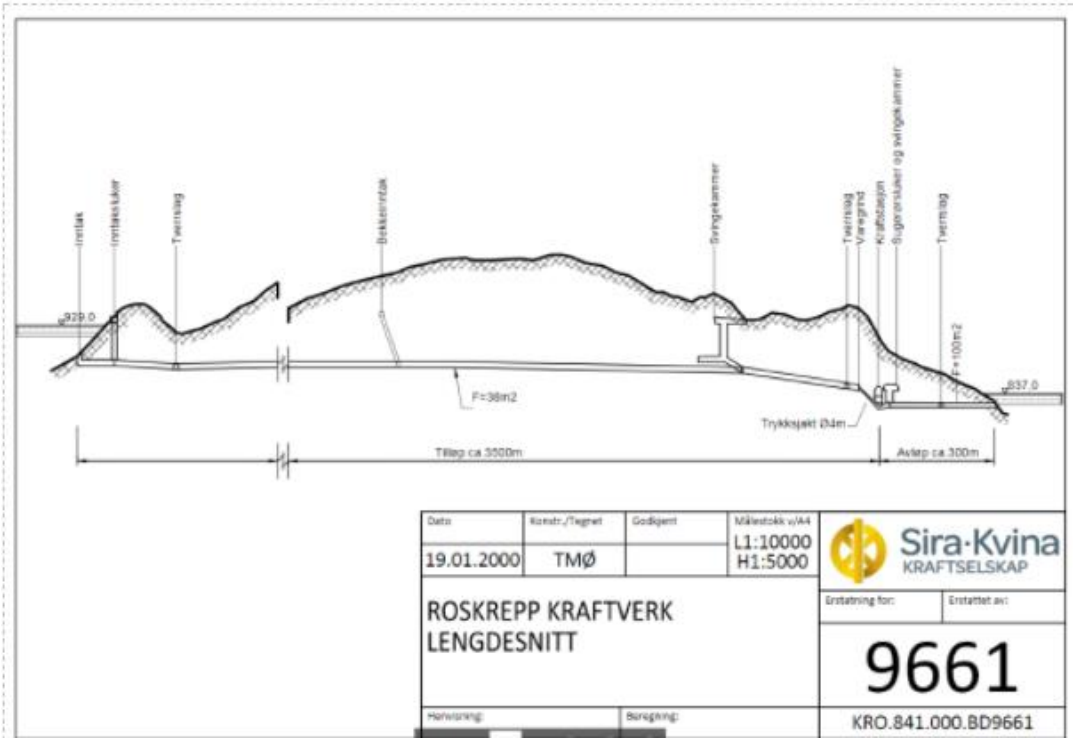

Figure 3 - Longitudinal profile of Roskrepp headrace tunnel (2000)

Roskrepp powerplant is a part of the Kvina-watercourse. The operation of Roskrepp power plant started in 1980 and has an annual production of about 105 GWh. It is the smallest powerplant of Sira-Kvina with a head loss of 92 meters, as shown in Figure 3, and an effect of 50 MW from the generator.

The electricity price is often high during winter season and is therefore mostly used during winter. This leads much drainage in Roskreppfjorden (the magazine) which leaves room for snowmelt and rainfall in spring, summer, and fall.

1.2 Objective and Scope

The headrace tunnel of Roskrepp has a 2896-m layer of asphalt. The headrace tunnel itself is 3500 m long. The main objective is to investigate the rock and asphalt condition in the tunnel and evaluate the stability situations that can occur if Roskrepp hydropower plant turns into a pumped-storage plant. The asphalted headrace tunnel is particularly vulnerable to variations in pressure. The scope of the thesis can be listed as follows:

- Relevant theory covering Norwegian design issues for unlined tunnel systems, mechanical properties of asphalt concrete and engineering geological properties of rock.
- Presentation of the engineering geological conditions along the tunnel alignment, including a theory-, method- and result part.
- Laboratory testing of the rock samples from the case project that includes method and result.
- Numerical analysis including a method- and a result part, for analyzing rock mass stability and stability regarding the asphalt lining.
- Physical modelling including a theory part, method, and results. Focusing on the asphalt stability in dynamic movement.
- Discussion from the findings, conclusion of the work and further studies.

1.3 Limitations

The main focus of the thesis will be on stability assessment of the rock mass along the tunnel alignment, and stability assessment of the asphalt lining regarding rapidly change of water pressure in the headrace. The discussion part of the assessment of the rock mass stability will include literature study, filed investigation, laboratory testing, and numerical analysis. The discussion part of the stability assessment of asphalt lining will include literature study, numerical analysis, and physical model test.

2 RELEVANT THEORY

This chapter presents relevant theory from literature study that can be used regarding the objective of the thesis.

2.1 HYDROPOWERPLANT PRINCIPLES

Hydropower is a renewable and an environmental energy resource. More than 99 % of total annual production in Norway is generated from hydropower. Worldwide it is in the range of one sixths of the total production (Statkraft, 2017). The principle of hydropower is to use the energy from streaming water. The water streams from an upper reservoir to a lower reservoir. Turbines are located in a powerhouse near the lower reservoir to get as much mechanical energy from the streaming water as possible. Placed close to the turbines, a generator turns the mechanical energy into electrical energy. The streaming water from the upper reservoir can be transported through different types of waterways, such as channels, tunnels and pipelines (Lia, 2017). There are different kinds of hydropower plants such as: low- and high-pressure power plant and pumped-storage power plant. Roskrepp hydropower is a high-pressure powerplant, consisting of an unlined headrace tunnel.

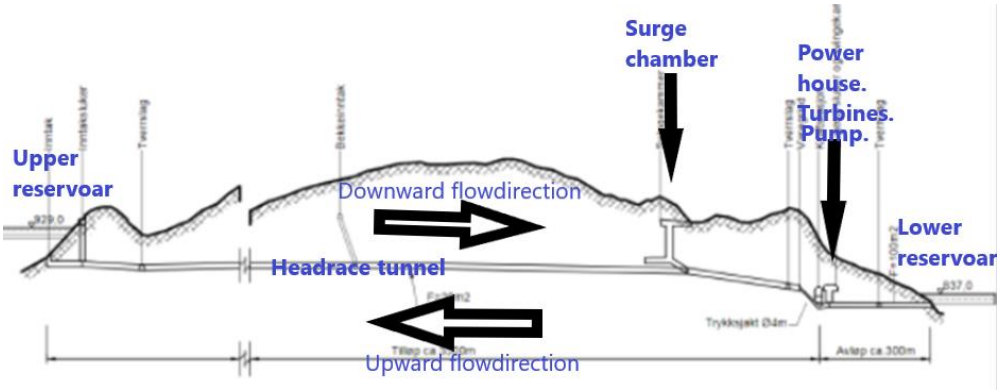

Figure 4 - Illustration of hydropower- and pumped-storage concept.

2.1.1 High-pressure Power Plant

High pressure powerplant is the most common powerplant in Norway. It has less quantity of water compared to low-pressure powerplant, and has steep underground headrace tunnels (Fornybar, 2016). Excluding the upward discharge direction, Figure 4**Feil! Fant ikke referansekilden.** illustrates the concept of a high-pressure hydropower plant. High-pressure headrace tunnel is usually equipped with a surge shaft for the purpose of releasing the potential high water pressure in the headrace that can occur when change in discharge (Guttormsen, 2014).

2.1.2 Pumped-Storage Plant

Pumped-storage powerplants are different from conventional hydropower plants. The principle of pumped storage hydroelectricity is illustrated in Figure 4. When demand for electricity is low, pumped-storage powerplants can store electrical energy by pumping water from a lower reservoir to an upper reservoir. They use streaming water to generate power, like conventional projects, but they also use reversible turbines to pump the water back to the upper reservoir (Hino and Lejeune, 2012).

2.2 DESIGN ISSUES FOR UNLINED HEADRACE TUNNELS IN NORWAY

An unlined tunnel can be defined as a tunnel that does not contain any form of lining over the most of its length (Brox, 2011). Dealing with operations of unlined headrace tunnels, different design issues must be considered in the process. Even though many unlined headrace tunnels have not faced any big design issues, preventing something in the tunnel from happening during operation and maintenance work can give economically savings. This chapter will focus on the designing issues of unlined headrace tunnels regarding stability assessment of Roskrepp headrace tunnel, and its possibilities of turning into a pumped storage station.

2.2.1 Geological Investigation

Geological aspects must be mapped and evaluated before positioning a headrace tunnel. Unlined tunnels are usually an indication of good rock conditions, but there can still be a possibility of having sections of bad rock conditions. To optimize the design an experienced tunnel design engineer/engineering geologist must be retained during and after construction. He/She can evaluate the sections where the lining is warranted. The evaluation of the rock condition should include detailed geological information such as (Brox, 2011):

- Rock type
- Jointing patterns: can have many joint sets and unfortunately orientation what that cause rock fall.
- Mineralogy/petrology if infillings in joints. Some infillings can cause swelling if in contact with water.
- Deterioration observed during excavation from natural exposure during the construction period.

Detailed information about engineering geological properties of rock regarding headrace tunnel is presented in chapter 2.4.

2.2.2 Hydraulic Gradeline

To prevent negative pressures in the tunnel, the hydraulic gradeline must be above the tunnel for all modes of power plant operation, including hydraulic transient. Assessment of head losses by friction along the tunnel is therefore required (Benson, 1989). In this case the friction varies with the type of rock.

2.2.3 Mass oscillation

Regulating of valve, such as start/stop of pumps and turbines, causes change in water flow. This leads to a pressure surge in the form of elastic waves in pressure line/headrace tunnel. These elastic waves propagate in a high velocity and reflects at the end of the line/headrace tunnel or at

free water surface in the system. Excluding the elastic properties and consider the fluid as incompressible, it will go by the name of mass oscillation. With fast changes, such as start/stop of turbines, the increase of pressure will become substantial. To release the pressure in the headrace tunnel, a surge chamber is built with free water surface (Guttormsen, 2014).

With stable water flow in the system, the height of the water in the surge shaft will be stable as well (equilibrium). As for stopping/starting turbines, this water level will oscillate, move up and down. This movement is presented in presented in Figure 5, showing the mass oscillation in meters versus time.

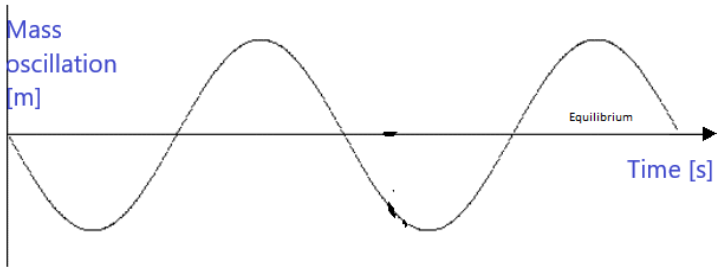

Figure 5 Mass oscillation principle.

It is possible to find the up- and down surge in the shaft, natural frequency and the time period of the mass oscillation through formulas presented below (Nielsen):

$$\Delta z = \Delta Q \sqrt{\frac{\frac{L}{A_t}}{aA_s}} + \frac{1}{3} h_f \qquad [2.1]$$

Formula [2.1] is the up-surge from steady state level in the shaft due to turbine shut down. ΔQ equals the flow of the tunnel (Q) minus the flow through the turbine ($Q_{turbine}$), L is the length of the tunnel, A_t is the tunnel area, A_s the surge shaft area, a the acceleration (gravity) and h_f is the head loss at steady state before shut down. Assuming h_f to be zero, will give the up-surge for Roskrepp situation a value of:

$$54.22 \frac{m^3}{s} * \sqrt{\frac{\left(\frac{3500m}{38.1\ m^2}\right)}{9.81 \frac{m}{s^2} * 60m^2}} = 21.42\ m.$$

Values are collected from scanned information presented in appendix G. The down surge due to turbine start-up is presented in formula [2.2].

$$\Delta z = -\Delta Q \sqrt{\frac{L/A_t}{aA_s}} + \frac{1}{9} h_f \qquad [2.2]$$

where h_f is the head loss at steady state after turbine start-up. Assuming h_f to be zero, this will give a value of -21.42 m. Natural frequency and time period is presented below in formula [2.3].

$$\omega = \sqrt{\frac{g}{A_s \frac{L}{A_t}}} \text{ and } T = \frac{2\pi}{\omega} \qquad [2.3]$$

Respectfully it will lead to ω = 0.04 frequency per second, and T= 149 seconds per frequency for Roskrepp situation.

2.2.4 Lifting- and Pulsating Force regarding Asphalt Lining in Headrace tunnels

Lifting Force

As the up-surge is on its way down, pressure under asphalt lining might not be able to align with the mass oscillation. This can lead to pressure under asphalt lining pointing up under the asphalt lining, while the water pressure over, is pointing downwards. This can work as a lifting force regarding the asphalt liner. If trapped air under asphalt are present, this will work as lifting force as well (Solvik, 1992).

Pulsating Force

With mass oscillations caused by turbine shut down, pulsating forces in the headrace tunnel will occur. This will also influence the asphalt stability. With pulsating force, such as velocity reduction, gravel under asphalt will move back and forth. This might be crucial regarding the asphalt stability (Solvik and Tesaker, 1997). Combining lifting- and pulsating forces over time, asphalt lining has a chance of destruction.

2.2.5 Dewatering

To identify the amount of potential scour and deterioration that has taken place, and quantify maintenance repairs if necessary, inspecting unlined pressure tunnels must be done. During hydraulic operations, all rock will undergo some form of deterioration over time, including dissolution of fracture infillings of soft materials, erosion of clay gouge within shear zones, as well as pitting of mineral constituents within a competent matrix such as feldspars within granite.

On the other hand, it is important to be aware that removal of all water (dewatering) of an unlined pressure tunnel can cause instabilities, such as rock block fall. This can happen regardless of the rate of dewatering. Suggested rates of dewatering depends on the quality of the rock in the tunnels. For fair quality rock conditions, lower rates are suggested. For good quality rock conditions, higher rates are suggested. The rate usually vary from 1.0 to 10 m/hour of total operating head (Brox, 2011).

The expected amount of rock debris after dewatering depends on the regulation of maintenance and inspections of dewatering. If regular and controlled dewatering has taken place, only minimum amount of rock debris can be expected to be present when inspecting the tunnel. For unlined pressure tunnels where previously inspections or well maintenance/upgrading have not been taken place over their operating life, an appreciable amount of rock debris can be generated because of dewatering, and should be anticipated for clean up during the first maintenance period (Brox, 2011).

For a free surface flow, gravel will move downwards because of gravity and the slope. This can cause up-lift of asphalt and damage it, as illustrated in Figure 6. It usually happens when dewatering the tunnel for maintenance work and inspections.

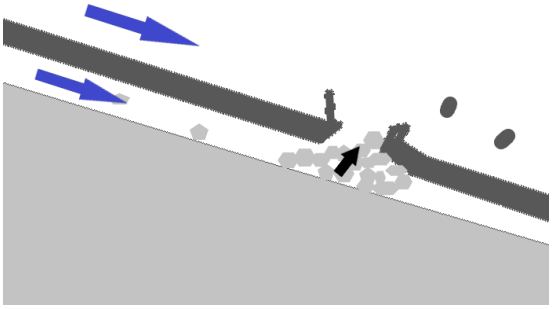

Figure 6 - Destruction of asphalt lining caused by buildup of gravel under asphalt lining.

When dewatering, the floor in the headrace tunnel will be the last part containing water, caused by the gravity force. This can cause large pressure working upwards under the asphalt layer and cause an uplift, or worst case, a rip-off of the asphalt layer. To prevent overpressure caused by the hydraulic head loss that otherwise may accumulate in stagnant water bodies under the lining,

the asphalt should be drained with small continuous or regularly spaced openings along the connection with the tunnel wall (Solvik, 1992). If the tunnel has a steep slope, 1:20 or steeper, special attention must be taken care of regarding the excess pore pressure which arises during emptying. It is not practical to empty the tunnel slowly enough for the pore pressure to follow the water table in the tunnel, because it is too time consuming (Solvik and Tesaker, 1997).

Dewatered inspections should be carried out by a team of qualified personnel, including an engineering geologist familiar with site geology along with a tunnel engineer well experienced in tunnel stability and safety. Rescue teams and medical services should always form part of any manual inspection of a previously operating unlined pressure tunnel. Should comprise a comprehensive documentation of all relevant tunnel condition including photographing of all tunnel surfaces, mapping of all signs of deterioration (scour, rock block fall, as well as the conditions of all intact and competent support and past repair works)(Brox, 2011).

2.2.6 Hydraulic Jacking

Hydraulic jacking, or uplift, can develop if water pressures are greater than the in-situ compressive stress. This can lead to openings of already existing joints, all depending upon the deformability of the rock mass and the area over which the hydraulic pressures act (Benson, 1989). Hydraulic jacking can occur in any direction where movement of rock masses can develop due to lack of adequate compressive in-situ stress. Jacking of rock blocks can occur into adjacent underground openings or opening of fractures in a compressive rock mass. One of the potential outcomes of hydraulic jacking is jacking of large masses of rock from tunnel that can result in excessive leakage and large-scale landslides or instabilities. Benson (1989) explains that hydraulic jacking in lateral direction can open vertical fractures that can allow excessive seepage to the surface.

The stress field may be highly variable for deformed rock masses that have zones, or beds of stiff and flexible material. A dilate in fractures caused by the water pressure can happen in low-stress deformable rock surrounding the tunnel. Even if the overall rock cover is adequate, this water

pressure can force an open pathway to access added tunnel or nearby powerhouse. This effect has been noticed in deformed granite masses, and between low stressed deformable sandstone and higher stress brittle siltstone. When dealing with compressible rock, care must be taken to obtain representative tests of those rocks where hydraulic jacking can occur. Material boundaries, probable stresses, permeability and deformability must be determined by appropriate geologic and testing methods (Benson, 1989).

To prevent hydraulic jacking, one should ensure that the hydraulic pressure within the tunnel is always less than the rock stress, or that the time of application of the hydraulic stress is too short to prevent hydraulic jacking. Ensuring that hydraulic jacking will not occur, measurements of rock stresses or estimation of stress levels by stress analysis are usually carried out. Overcoring is a possible measurement method.

It is being recommended that designing to control hydraulic fracturing by grouting and/or drainage should only be used where potential failure can be tolerated, or where a problem had arisen that cannot reasonably be solved by a more direct approach (Benson, 1989).

Failures caused by hydraulic jacking often takes many months before fully repaired. This results in big economical losses. It is therefore recommended a careful and conservative design of hydropower tunnels to prevent problems of this nature.

2.3 MECHANICAL PROPERTIES OF ASPHALT CONCRETE

2896 meters of the 3500 meters headrace tunnel in Roskrepp is covered with an asphalt concrete layer. Roskrepp hydropower plant has an asphalted layer for economic reasons. Instead of taking all the blasted rock materials out of the tunnel, it was possible to lay asphalt over it. This is a method that has been used before in other headrace tunnels. Rebuilding the hydropower plant into a pumped-storage plant will cause change in water pressure in the headrace tunnel. The change of water pressure can cause damage on the asphalt layer, and it is therefore important to

investigate the mechanical properties of the asphalt concrete. Figure 7 show asphalt layers used in the physical model test of Roskrepp headrace tunnel.

Figure 7 – Asphalt layers used in physical testing conducted by Peab Asfalt.

The general definition of asphalt is a material that contains 5-6 % of bituminous binder and 94-95% of rock materials (Statens vegvesen, 2017). Bituminous binder binds the rock materials together and prevents water intrusion in the road construction. It also helps the asphalt to resist deformation and at the same time give flexibility. The most important factors to include when choosing the hardness is the climate, traffic conditions and wanted lifespan (vegvesen, 2014). There are different types of asphalt for different uses, such as traffic load, costs, access to materials etc. Types of asphalt are listed below (Statens vegvesen, 2017):

- Asphalt concrete (AC)
- Asphalt concrete with gravel (AC)
- Stone Mastic Asphalt (SMA)
- Soft Asphalt (SA)

2.3.1 General Information of Asphalt Concrete

Asphalt concrete, also known as hot-mix asphalt (HMA), can be defined through the consistency and performance of paving. It consists of asphalt binder and aggregates mixed together at a high temperature and placed and compacted on the road while still hot (Mamlouk and Zaniewski, 2011).

Statens Vegvesen has certain requirements the asphalt must fulfill if they were to build a highway. Some of the different types of requirements are mentioned below in Table 2. Evaluating the asphalt requirements of asphalt concrete for highways can give an indication on how the asphalt layer is in Roskrepp headrace tunnel. Using data from Handbook N200 (Statens vegvesen, 2017).

Table 2 Requirement for type of asphalt. Statens vegvesen.

Rock materials	Bituminous binder	Paving
Grading	Type	Temperature
Wear resistance	Quality	Air Voids
	Quantity	Compression

(Entreprenørforeningen - Bygg og, 1999, vegvesen, 2014)

Typical design of asphalt contents of binder range from 4% to 7% by weight of total mix (Mamlouk and Zaniewski, 2011). It is possible to get an indication of the value of the air void of the asphalt concrete at Roskrepp. Figure 632.4 in Handbook N200, presents relevant data (Appendix A). The air void is supposed to be between 2.0-7.0 % for highways. These numbers might also be realistic when trying to have an indication on how the asphalt is in the headrace tunnel to Roskrepp. There are also requirements for the rock materials. Properties that is being evaluated are:

- Flakiness Index (the flakiness of the rock material)
- Los Angeles-value (resistance to crushing)
- The Mill Value (resistance to studded tire)
- Crushing degree of the rock material

The rock materials should also not contain too much humus (vegvesen, 2014).

Research on how crack sealed asphalt concrete behaves by varying temperature and time of loading have been bone by Ziari et al. This research was for crack sealed pavement behavior under Iran conditions (Ziari et al., 2007). According to the test described in the article, asphalt concrete with lower bitumen contents are more resistant to rutting compared to asphalt with

higher content of bitumen. It is maybe possible to see this through the rapidly water pressure caused by a potential pumped-storage plant in Roskrepp headrace tunnel.

2.3.2 Strength

It is possible to find the strength of the asphalt mix based on Mohr-Coulomb theory. Many factors can affect the uniaxial compressive strength of an asphalt concrete, and the asphalt mix is rarely the same. This makes values of the mechanical properties vague, but there might be a possibility to find a trend value. Zhang et al. (2013) presents a typical stress-strain curve in a uniaxial strength test on an asphalt concrete at 40 Celsius in Figure 8.

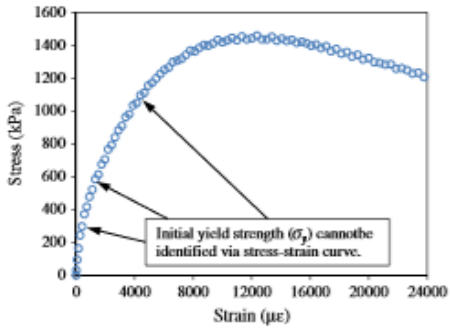

Figure 8 - Typical stress-strain curve in a unoaxial compressive strength test of an asphalt concrete at 40 degree Celsius.(Zhang et al., 2013)

By using the figure presented above, it appears like the UCS value is approximately 1.5 MPa, for a typical asphalt concrete at 40 Celsius. The temperature seems to affect the strength. Zhang et al. (2013) shows results from triaxial compressive test of different specimens of asphalt concretes at different temperatures in Figure 9.

Table 4
Ultimate yield strength and temperature factors for asphalt concrete.

Temperatures		σ_u	a_T	
°C	K	kPa	Calculated a_T based on data of σ_u	Modeled a_T based on Arrhenius function (Eq. (9))
40	313.15	2224	1.02	1.00
45	318.15	2094	0.96	0.88
50	323.15	1746	0.80	0.78
55	328.15	1609	0.74	0.69
60	333.15	1199	0.55	0.62

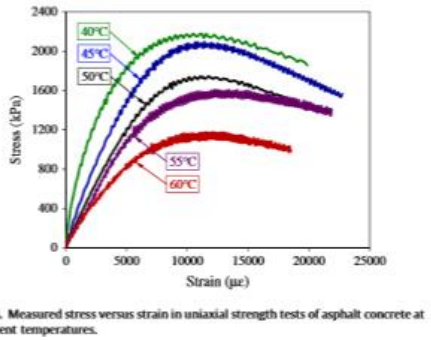

Fig. 4. Measured stress versus strain in uniaxial strength tests of asphalt concrete at different temperatures.

Figure 9 - Results from triaxial compressive test of different specimens of asphalt concrete at different temperatures.(Zhang et al., 2018)

Seo et.al (2017) performed a test of asphalt concrete to find the compressive strength. This test was mainly used for dam purposes. The test was conducted at three confining pressures; 36, 69 and 138 kPa in ambient temperature (25 Celsius). Nine specimens were used for three mixes of asphalt concrete – two specimens on one mix. The average stress results landed on; 2.77, 2.54 and 2.23 MPa, see Figure 10. Using the mean value of 2.51 MPa, for input parameter to the numerical analysis in chapter 5.

Table 4
Summary of average stress results.

Mix	Stress		
	Average (MPa)	Standard Deviation	C.O.V. (%)
F10	2.77	0.141	5.1
F12	2.54	0.101	4
F14	2.23	0.019	0.87

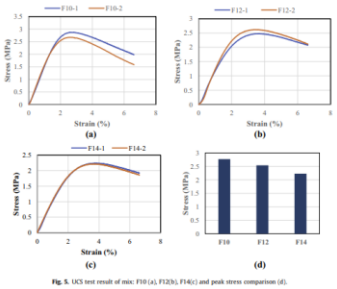

Figure 10 - Stress results of asphalt concrete.(Seo et al., 2017).

2.3.3 Elasticity

Apeagyei et al. (2012) presents in their paper a curve of the elasticity of typical hot mix asphalt for Virginia mixes at different temperatures and reduced frequency, see Figure 11. This might give an indication of the elasticity for other typical asphalt concrete mixes.

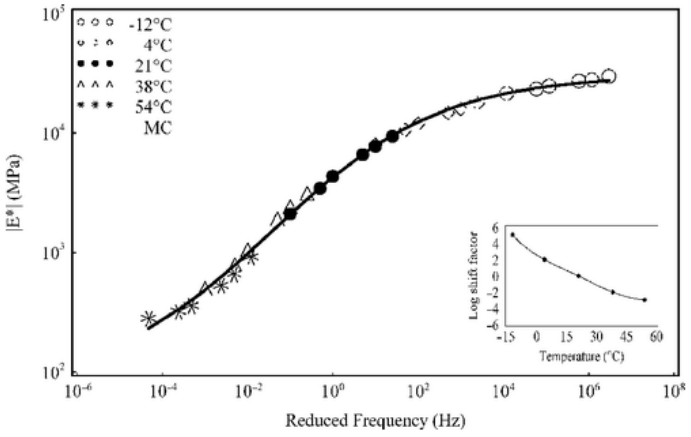

Figure 11 - Typical HMA |E| master curve for Virginia mixes (T = 25 Celsius).(Apeagyei et al., 2012)*

Articles shows that each asphalt concrete mix tends to have their own elasticity values. Comparing asphalt concrete mixes of around 20-30 Celsius, it seems like most values of elasticity lands on around 5000 MPa. This value will be used in the numerical analysis.

2.3.4 Permeability

Research done by Vardanega and Waters (2011) presents results of the permeability from 23 hot mix asphalt construction projects. The primary indicator of permeable asphalt concrete is high air void. Other parameters that affect permeability in the asphalt concrete are:

- The percentage of bitumen binder in the asphalt mix
- Compaction effort
- Type of aggregate
- Nominal aggregate size (NMAS)
- Lift thickness (if lift thickness increases, the permeability decreases)
- Aggregate mix gradation
- Air voids in the mixture

The grading of the asphalt mix and the air void in the asphalt mix have a major influence on permeability. The degree of connectivity of the pore structure affects the power on the air voids versus permeability relationship (Vardanega and Waters, 2011). According to Vardanega (2011) X-ray techniques can be used to assess air void gradients and distributions in compacted asphalt concrete mixtures.

2.4 ENGINGEERING GEOLOGICAL PROPERTIES OF ROCKS

It is important to understand the rock mechanical properties when assessing the tunnel stability of Roskrepp headrace tunnel. Rock mechanical properties such as rock strength and elasticity are relevant to evaluate and understand the behavior of the rock mass, and is according to many, the most important mechanical parameters of rock (Li, 2015).

2.4.1 Rock Stresses

Geological materials are preloaded by *in-situ* stresses. Knowledge of the *in-situ* stresses is important since both high and low *in-situ* can impact the stability. If the stresses set up around an underground excavation exceed the strength of the rock mass, stability problems can occur (Palmström and Stille, 2010). This concludes that stress is a depending factor of the rock strength and the elasticity of the rock mass, and is defined as (Li, 2015):

$$\sigma = \frac{F}{A} = \frac{force}{area} = \frac{[N]}{[m^2]}. \qquad [2.4]$$

These stresses are usually handled as a three-dimensional case of $\sigma_1 \geq \sigma_2 \geq \sigma_3$ for rock materials. *In-situ* stresses can be influenced by different factors such as gravitation (a), topographic (b), tectonic (c) and residual (d) (Nilsen and Palmström, 2000).

a) Gravitational Stresses

The gravitation can influence *in-situ* stresses. Gravitational stresses are normally expressed as vertical stress, σ_v, major horizontal stress, σ_H, and minor horizontal stress, σ_h. The vertical stress is directly expressed through gravitational acceleration, g [m/s^2], and are presented below in formula [2.5].

$$\sigma_v = \rho g h, \qquad [2.5]$$

where ρ [kg/m^3] is the density of the cover rock mass and h [m] the cover height (see Figure 12). The horizontal stresses are in many cases connected to the vertical stress (Li, 2015). An example on how the horizontal stresses can connect to the vertical is shown in chapter 3.1.3.

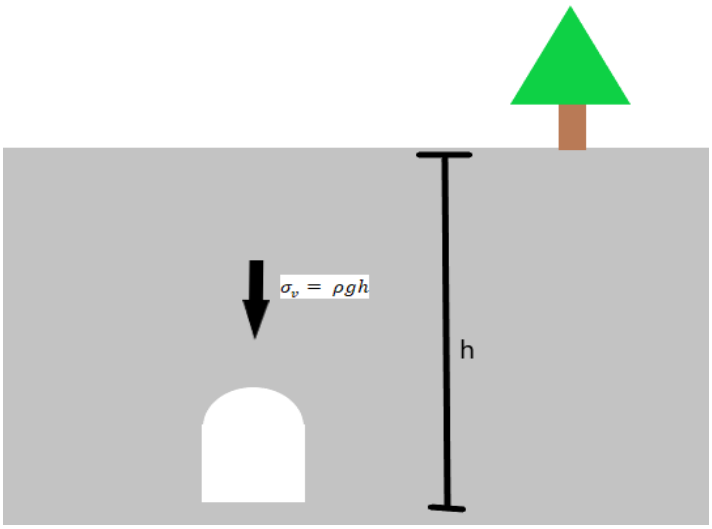

Figure 12 - Gravitational stress situation.

b) Topographic Stresses

The topographic surface can influence *in-situ* stresses. According to Li (2015), the principal stresses in the surface-nearby areas becomes either parallel or normal to the slope surface because of traction-free boundary. Figure 13 illustrates how the topography influences the *in-situ* stresses. The minor stress is always facing normal to the slope and the largest stress are usually parallel to the slope. The differences of the magnitude between minor and largest stress decreases as the distance from free-surface increases. They become more isotropic.

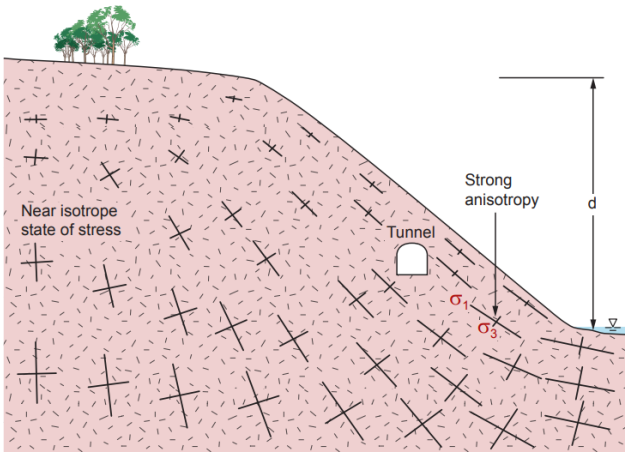

Figure 13 - Topographic stress situation. (NGI, 2015)

c) Tectonic Stresses

Global patterns of tectonic stresses in the lithosphere has been noticed. Measurements and observations have been done in Norway and are shown in Figure 14.

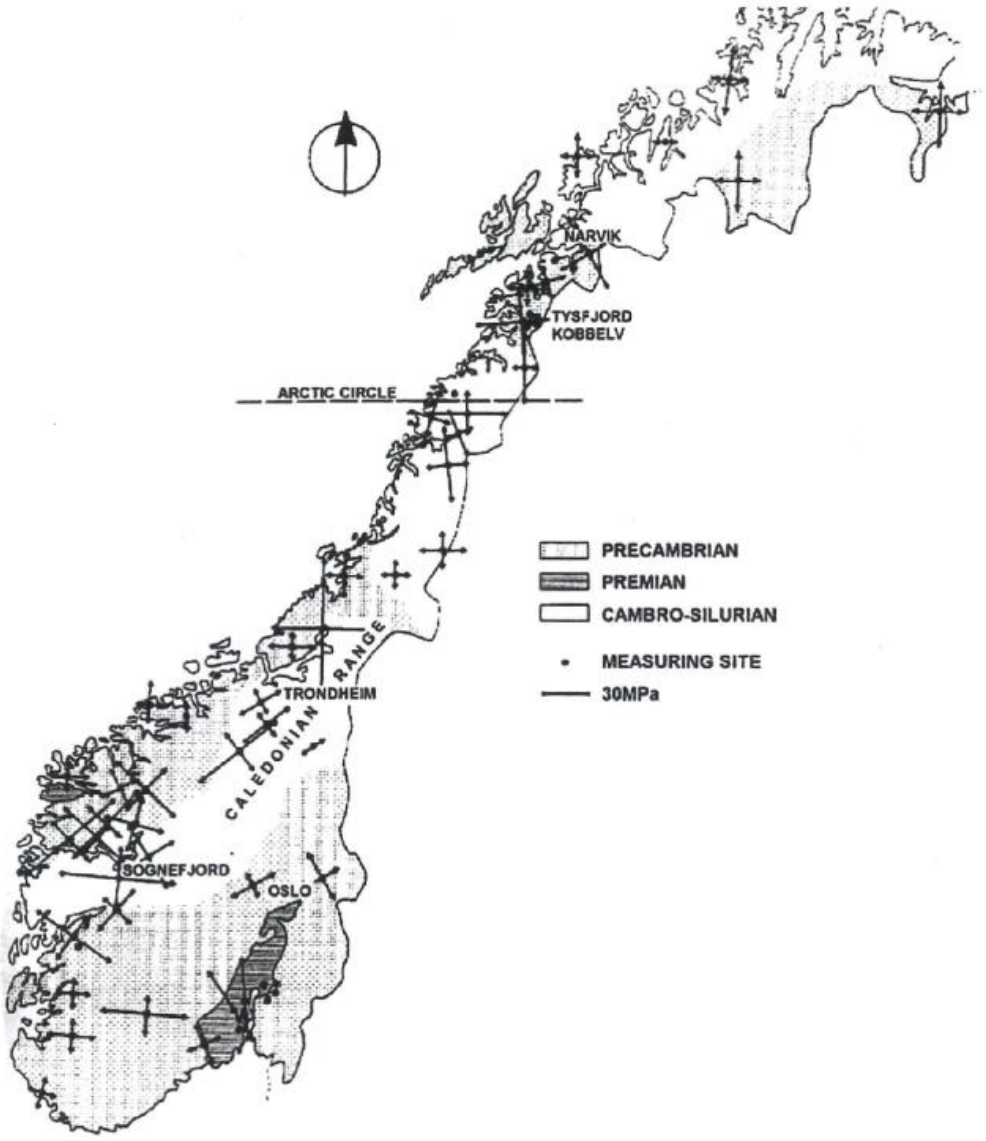

Figure 14 - Tectonic stress map of Norway.(Myrvang, 2001)

d) *Residual or Internal/"locked-in" Stresses*

In Norway residual stresses are often caused by deglaciation. Residual stresses are related to a system of balanced tensile and compressive forces contained in domains. These can be ranged from the microscale to the macroscale.

2.4.2 Rock Strength

The strength and hardness of the different rock types can vary. There are different methods for evaluating the rock strength, σ_{ci}, such as laboratory testing and empirical methods. The most common method for laboratory testing is the Uniaxial Compression Strength Test that classifies the rock strength as uniaxial compressive strength (ISRM, 1979). Point load test is another laboratory test that evaluates the rock strength and uses the correlation between the point load index and the UCS to find a respectful value. More specific information of UCS testing is explained in chapter 4.1.4. Empirical methods, such as Rock Mass Rating (RMR), uses the GSI, Geological Strength Index, to estimate rock strength values (Hoek et al., 1995).

One of the structural features that reduces the rock mass strength is the schistosity planes of the rock (Panthi, 2006). Schistosity is a mode of foliation and reflects an intensity of metamorphism. (The Editors of Encyclopædia Britannica, 2006, Rast and Crimes, 1969).Shrestha and Panthi analyzed the plastic deformation behavior of schist and schistose mica gneiss at Khimiti headrace tunnel in Nepal in 2014. The report informed that instability and squeezing problems occurred in the weak sheared schist and schistose mica gneiss (Shrestha and Panthi, 2014).

2.4.3 Elasticity

The fundamental law in elastic theory is the Hooke's law; the stress is proportional to the strain. The relation between stress and strain is expressed in equation [2.6].

$$E = \frac{\sigma_z}{\varepsilon_z} \qquad [2.6]$$

The deformation capability of the rock is represented by the Young's modulus *E*. When loading uniaxial of a cylindrical specimen; σ_z represents the axial strength and ε_z represents the strain. ε_z is the strain and is a relative deformation with respect to the original length of the cylindrical specimen.

In rock mechanics, tensile stress, σ_t, has a negative sign unlike classic mechanics. In rock mechanics, it is the compressive stresses that are most dealt with and has therefore positive sign.

As the specimen is compressed axial, it will expand radial (or lateral) and will have a negative sign. A constant, called *Poisson's ratio* (ν), expresses the relation between these movements in different directions. See equation [2.7].

$$\nu = -\frac{\varepsilon_x}{\varepsilon_z} = -\frac{\varepsilon_y}{\varepsilon_{z\,z}} \qquad [2.7]$$

To have a positive ν, negative signs are put in the equation. A plane that is inclined to the axis of the specimen, has an angle α and a resultant stress, that can be expressed through equation [2.8].

$$\sigma = \sigma_z * cos\alpha \qquad [2.8]$$

If the strain of a material returns to zero, but by a different path, after loading and subsequent unloading to zero stress, it is called an elastic material. This effect is called hysteresis.

A complete stress-strain curve is shown in Figure 15. This type of curve can be established in a stiff machine test, such as in a Uniaxal Compressive Strength test.

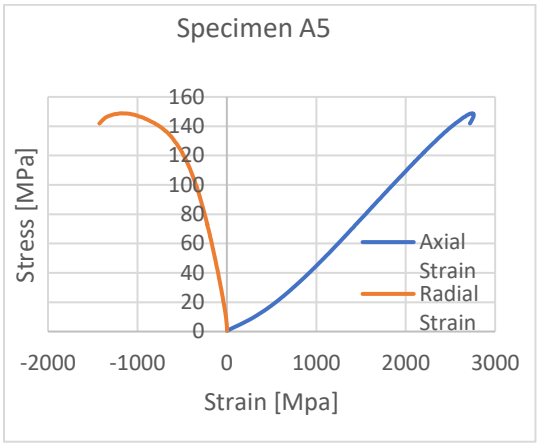

Figure 15 - Stress-strain curve for rock specimen A5, tested in laboratory.

2.4.4 Failure Criteria

Too high stresses and too low stresses can both lead to rock failure in a tunnel. It is therefore important to understand the rock stress conditions when dealing with a tunnel and rock support (Li, 2015).

According to Li (2015) Mohr Coulomb criterion is the best suit to describe the failure if the rock under compressive stressing. Uses Mohr's Circle in a σ-τ diagram, where the ultimate stress, σ_1 and the confining stress, σ_3 are presented in a Mohr's Circle. Several triaxial tests on the same rock sample gives many Morh's circle. This gives a curve of the rock strength by using the envelope of the Mohr's circles, shown in Figure 16**.**

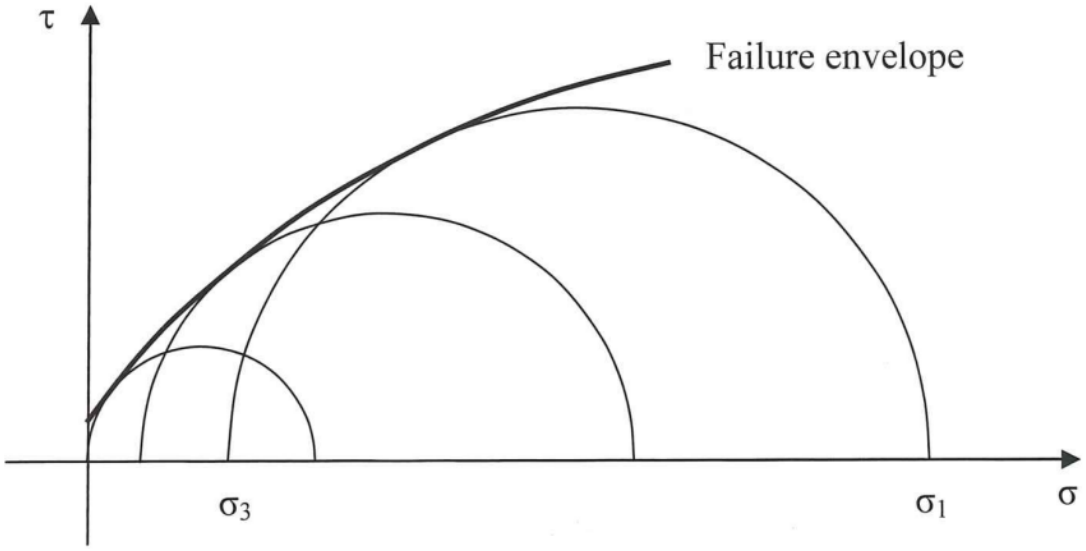

Figure 16 - Morh's circle. (Li,2015)

The shear failure can be found as well through Mohr-Coloumb criterion:

$$\tau = c + \sigma_n tan\varphi \qquad [2.9]$$

Where τ is the shear stress, σ_n represents the normal stress, c is the cohesion, and ϕ is the internal friction angle.

Hoek and Brown (1980) proposed an empirical strength criterion for rock based on reviews on the published information on intact rock strength. The Hoek-Brown criterion for intact rock can be presented as:

$$\frac{\sigma_1}{\sigma_c} = \frac{\sigma_3}{\sigma_c} + \left(m\frac{\sigma_3}{\sigma_c} + 1\right)^{1/2} \qquad [2.10]$$

(Hoek and Brown, 1980 , Myrvang, 2001)

m is the material constant for intact rock and has different value for different rock types presented in Table 3

Table 3 - Rock types and their material constant value.

m	Rock type
7	Carbonate rocks with well developed crystal cleavage (dolomite, limestone, marble)
10	Lithified argillaceous rocks (mudstone, siltstone, shale, slate)
15	Arenaceous rocks with strong crystals and poorly developed crystal cleavage (sandstone, quartzite)
17	Fine-grained polyminerallic igneous crystalline rocks (andesite, dolerite, diabase, rhyolite)
25	Coarse-grained polyminerallic igneous and metamorphic rocks (amphibolite, gabbro, gneiss, granite, norite, quartz-diorite)

2.4.5 Joints

Detailed jointing normally dominates in a tunnel and can be defined based on their size and composition based on their origin. According to Nilsen and Palmström (2000), are the most important characteristics of joints for engineering purposes such as:

- Roughness
- Possible filling materials
- Orientation
- Length and continuity
- Condition of join wall with regards to alteration or coating (Nilsen and Palmström, 2000)

Joints can have different degree of roughness, depending on rock types and other factors. They can for example be rough and irregular, or smooth and undulating, as shown in Figure 17.

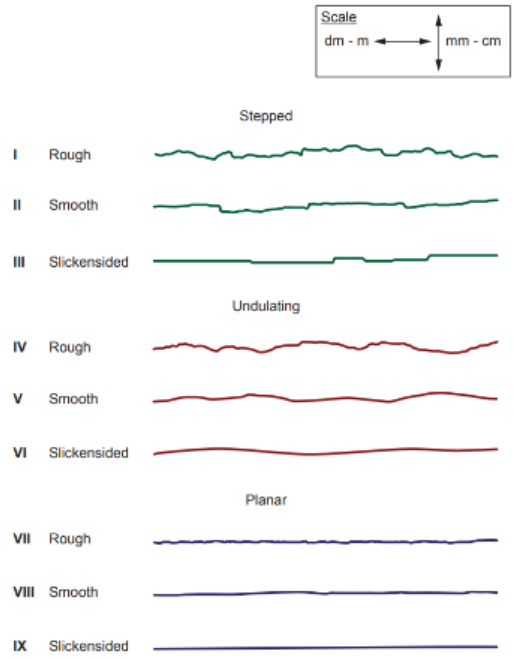

Figure 17 - Description of joint parameters.(NGI, 2015)

Infilling in joints can be crucial during and after excavation in a tunnel. Most common infillings materials can be divided into four main groups:

- Inactive minerals (chaolite, iolite, limonite, zeolite etc.).
- Minerals with very low inner friction, especially in wet condition (chlorite, talc, graphite etc.)
- Dissolved minerals (carbonates).
- Minerals with swelling characteristics (swelling clay or smectite) (Aksu et al., 2015).

Minerals with swelling characteristics is the most common infilling group causing instability problems (Nilsen and Broch, 2010). They can lead to major collapses and/or blockages during operation due to turbulent flow conditions (Benson, 1989). Infillings of minerals in jointed rock material can be difficult to discover in field. Laboratory testing is therefore often used to engage more knowledge about the amount and type of minerals in a rock. The most common laboratory tests for swelling is mineralogic analysis, determination of plastic characteristics and direct measurements of swelling and swelling pressure (Nilsen and Broch, 2010).

Knowledge of the orientation of the joint sets can be important when designing a tunnel. Rock blocks developed by two to three joint sets that crosses each other, can lead the blocks to fall out from the ceiling of a tunnel or along a steep rock wall.

2.4.6 Weakness Zones

It is according to Nilsen and Broch (2012) the support condition for the tunnel that is usually influenced by weakness zones. Weakness zones can be divided into two main groups; weak bedrock- and tectonic fracture zones. For the Norwegian landscape, most of the weakness zones can be recognized by areas of valleys and fjords where erosion from ice has taken place. Weak bedrock can in many cases contain of large amount of parallel oriented minerals such as talc, chlorite, glimmer etc. This leads the rock mass to easily split in same mineral orientation. Another example of weak bedrock can be of weathered rock material that can cause reduction of binding force between the minerals.

Tectonic fracture zones are weakness zones caused by tectonic stresses. Normally it is characterized of movements along two planes by strain or stress. If the formation of these zones is not clear, they can be divided into its appearance and is then called either slit zones or crush zones. Slit zones can be filled with clay, calcite, silt, soil etc., with normally unweathered and unfractured rock mass at the sides. Crushed zones can vary in appearance and its degree of stability. Degree of crushed rock material, the amount and type of clay minerals are the most common characteristics of crushed zones.

History shows that caving problems from weakness zones have caused cancelation of the construction work. These kinds of weakness zones usually contain crushed or decomposed rock material. There are also cases where caving has happened after tunnel excavation. These cases are usually happening to water tunnels where the weakness zones are containing of swelling clay (Nilsen and Broch, 2010).

3 ROSKREPP HEADRACE TUNNEL AND FIELD INVESTIGATION

Engineering geological investigations can be performed during the whole process of building a tunnel; before, during and after. In this case, the tunnel is already completed. Since the headrace tunnel of Roskrepp was filled with water, it was not possible to investigate the rock conditions inside the tunnel. To predict the rock conditions in the tunnel, pre-investigation methods and information from previous investigation of the tunnel have been used.

Engineering geological investigations in this case are:

- Pre/Desk-studies
- Field mapping
- Processing results from field

3.1 THEORY

Pre/Desk-studies can be performed before field investigations. Relevant information that can be collected are:

- possible weakness zones
- rock type distribution
- water conditions
- stress conditions
- foliation and marked detail joint orientation

This information can be collected by: flight photo, topographical map, previous geological maps of the area if possible and information from the power plant. The collected data can be helpful during field mapping.

3.1.1 Location

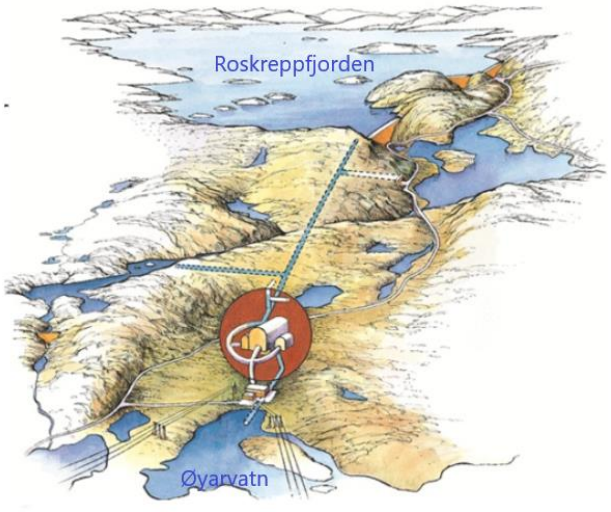

Figure 18 - Illsutration of Roskrepp hydropower plant (Sira-Kvina, 2017a)

As illustrated in Figure 18, there is a road (highway 978) crossing Roskrepp area, and it is located between Suleskard in Sirdal and Brokke in Setesdal. Roskrepp power plant is the upper part of the Kvina-watercourse and takes place at the county border between Vest- and Aust-Agder. The two magazines involving Roskrepp powerplant is Roskreppfjorden, the upper magazine, and Øyarvatn, the lower magazine.

3.1.2 Topography

Roskreppfjorden, the upper magazine, is 929 meters above sea level. The headrace tunnel starts in the end of the magazine, where the rock filled dam is located. The length of the headrace tunnel is approximately 3500 meters and ends in the hydropower station close to Øyarvatn, which is 837 meters above sea level. This makes it a head loss of 92 meters. To get an overview of the locations of the magazines see Figure 19 and Figure 20.

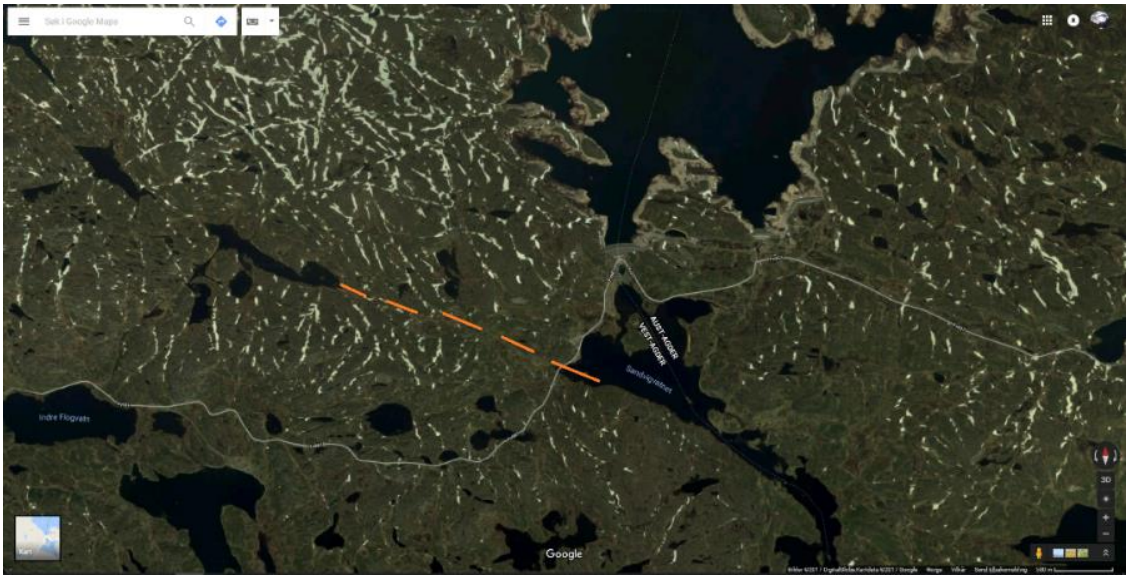

Figure 19 - Satelite photo by Google Maps of Roskrepp area. Orange line illustrates weakness zone 4.

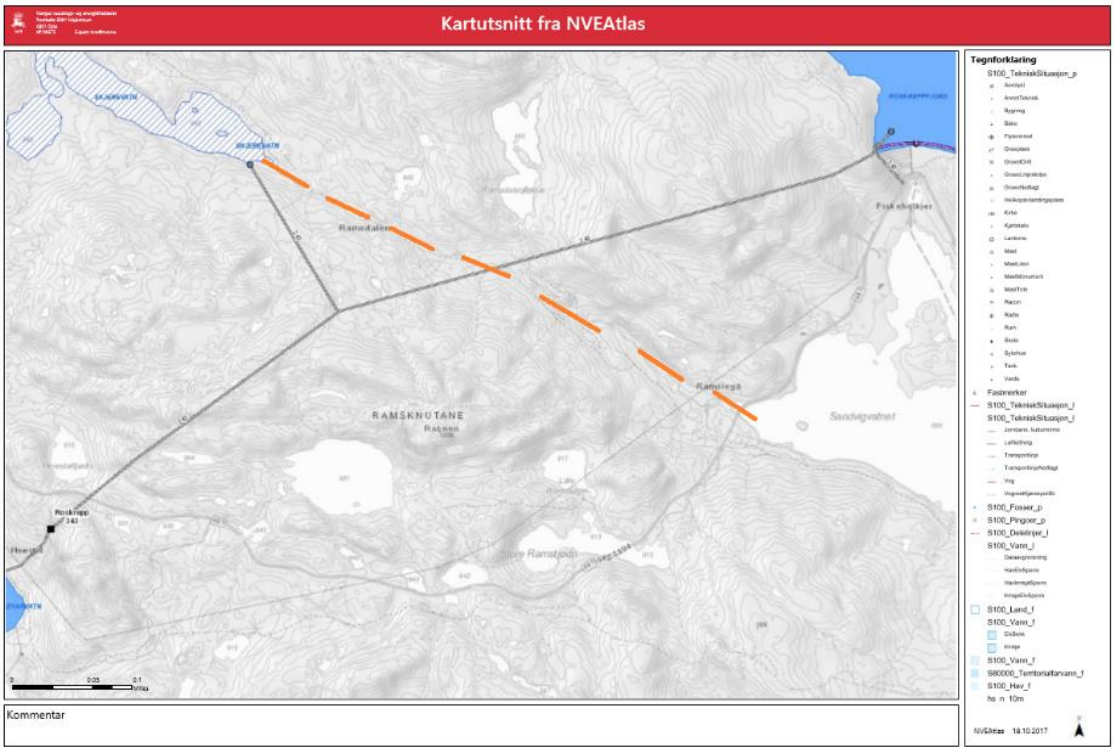

Figure 20 - Topographic map by NVE Atlas of Roskrepp area. Orange line illustrates weakness zone 4.

The highest point between the two reservoirs is approximately 1040 meters above sea level. A river crossing the tunnel area, is also a part of the widest valley, Ramsdalen, between Øyarvatn and Roskreppfjorden (orange line in the figures above). The streaming water in Ramsdalen comes partly from a reservoir, called Skjerevatn. This reservoir distributes electric energy to the

hydropower plant as well as Roskreppfjorden. A brook intake connects to the headrace tunnel, see Figure 20. There are many lakes in different scales in the area that are not connected to the hydropower system. Smaller valleys crossing the "headracetunnel-section". The water streams from Øyarvatn to the next power plant, Kvinen. The water runs through five power plants before it flows to the ocean in Åna-Sira.

3.1.3 Stress Situation

No measurement of *in-situ* stresses has been found during research in this thesis. A doctorial paper of measurements taken from Bykle (Ferjerskov, 1996). This location is approximatel 35 km in air-distance from Roskrepp area (Figure 21), which is the nearest measurements found. According to bedrock map from NGU (Figure 22), Bykle area consists mostly of the same rock types as Roskrepp - granite and gneissic rocks.

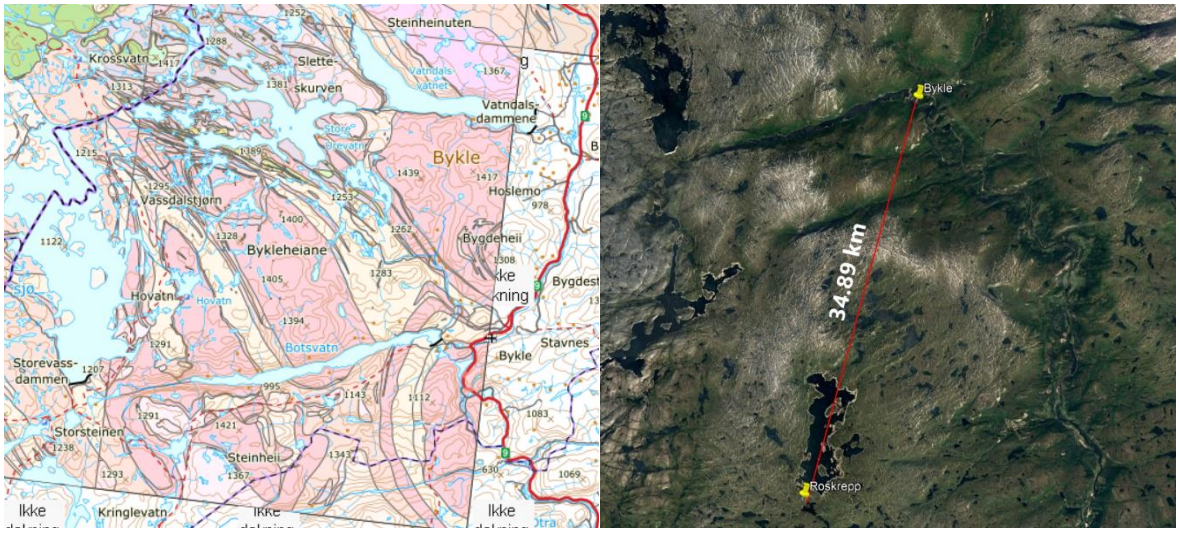

Figure 21 – (Wright) Distance between Bykle and Roskrepp.

Figure 22 – (Left) Bedrock map, from NGU.

Measurements and relations between the measurements are presented below in Table 4.

*Table 4 - Measurements from Bykle. *Does not include these measurements because of lack of relation to measurements from Bykle01 and Bykle02.*

	Latitude	Longitude	Depth	σ_H-direction	σ_H [MPa]	σ_v [MPa]	σ_h [MPa]	σ_H/ σ_v [MPa]
Bykle01	59.350	7.299	400	93	20.4	9.8	5.4	2.1
Bykle02*	59.350	7.299	400	26	6.4	7.3	4.3	0.9
Bykle03	59.350	7.299	400	106	11.0	8.2	5.2	1.3

Mean value of the relation between σ_H/σ_v of Bykle01 and Bykle02 is 1.7. Choosing this value for further calculations of stress values for Roskrepp area. By using the formula

$$\sigma_v = \rho g h \quad [3.1]$$

parameters from Roskrepp area can be used. Assuming

$$\sigma_h = \sigma_v \quad [3.2]$$

$$\sigma_H = 1.7\sigma_v \quad [3.3]$$

Fokusing on Bykle01 and Bykle03, the σ_H – direction will be approximately N100E. This can be correct if comparing with the tectonic stress map from chapter 2.4.1.

3.1.4 Geological History

The main part of the bedrock in the south part of Norway was formed for about 1500-1040 million years ago. These bedrocks are one of the oldest rock types in Norway and has been influenced by the Sveconorwegian orogeny for about 1130-900 million years ago. The rocks were strongly folded and metamorphosed. Unlike many rocks in Norway who has been influenced by the making of the mountain chain, few areas of granite in the south of Norway were formed in the earth crust for 925-930 million years ago (Ramberg et al., 2007).

According to NGU bedrock map, a pre-investigation from 1961, and field mapping, is the Roskrepp area dominated by the rock types of granite and granitic gneiss.

Granite is a magmatic rock that is crystalized from magma. Magma has been crystalized below surface, and the granite is therefore classified as a pluton/an intrusive rock. Plutons tends to have bigger minerals compared to rocks crystalized in the surface and in the magma chambers (Bruhni, 2017). The minerals are usually of quarts, K-feldspar (orthoclase- or microcline perthite) and Na-rich plagioclase. The granite can occasionally contain some dark minerals such as glimmer (biotite and muscovite), amphibole and pyroxene (Raade, 2016). This rock type is usually considered as a hard rock.

The granitic gneiss is most likely from a regional metamorphose. Granitic gneiss is classified as an orthogenesis, which means that it comes from a magmatic rock. It is likely that it was metamorphosed during the Caledonian orogeny that took place 750 to 400 million years from today (Bryhni, 2017). The minerals are usually of the same types as the granite.

Shear zones influences the south part of Norway. These zones are steep, linear belts where the rocks have been exposed to plastic deformation. The strongly deformation along the shear zones is most likely made by sideways faults between the earth blocks during the development of the Sveconorwegian orogeny (Ramberg et al., 2007).

Including Ramsdalen, smaller valleys in the area can be considered as weakness zones regarding the stability in the headrace tunnel. To see all the possible weakness zones, see geological map. According to a pre-investigation in 1961 it was also expected to hit stability problems in the southern part of the headrace.

A geological report from investigations of the drainage tunnel in 1979, can give an indication of the geological conditions of the headrace because of its closeness: *"This zone is in the transition between overlaying, coarse-grained granite and underlaying dark, biotite-rich gneiss (or biotitic amphibolite?). The granite is massive and homogenic, while the dark gneiss has a markedly and almost perpendicularly cracking pattern."*

3.1.5 Groundwater Table and Hydrostatic Line

Limited possibilities to predict water leakage into the headrace tunnel reported in 1961. Possibilities of water leakage if rock mass contains of jointed material and nearby reservoirs. Øyarvatn and Skjervatn can influence if something were to happen to the water in the headrace tunnel.

The ground water table is most likely to follow the topography, along with the water table to Roskreppfjorden. The water table of Roskreppfjorden varies from the highest level at 929 meters to the lowest level at 890 meters. An illustration on the variation of groundwater table in the tunnel area is shown in Figure 23.

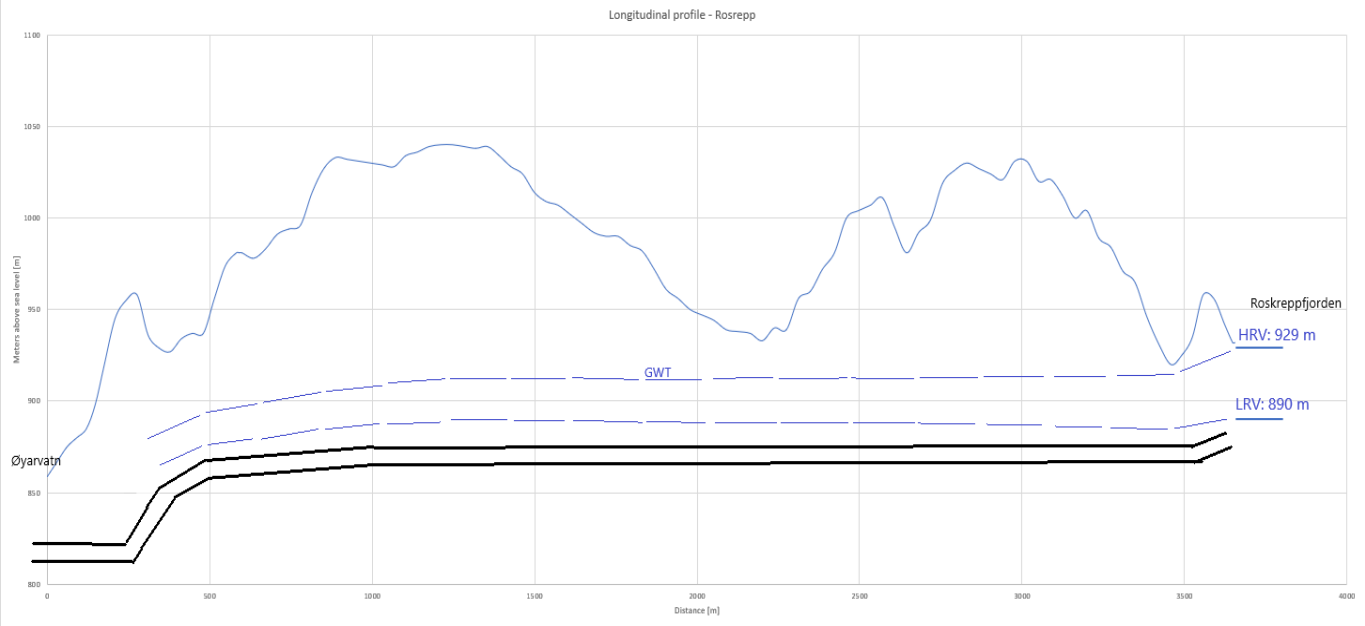

Figure 23 - Potential groundwatertable for Roskrepp headrace tunnel.

Most of the headrace tunnel will be under the groundwater table at all time. This leads to the possibility to assume that the water pressure will be equal around the tunnel face periphery (see Figure 24). Even though the water pressure will be equal around the tunnel face periphery at all time, the magnitude of the water pressure will increase as getting closer to Øyarvatn.

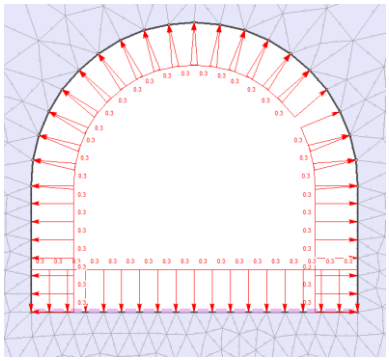

Figure 24- Water pressure in the tunnel periphery

3.2 METHOD

Field mapping collects information that are only possible at site. Rock types and its distribution are mapped in a geological map as well as potential weakness zones. Orientation of joints are measured, and the quality of the rock is evaluated. Certain tools can be useful to bring such as:

- Compass with clinometer (for measuring strike and dip of joints)
- Map over the area
- Geological hammer
- Notice book
- GPS
- Camera (Nilsen and Broch, 2010)

3.2.1 Geological Mapping

For a good overview of the engineering geological aspects of Roskrepp area, a geological map is developed. The geological map is a flight photo map that combines information collected before, during and after field investigations. Information that is possible to see in a geological map can be:

- Rock types and transition zones
- Weakness zones
- Topography
- Water conditions

Information that can be collected before field investigations is possible weakness zones, water condition and maybe an idea of rock types and transition zones. This information can be clarified from observation at site. GPS can be used to note the locations where measurements and other notifications is observed. After field investigation, a thorough geological map can be done. The aim was to present the map by using Autocad, but because the hydraulic model testing was

unexpectedly time consuming, it was not possible to do Autocad version. Raw data in a colored map by hand has been used in this thesis.

3.2.2 Joint Measurements

As mentioned in chapter 2.4.5, measuring joints to find potential joint sets and its dip/dip direction can be important to the assessment of the stability to the headrace tunnel. Using compass with clinometer when measuring strike and dip of joints. Location found from GPS with measurement are noted. Trying to find joint sets and at the same time exclude mechanical joints. Many measurements should be taken to find a potential trend of different joint sets. If infilling in the joints, it should be noted. Flight photo can also be used to help find some trends of joint sets. After field investigation, all the joint measurements are gathered in a joint rosette. This rosette can give a good overview and find trends of joint sets and is orientation and dip.

3.2.3 Q-system

Rock mass classification is determined in field by using the Q-system. To classify the rock mass quality, Barton, Lien & Lunde launched the Q-system at NGI in 1974. It is a method that can indicate what kind of support the tunnel needs in certain areas and an indication of the quality of the rock mass. It is an empirical method based on a numbered of tunnels. The Q-system uses six parameters described in Table 5.

Table 5 - Description of parameters used in the Q-system

Symbol	Description
RQD	Rock Mass Designation
J_n	Joint set number
J_r	Joint Roughness Number
J_a	Joint Alteration Number
J_w	Joint Water Reduction Factor
SRF	Stress Reduction Factor

(Nilsen and Broch, 2012)

The Q-value can vary from 0.001 (worst quality) to 1000 (best quality). Recommended support is decided with help from a diagram presented in Figure 25. Finding the recommended type of support, the "Equivalent dimension" is estimated. This value depends on the span (or wall height) of the tunnel and the Excavation Support Ratio, ESR. Increasing span of height usually results in increase of need of support. The safety requirements will also change depending of the use of the tunnel (NGI, 2015).

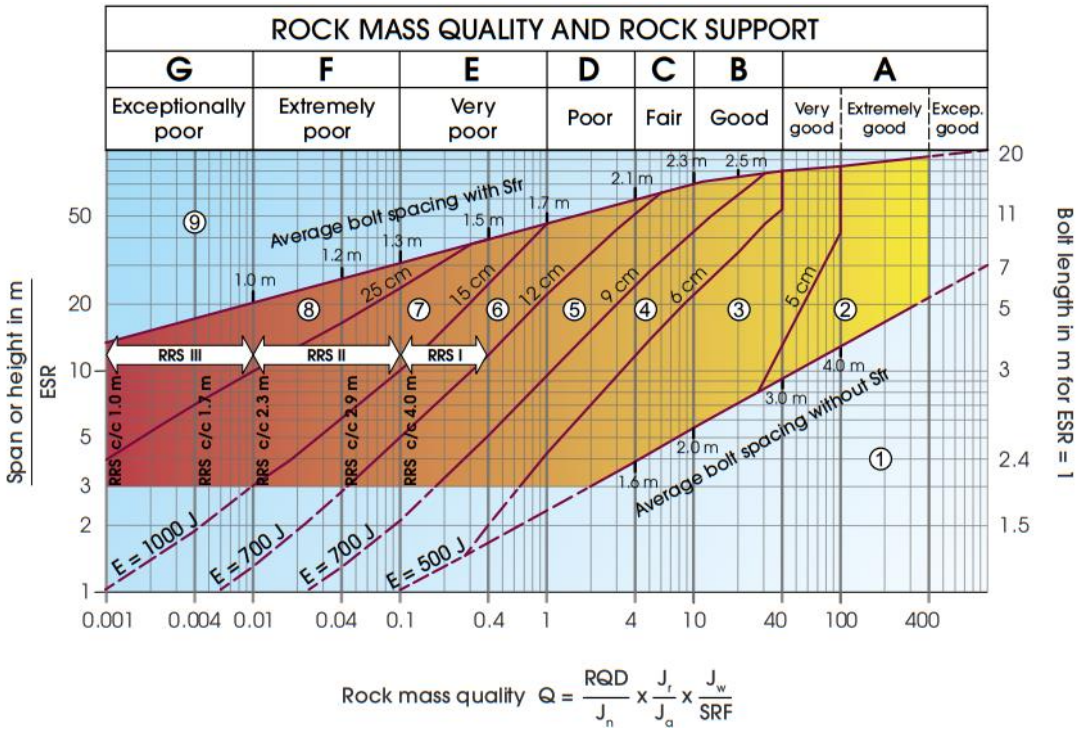

Figure 25 - Q-system diagram. (NGU, 2015)

To indicate the amount and what kind of support is recommended, ESR-value and span (or height) of the tunnel is used. ESR-value is estimated to be 1.6 when reading of the Q-system Handbook from NGI. It is a water tunnel where the traffic of people is low. If it were to be a highway tunnel the ESR-value would have been 1.

The height of the tunnel is estimated to be around 6.2 meters. The "Equivalent dimension" will be:

$$Equivalent\ dimension = \frac{height\ of\ the\ tunnel\ [m]}{ESR} = \frac{6.2\ m}{1.6} = \mathbf{3.9} \qquad [3.4]$$

This will be used when deciding the Q-value.

Rock Mass Rating –system is another method to classify the rock mass. This method is similar to the Q-system, but does not include the stress situation in the rock. Hence, the RMR-system includes uniaxial strength of the rock, which is excluded in the Q-system. In Norway the Q-method is mostly used (Hoek, 2007).

3.3 RESULTS

After field mapping it is important to process the results collected at field and maybe do some analysis if possible. Results can be presented through:

- Engineering geological map
- Joint rosette (includes the strike and dip measurements)
- Q-values
- Longitudinal profile (includes the orientation of weakness zones, rock distribution.)

3.3.1 Engineering Geological Map

The engineering geological map, in appendix C, shows two rock types that was discovered in field; granite and granitic gneiss. Previous geological reports from 1961 and 1979 and NGU bedrock map is backing up the observations.

A large area between the upper and lower reservoirs seems to be containing of coarse-grained granite, see Figure 26. This rock type is usually considered as a hard rock. It can be strong when dealing with a tunnel, but if it is very coarse-grained, it can on the other hand become a weak rock. It was possible to break the coarse-grained granite easily at the surge chamber of Roskrepp with a geological hammer.

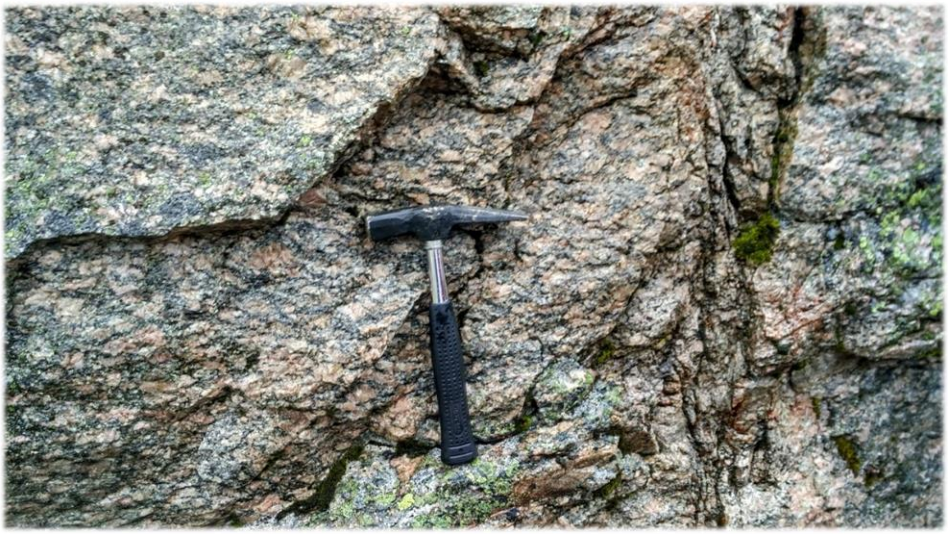

Figure 26 - Coarse-grained granite from Roskrepp area. (Bibek Neupane)

No clear transition zone between granite and granitic gneiss was discovered during field mapping, but there was some tendency to see metamorphic character in the granite in some locations. Most of the granitic gneiss was spotted in the upper and lower areas of the tunnel area.

Figure 27 - Granitic gneiss from Roskrepp area, close to Øyarvatn. (Bibek Neupane)

From field observation and research through the previous report of Roskrepp area, it is possible to state that the granitic gneiss has some tendency schistosity. Figure 27 shows layers of darker minerals in the same orientation as the cracking pattern. The cracking pattern is most likely the foliation.

3.3.2 Joint Rosette

Measurements on different joints was taken during field mapping. Strike and dip of the joints was measured by using a compass with a clinometer (see Figure 28).

Figure 28 - Measuring joints close to the added tunnel and the dam of Roskreppfjorden. (Bibek Neupane)

121 measurements of different joints were taken from the Roskrepp area. 101 of the total measurements was representable. No further analysis for the remaining 20 measurements. A joint rosette was made (appendix D) from the measured joints and the orientation of the tunnel is marked as well, see Figure 29. The tunnel has two orientations, where “tunnelstrike 1” indicates the first orientation of the tunnel from Roskreppfjorden to Øyarvatn, and “tunnelstrike 2” as the second orientation.

Three main joint sets were discovered in field. One of them was the foliation of the rock mass. The foliation is often the weakest joint when it comes to stabilization in a tunnel. The pre-investigation from 1961 measured the foliation. It was evaluated to be about N140E/50NE. From measurements taken in field the foliation was approximately N120-140E/40-50 NE. These two observations are close to each other. The foliation in this case is beneficial relative to the tunnel orientation. It will most likely not cause any stability problems itself if the schistosity is low.

The most favorable orientation of a joint set would be perpendicular to the tunnel direction, as indicated above. From Figure 29 it is possible to see that the orientation of "joint set 2" is close to the tunnel directions. This is not beneficial when it comes to the tunnel stabilization. The combination of the main joint sets can maybe cause rock fall in the headrace tunnel.

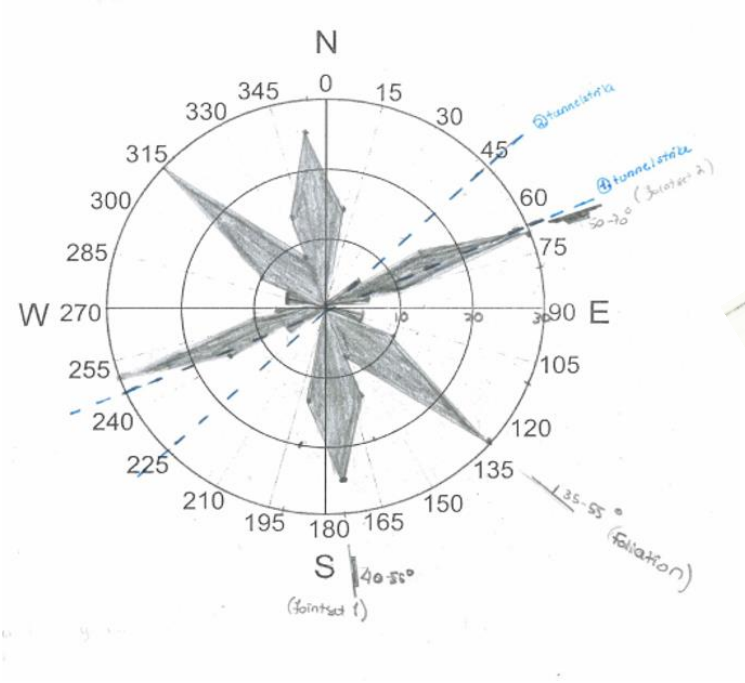

Figure 29 - Joint rosette of Roskrepp.

Figure 30 - Joint rosette of Roskrepp measurements from 1979.

Figure 30 shows a joint rosette from 1979, from the outlet tunnel of Roskrepp. Comparing the two joint rosettes, there are similarities regarding the main joint sets. The notes taken of the main joints from investigations in 1979 are listed below:

1) N120-140 E/40-45 NW, crack distance: 0.1-0.5 m, smooth
2) N20-40E/ 40 SØ, crack distance: around 0.75 m average
3) N100E/80 NW, crack distance: average 0.5 m

The foliation in the outlet tunnel is described as smooth, with a crack distance of 0.1-0.5 m. This might give an indication of how the weakness zones with the same orientation are in the headrace tunnel (WZ1, WZ2, WZ3, WZ4 and WZ7). The crack distance might not be the same everywhere, but there is a possibility that the foliation joints are containing of smooth materials.

The surge chamber was investigated as well. The report (1979) says that the chamber is quite breakable by a zone of clay. The granite is massive and homogenic, while the dark gneiss has a markedly and almost perpendicularly cracking pattern. The crack distance is about 0.5 meters. The gneiss gives a blocking pattern, but gives also an unstable area, where the most marked crack-direction is parallel to the clay zone. It seems like the gneiss turns into granite about two meters away from the clay zone.

3.3.3 Q-measurements

To evaluate the rock mass quality, Q-measurements was performed at three different locations spread along the tunnel area (see geological map and longitudinal profile). Two measurements in each location. The results are presented below in Table 6. The Q-value can vary from 0.001 (worst quality) to 1000 (best quality).

Table 6 Results of Q-measurements.

Description of location	At the added tunnel		At the surge chamber		In the access tunnel	
	Q_1	Q_2	Q_3	Q_4	Q_5	Q_6
RQD	95	90	70	80	85	95
J_n	9	9	6	6	5	5
J_r	3	3	3	3	1.25	2
J_a	1	1	2	2	3	3
J_w	0.9	0.9	0.85	0.9	0.9	0.9
SRF	1	1	1.5	1.5	1	1
Q-value	**29**	**27**	**9.9**	**12**	**6.4**	**11.4**
Comments			Granitic gneis	Granite, very coarse-grained		

At the added tunnel:

Q_1 and Q_2 was measured outside the entrance of the added tunnel. This area had some metamorphic character and is according to the values classified as a rock mass area with “good” quality.

At the entrance of the surge chamber:

Figure 31 shows the sections where Q_3 and Q_4 was measured. The location is right outside the entrance to the surge chamber which is located close to the last part of the headrace tunnel. Q_4 was taken from a wall of very coarse-grained granite that was easily to break with a geological hammer, but because of the lack of joints, this section resulted with a Q-value of 12. The wall of granitic gneiss where Q_3 was measured consisted on the other hand of more joints. This resulted with a Q-value of 9.9. The two Q-values are close to the line between "fair" and "good" quality.

Figure 31 - Coarse-grained granite (left) and granitic gneiss (right) at the area of surge chamber. (Anna Helene Mong Urdal)

At the access tunnel:

Q_5 and Q_6 was measured at the access tunnel, which is close to the last part of the headrace tunnel. Q_5 is in the range of "fair" rock mass quality, while Q_6 is in the range of "good" quality. As for the measurements at the surge chamber, it seems like the total result of the rock mass from the access tunnel is between fair and good quality. The distance from these two locations are not too far away from each other.

Using ESR-value, recommendations of support can be found. Support category 1 is the best category when dealing with support. If the tunnel where to be used as a highway, the support would have been heavier than it is now (support category 2 and mostly 3).

- For the rock mass in the first part of the water tunnel: support category 1 (bolt spacing right under 3 meter).
- For the rock mass closer to the last part of the water tunnel: support category 1 (bolt spacing 2 meter)
- For the rock mass in the last part of the water tunnel: support category 1, but close to support category 3 (bolt spacing 2 meter)

3.3.4 Longitudinal Profile

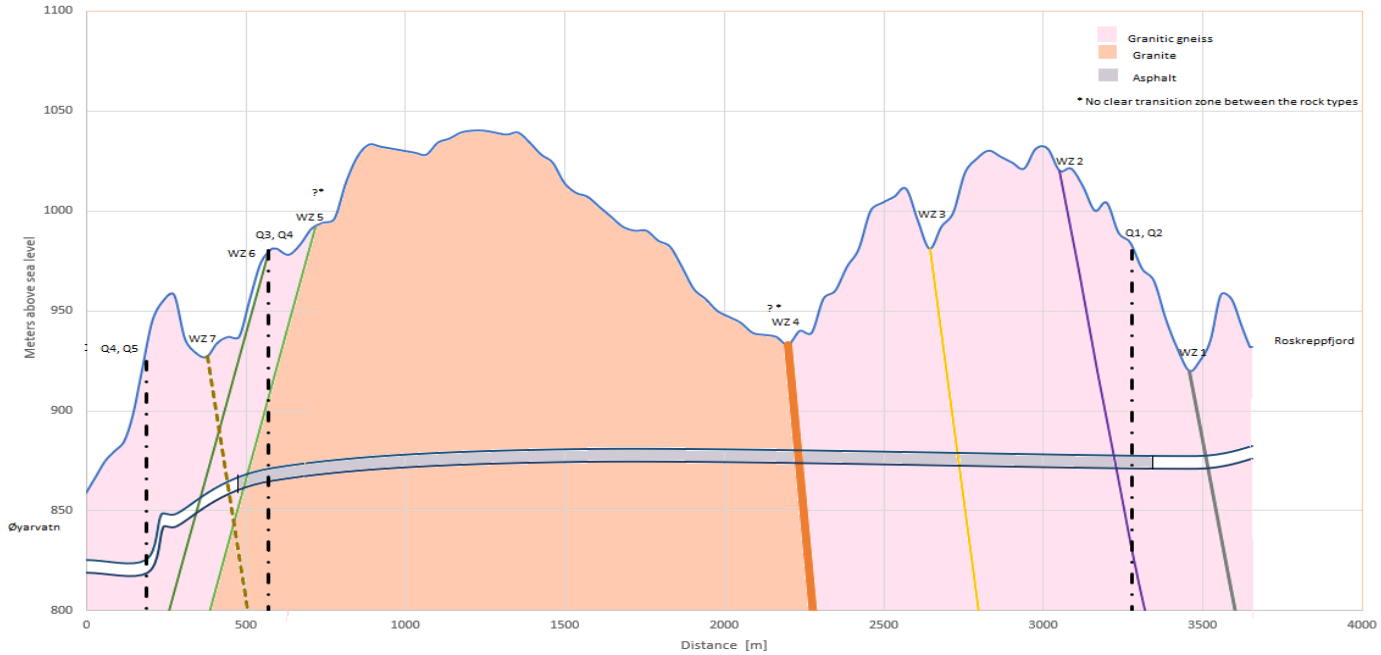

Figure 32 - Longitudinal profile of Roskrepp. (Øyarvatn: south-west direction, Roskreppfjorden: north-east direction). WZ = weakness zone, Q = q-value measurement.

Figure 32 show the longitudinal profile of Roskrepp (appendix F). The longitudinal profile is done through topographic coordinates from NVE Atlas in combination with excel.

In addition to pre-studies and field mapping, it seems like there are six to seven weakness zones that might be of interest of crossing the tunnel. The weakness zones that is being considered are numbered from one to seven in the longitudinal profile. Starting with number one as the weakness zone closest to Roskreppfjorden.

As predicted from pre-studies, weakness zone 4, was large (see Figure 33). The valley of the weakness zone is approximately 40 meters wide. The orientation of this zone was the same as the foliation. There is a possibility that this zone can be of crushed rock material.

Figure 33 - Weakness zone 4, Ramsdalen. (Bibek Neupane)

The weakness zones 1, 2 and 3, has also been predicted to have the same orientation as weakness zone 4, the orientation to the foliation. These were spotted from the topographic map because of their valley-characteristics.

The last weakness zones that is being considered are located further south, closer to the power station. There is one weakness zone that is more uncertain of its existence than the other weakness zones, labeled as weakness zone 7 (WZ7 in longitudinal profile). Because of its valley-characteristics and the observations closer to Roskreppfjorden, it was concluded to have an orientation like the foliation.

Weakness zone 5 and 6 has a different orientation than the other weakness zones. Form investigation in 1979, inside the surge chamber area (located close to the Q3 and Q4 measurements, see longitudinal profile), it was spotted a zone of clay. The zone of clay was, according to this report, the transition zone between overlaying, coarse-grained granite and

underlaying dark, biotite-rich gneiss. This might indicate that both of the weakness zones, 5 and 6, might contain clay minerals. The clay containment can weaken the stability in the tunnel.

According to a report from 1961, from pre-investigation, it was predicted that the weakness zones in the southern part of the headrace tunnel (WZ5, WZ6 and WZ7) would make most stability problems. Weakness zone 4 was also mentioned. A part where it might be some problems when excavating and stabilizing.

4 LABORATORY TESTING - ROCK SAMPLES

Two rock samples, granitic gneiss (marked as group A) and granite (marked as group B), from Roskrepp area has been tested at the laboratory (see Figure 34). This chapter will first give a brief description of tests used on the rock samples, and then show results from the testing in laboratory.

Figure 34 - Rock specimens used in laboratory testing. Group A reprents the granitic gneiss and Group B represents granite. Both rock samples collected from Roskrepp area.

4.1 METHOD

4.1.1 Density

The density of the two rock samples are determined by the weight and the volume of the specimens (A1-A5 and B1-B4). Every specimen was measured (mass, diameter and length) in laboratory. These specimens are used in the UCS – test. The density is calculated from the formula:

$$\gamma = \frac{mg}{V} \left[\frac{kg}{m^3}\right] \qquad [4.1]$$

where m is the mass, g is the gravitational acceleration and V is the volume of the specimen.

Using the mean value from the specimens from each rock sample and obtain a density of:

- 2741 kg/m^3 for group A (granitic gneiss)
- 2573 kg/m^3 for group B (granite)

4.1.2 Sonic Velocity Test

Figure 35 - Tilt testing of A2 - granitic gneiss.

Testing the P-wave of rock specimens. Three to four cores of each rock sample with the length of 2,5 of the diameter is tested. Layering /weakest direction should be normal to the core for obtaining the best result, because the P-waves tends to be faster along foliation lines or other weaker lines.

Travel time, *t*, is measured by an instrument that uses electrical sound, as shown in Figure 35. The machine calibrates before testing of each sample. Applying ultrasound gel on the axis area for accomplishing directly contact with the surface. To find sonic velocity, *v*, for P-waves, the equation below is used:

$$v = \frac{s}{t} \qquad [4.2]$$

The distance, *s*, corresponds to the length of the core. Low velocity can indicate weak rock mass.

4.1.3 Tilt Test

Figure 36 – (left) Three rock specimens from same rock sample, ready for tilt-testing of granite.

Figure 37 – (wright) Tilt-testing of granite.

Tilt test finds the basic friction angel, φ_b. Three specimens from the same rock is used and placed in a pyramid, see Figure 36. The two specimens under the upper specimen are fixed and will not move as the inclination to the plane increases. The apparatus tilts by a hydraulic pump until the upper specimen starts sliding. Basic friction angle can be read by the inclinometer that is attached to the apparatus, see Figure 37.

The test is performed in three different combinations with three repetitions for each combination. Each specimen is divided in four parts in axial direction numbered from A to D. The two specimens under the upper specimen are faced with their A's , B's or C's to each other, depending on the specimen number. These numbers are faced upwards and against each other. The upper specimen is tested three times for each number from A to D. After twelve tests on the upper specimen, there is a shift of positioning of the specimens, and twelve more tests is done. This procedure is done for all three specimens joining the test.

Mean value of the friction angles are calculated.

4.1.4 Uniaxial Compressive Strength Test

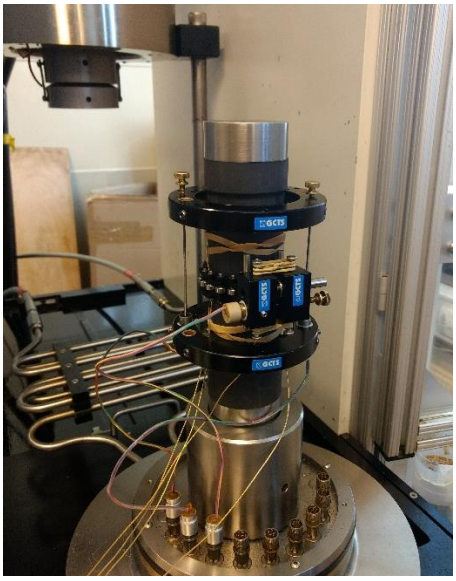

Figure 38 - USC testing.

Uniaxial strength of a rock sample is normally found through UCS test and/or Point Load test. Point Load test is an easy method for finding the strength of a rock and can be used both in field and in lab. UCS is a more complicated, time consuming method that can only be performed in a laboratory. On the other hand, UCS test gives more accurate results than the Point Load test. Because of small amount of specimen of each rock sample from Roskrepp area, UCS test was used in this thesis only.

A specimen, covered in rubber, is put into a test machine, see Figure 38. LVTS-sensors are detached to the core for measuring deformation in two directions; axial (ε_{axial}) and radial (ε_{radial}). The machine applies axial loading to the core until failure occurs. Data of the deformation in the two directions in consonance with the increasing load is being logged and presented in a graph. Before failure occurs, the graph tends to have a linear form, and it is therefore possible to see a connection between the deformation and axial stress by using Hooke's law:

$$\sigma = \mathrm{E}\varepsilon_{aksiell} \qquad [4.3]$$

The uniaxial compressive strength can be found through reading the graph from the logged data. The peak value of the logged stresses represents the failure point, and therefore the uniaxial

compressive strength. Poisson's number (ν) is found through the relation between the tangents to axial and radial deformation at the graph and calculation in equation [4.4].

$$\nu = -\frac{\varepsilon_{radiell}}{\varepsilon_{aksiell}} \qquad [4.4]$$

E-modulus is decided from the tangent at 0.5UCS.

Acoustic sensors where detached to the specimen as well as the LVTS-sensors for measuring micro cracking under the UCS test. This part will not be included in this thesis, but will be furtherly investigated by PhD student, Bibek Neupane.

4.1.5 Brazilian Test

Figure 39 - Measurement used for Brazilian testing.

The Brazilian test is an indirect method to find the strain, σ_t, of the rock. Ten to sixteen disc-formed rock samples with a thickness, *t*, of 0.5*diameter (D) are used to get a more reliable result of the strain. A line load along the side of the disc is applied with a velocity of 1 sec/0.2 Newton and causes induced stress on the disc (Figure 39). The load should be applied normal to the rock layering if possible. The peak load (P) are noted after induced failure occurs. The strain of the rock is found through calculation by equation [4.5].

$$\sigma_t = \frac{\frac{2}{\pi}P}{Dt} \qquad [4.5]$$

The test is valid if failure goes from upper to lower point and are not moving while applying load.

4.1.6 XRD- Test

X-ray diffraction analysis (XRD) is a semi-quantitative analysis that identifies types of minerals and its containment in a rock sample. The test is performed through registration of interference that occurs by reflection of the x-rays from crystal lattice in the mineral. In a given crystal structure, the reflected x-ray will reflect if the difference in travel time is equal to a whole number of wavelengths. (Nesse, 2000, Nilsen and Broch, 2010)

4.2 RESULTS

4.2.1 Sonic Velocity Test

Table 7 - Results of sonic velocity test

Specimen number	s – Distance [mm]	t – Travel Time [micro seconds]	v - Velocity [m/s]
A1	128.40	28.5	4505.26
A2	128.70	27.7	4646.21
A3	128.28	31.6	4059.49
A4	128.29	30.7	4178.83
A5	129.10	30.8	4191.56
Main velocity group A			**4316.27**
B1	127.63	23.4	5454.27
B2	127.37	24.2	5263.22
B3	122.01	21.4	5701.40
B4	124.79	22.8	5473.25
Main velcity group B			**5473.04**

Results from sonic velocity test is presented in Table 7. Air chambers can slow down the travel time of a rock specimen and cause a decrease in a potential velocity in this test. Hence, porous rocks mass tends to have lower velocity than dens rock mass. Cracks in a rock specimen can also cause a decrease in velocity.

Foliations can increase the travel time for the p-wave if tested parallel to the test-direction. Because of that, foliation should be normal to the test-direction.

Calculation of the velocity for the granitic gneiss and the granite resulted with values of approximately 4316 m/s and 5473 m/s. The granite is therefore the sample with the shortest travel time. Combining the results from sonic velocity and the measured density of the specimens, the density does not seem to be a main factor of the velocity difference. Using the mean value from the specimens from each rock sample and obtain a density of 2741 kg/m^3 for the granitic gneiss (group A), and a density of 2573 kg/m^3 for the granite (group B). Secondary waves were not measured in this test.

4.2.2 Tilt Test

Table 8 - Results from mean values of tilt test.

Test	Mean core [°]
A2 - AA	34.5
A3 - BB	33.8
A4 – CC	34.3
Mean total A	**34.2**
B2 - AA	31.3
B3 – BB	31.3
B4 - CC	29.6
Mean total B	**30.7**

Table 8 presents mean values of the results from tilt test. All results from tilt test can be found in appendix H. As expected, the friction angle of the two rock samples had a value close to 30°. Group A, the granitic gneiss, has a larger friction angle, and can handle more inclination before rockfall.

4.2.3 Uniaxial Compressive Strength Test

*Table 9 - Results from UCS-testing. *Rock specimens presented in figure 40 and 41.*

Specimen number	UCS (MPa)	E-modul (GPa)	ν-Poissons Ratio
A1	136.5	64.34	0.27
A2	155.9	69.12	0.31
A3	146.0	61.23	0.29
A4	153.8	63.89	0.28
A5*	148.8	65.59	0.27
Main values group A	**148.2**	**64.83**	**0.27**
B1	133.7	70.52	0.27
B2*	172.8	67.93	0.27
B3	135.0	60.41	0.3
B4	201.8	69.09	0.27
Main values group B	**160.8**	**67.0**	**0.28**

USC results are represented above in Table 9, after running the specimens through UCS testing. UCS-value is the peak value of the deviator stress (axial stress), and a mean value are calculated for each rock sample. E-modulus and poisons ratio are calculated by 50% of UCS with a data-interval of 10% of UCS. A mean value is calculated for each rock sample. These values can furtherly be used in numerical analysis for the stability assessment for Roskrepp headrace tunnel.

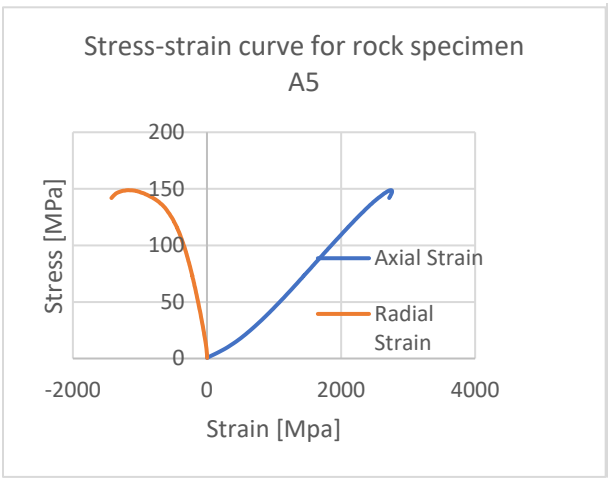

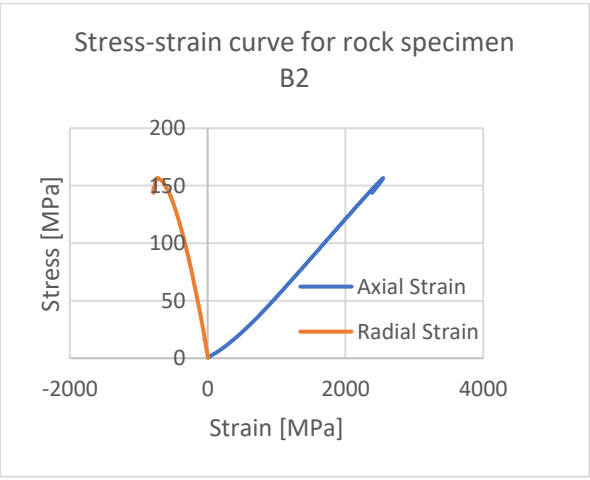

Figure 40 – (left) Stress-strain curve of rock specimen A5 from UCS results.

Figure 41 – (wright) Stress-strain curve of rock specimen B2 from UCS results.

4.2.4 Brazilian Test

Table 10 - Results of brazilian test

Disc number	D - Diameter [mm]	t- Thickness [mm]	P - Power [N]	σt – Tensile Strain [Mpa]
A*1	50.16	25.60	2606	12.93
A*2	50.18	25.85	3465	17.01
A*3	50.22	25.52	3347	16.63
A*4	50.22	26.01	3478	16.96
A*5	50.20	25.96	3953	19.32
A*6	50.20	25.60	3519	17.44
A*7	50.21	25.62	2817	13.95
A*8	50.25	26.14	2252	10.92
A*9	50.21	26.19	2806	13.59
A*10	50.16	25.98	2549	12.46
A*11	50.18	25.76	2424	11.94
A*12	50.22	26.06	3048	14.83
A*13	50.20	25.99	2866	13.99
A*14	50.22	25.97	3461	16.90
A*15	50.21	26.26	3465	16.74
A*16	50.21	26.10	2743	13.33
Mean value A*				**14.93**
B*1	50.16	25.91	2705	13.26
B*2	50.10	25.49	2644	13.19
B*3	50.15	25.90	2701	13.25
B*4	50.18	24.63	2538	13.08
B*5	50.12	25.02	2740	13.92
B*6	50.10	25.71	2558	12.65
B*7	50.05	25.02	3024	15.38
B*8	50.17	26.76	2758	13.08
B*9	50.05	25.18	2788	14.09
B*10	50.15	26.06	2221	10.82
Mean value B*				**13.27**

Table 10 presents the results from the Brazilian test for the two rock samples, granite and granitic gneiss. Finding mean value of the results from each disc, granitic gneiss has a tensile strength of about 14.93 MPa and the granite has a tensile strength of about 13.27 MPa.

4.2.5 XRD Test

The preparation and performance of the XRD-analysis was done by senior engineer, Laurentius Tijhuis, the results from the analysis are represented in Table 11. For a more detailed result, see appendix J.

Table 11 - Results of XRD tests

	Rock sample A (granitic gneiss) [%]	Rock sample B (granite) [%]
Quartz	29.04	32.30
Albite		37.78
Albite intermediate	35.71	
Microcline maximum	13.15	23.07
Diopside	4.47	1.34
Calcite	0.13	0.41
Chlorite IB		1.86
Muscovite 2M:1		2.93
Chalcopyrite		0.31
Biotite 1M Mica		
Spessartine	0.08	
Actinolite	9.89	

Noticing the mineral, chlorite, with low inner friction, especially in wet condition, are present for the granite.

5 NUMMERICAL ANALYSIS

Numerical analysis is used in this master thesis to help assessing the stability in Roskrepp headrace tunnel. A study on parameters has been done to see how much change the different parameters affects the stability in the rock mass. The chapter gives a description of numerical modelling with an explanation of the input parameters and the establishing of the model and presents the results in the last part of this chapter. The main focus in this chapter is the stability of the rock mass and the stability of the asphalt lining with increase of pressure under it.

5.1 METHOD

5.1.1 RS2

Using program RS2 to do numerical modeling. Numerical modeling has become a common tool in rock mechanics. It has, according to Trinh and Holmøy (2012), many advantages compared to empirical and analytical methods. Advantages and disadvantages of a numerical modeling are presented below in Table 12. (Myrvang, 2001, Trinh and Holmøy, 2012)

Table 12 - Advantages and disadvantages of using numerical modeling.

Advantages	Disadvantages
Gives detailed information of rock mass and performance of rock support (such as in support load, displacements, and stress distribution around a rock cavern).	Incorrect establishment of the model can cause incorrect outcome. This will be unfortunate to include in a potential discussion part.
Shows analysis of complex underground conditions and tunnel geometry.	
Through numerical calculations methods; stresses and deformation around a tunnel periphery can be found.	
The relation between installed support and the intact rock mass can be found.	

Because of a possibility of an incorrect establishment of a model, the potential discussion part should not be relied on a numerical modeling only. Results from other analytical methods, laboratory testing and experiences from similar projects should be included in a discussion part as well (Trinh & Holmøy, 2012).

There are two main groups of numerical models; continuums models and discontinuous models. Continuums modelling includes methods such as Final Element Method (FEM), Final Differential Method (FDM) and Boundary Element Method (BEM). These methods focus on the rock mass as a continuum medium. Discontinuous modelling includes a method such as Block Element Method. The model is presented as a coupled model; one for an intact rock mass and one for its discontinuities. The movement in the rock mass is described through the deformation mechanisms for plane sliding, separation, and rotation. The quality of the results should depend on the accuracy of the input parameters, no matter what type model is used (Myrvang, 2001).

5.1.2 Cases

In this master thesis three cases are being analyzed.

1) Granite with good rock conditions
2) Granitic gneiss with good rock conditions
3) Granitic gneiss in weakness zone 4

The purpose for this numerical analysis is to investigate the stability of the rock mass and the asphalt lining. Two scenarios are presented for each case; 0.0 MN/m^2 pressure under asphalt lining and 0.2 MN/m^2 pressure under asphalt lining. A pressure of 0.4 MN/m^2 pressure under asphalt lining are tested as well for last case, granitic gneiss in weakness zone, to see how the asphalt lining reacts with a potential maximum pressure regarding case of Roskrepp. These scenarios indicate when the headrace of Roskrepp is running with constant flow – 0.0 MN/m^2 pressure under asphalt lining and when turbines are shut down - 0.2 MN/m^2 and 0.4 MN/m^2 pressure under asphalt lining. 0.4 MN/m^2 is assumed to be maximum possible pressure under the lining, this can happen at the moment when max mass oscillation is present.

Focusing on yielded elements, stress situation, total- and vertical displacement.

5.1.3 Input Parameters

Material parameters for the rock mass were partly defined from Uniaxial Compression Test and Tilt Test. These values are not used directly in the analysis because of scaling and discontinuities in the rock mass. The software, RocData, determines rock mass strength parameters for different rock types based on the generalized Hoek-Brown failure criterion given as:

$$\sigma'_1 = \sigma'_3 + \sigma_{ci} * \left(m_b * \frac{\sigma'_3}{\sigma_{ci}} + s \right)^a \qquad [5.1]$$

Input parameters for rock mass with description used in this analysis are presented below in Table 13.

Table 13 - Description of relevant input parameters for RS2

Input parameters		Description	Calculation from:
σ_{ci}	In-situ stress	Uniaxial compressive strength.	Laboratory
GSI	Geological Strength Index	Defines the rock mass properties. Can be determined by using rock surface images from site and borehole core samples (if possible).	Table in RocData
D	Disturbing Factor	Depends on the tunnel opening and type of tunnel (TBM/conventional)	RocData
E_i	Elasticity modulus	Values calculated from stress-strain curve from lab testing of relevant rock specimens can be used. E-modulus has, according to Hoek and Brown (1997), normally a higher value in lab that in the field. E_i should therefore be scaled in RocData.	Laboratory
E_{rm}	Reduced Elasticity modulus	E_i tends to have a higher value in laboratory than in field, E_{rm}, is a reduced elasticity modulus calculated in RocData.	RocData

m_i	Hoek-Brown constant	Defines the ductility/brittleness of the intact rock. Typical values for ductile rocks: 10-12 Typical values for brittle rocks (quartzite, granite etc.): values approaching 20. (Hoek and Marino, 2000)	Table from RocData
m_b	Dilatance parameter	A measure of the expansion of the volume that can happen if the material splits. Dimensionless parameter for Hoek-Brown materials, varies from zero to m_b. If the material is plastic, Hoek-Brown can be defined. Soft rocks: usually low dilatance. Hard rocks: high dilatance.	RocData or $m_b = m_i * e^{\left(\frac{GSI-100}{28-14D}\right)}$
a_r	Residual parameters	The numerical analysis is doing plastic-elastic situation for simulating failure in the rock mass. The residual parameters describes the material behavior after yielding and can simply be determined by reducing GSI to GSI_r defined as 0.7GSI (Arngrimsson et al., 2010). Using calculation in this thesis.	RocData or $a_r = \frac{1}{2} + \frac{1}{6} * \left(e^{-\frac{GSI_r}{15}} - e^{-\frac{20}{3}}\right)$
s_r			RocData or $s_r = e^{\left(\frac{GSI_r-100}{9-3D}\right)}$
m_r			RocData or $m_r = m_i e^{\left(\frac{GSI_r-100}{28}\right)}$
σ_H	Field stress	Using measurement results discussed in chapter 3.1.3.	$\sigma_H = 1.7\sigma_v$
σ_h			$\sigma_h = \sigma_v$
σ_v			$\sigma_v = \rho g h$
θ	Field stress angle	Angle from horizontal to main stress	Topographical map.

To find correct input parameters for rock mass with lower rock mass quality (case 3), a table by Panthi (2017) can be used. Table 14 presents stress problems class in competent rock mass based on Q-system.

Table 14 - Stress problems class in competent rock mass based on Q-system (Panthi, 2017b) (Panthi, 2017a).

Stress Class	Description of potential stress induced instability	Ratio – intact rock strength and major principle stress (σ_{ci}/σ_1)	Ratio between maximum tangential stress and intact rock strength ($\sigma_{\theta\text{-max}}/\sigma_{ci}$)
SC 1	Low stress, near surface, open joints	≥200	<0.01
SC 2	Medium stress, favorable stress conditions	200-10	0.01-0.3
SC 3	High stress, very tight structure, usually favorable to blasting except for wall	10-5	0.3-0.4
SC 4	Moderate spalling after > 1 hour	5-3	0.5-0.65
SC 5	Spalling and rock burst after few minutes	3-2	0.65-1
SC 6	Heavy rock burst and immediate strain failure.	<2	>1

Case 3 represents the scenario of lower rock mass quality and is of granitic gneiss. Defined σ_1 and σ_3 in chapter 3.1.3, and found σ_{ci} from UCS testing. This gives:

$$\frac{\sigma_{ci}}{\sigma_1} = \frac{148.2\ MPa}{2.2857\ MPa} = 64.8 \qquad [5.2]$$

Which is in the stress class 2, medium stress, favorable stress conditions.

Finding maximum tangential stress by using equation [5.3].

$$\sigma_{\theta-max} = 3\sigma_1 - \sigma_3 \qquad [5.3]$$

and find that maximum tangential stess is 5.5126 MPa. Furtherly

$$\frac{\sigma_{\theta-max}}{\sigma_{ci}} = \frac{148.2\ MPa}{5.5126\ MPa} = 0.04. \qquad [5.4]$$

This gives a reduced uniaxial compressive strength, σ_{ci}*, and a reduced elastic modulus, E*.

$$\sigma_{ci} *= 0.96\sigma_{ci} \text{ and } E *= 0.96E. \qquad [5.5]$$

Chosen values for the asphalt concrete and the layer of the aggregate are taken from RocScience (Rocscience, 2018b, Rocscience, 2018a) and theory presented in chapter 2.3

Table 15 - Input parameters for asphalt and aggregate layer used in RS2 analysis.

	σ_{ci}	E_i	ν	φ
Aspahlt concrete	2,51 [MPa]	50 000[MPa]	0.3	
Aggregate		100000 [MPa]	0.3	35[°]

Table 16 presents input parameters used in RS2 analysis for the three cases mentioned.

Table 16 - Input parameters for rock mass situation for the three cases.

Input parameters	Granite Intact rock mass	Granitic gneiss intact rock mass	Granitic gneiss weakness zone	Taken from
h	160 [m]	160 [m]	50 [m]	Chosen location at longitudinal profile.
Expansion factor	25	25	8	Calculation from cover height.
GSI	70	75	30	RocData
σ_{ci}	160.8 [MPa]	148.20 [MPa]	142.72 [MPa]	Laboratory and Panthi (2017)
E_i	67.0 [GPa]	64.93 [GPa]	62.3328 [GPa]	Laboratory
m_i	32	28	28	Table in RocData
D	0	0	0.2	Table in RocData
σ_t	13.27 [MPa]	14.93 [MPa]	14.93 [MPa]	Laboratory
φ	30.7 [°]	34.2 [°]	34.2 [°]	Laboratory
φ_r	65.314 [°]	64.421 [°]	60.269 [°]	RocData
ν	0.28	0.27	0.27	Laboratory
E_{rm}	49.098545 [GPa]	53.00561 [GPa]	3.907225 [GPa]	RocData
m_b	10.961	11.47	11.47	RocData
s	0.036	0.062	$2.404e^{-0.004}$	RocData
a	0.501	0.501	0.522	RocData
m_r	5.2	5.1	1.7	Calculation from table13.
s_r	0.003	0.005	0.000	Calculation from table13.
a_r	0.5	0.5	0.5	Calculation from table13.
ρ	2573 [kg/m^3]	2741 [kg/m^3]	2741 [kg/m^3]	Laboratory.
Water pressure head	20 [m]	20 [m]	20 [m]	Approximately height measured from longitudinal profile
	0.20 [MN/m]	0.20 [MN/m]	0.20 [MN/m]	
σ_v	4038.6 [KPa]	4302.274 [KPa]	1344.5 [KPa]	Formula
σ_H	6865.6 [KPa]	7313.865 [KPa]	2285.7 [KPa]	Formula
σ_h	4038.6 [KPa]	4302.274 [KPa]	1344.5 [KPa]	Formula
θ	0	0	0	Longitudinal map.

5.1.4 Establishment of the models

Establishment of the models starts with insert two stages. First stage is for tunnel excavation including aggregate- and asphalt lining insertion, and second stage is for insertion of water pressure under lining (Figure 42).

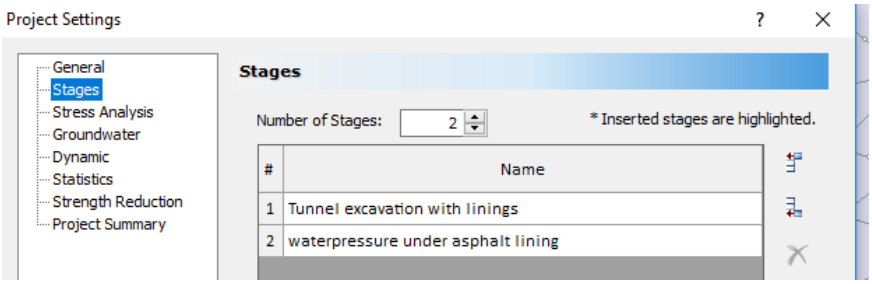

Figure 42 - Stage insertion.

As being in stage one, geometry of the tunnel periphery is applied with the coordinates:

x	y
0	2.7
0	0
7	0
7	2.7

To accomplish the ceiling of the tunnel periphery, arc is applied with 20 segments.

External boundary is applied as a box with expansion factor of 25 for the good rock condition cases and 8 for the weak rock condition case. Material boundaries for rock mass are applied for each case with their properties from input parameters presented in Table 16.

Next step is applying mesh setup for meshing and discretization. Graded meshtype with 6 noded triangles as element type. Gradiation factor of 0.1 and default number of nodes on all excavation of 60. Explained in Rocscience (2018) will the discretization of the boundaries, indicated by red crosses, form the framework for the finite element mesh. After discretization is done, finite element mesh is applied.

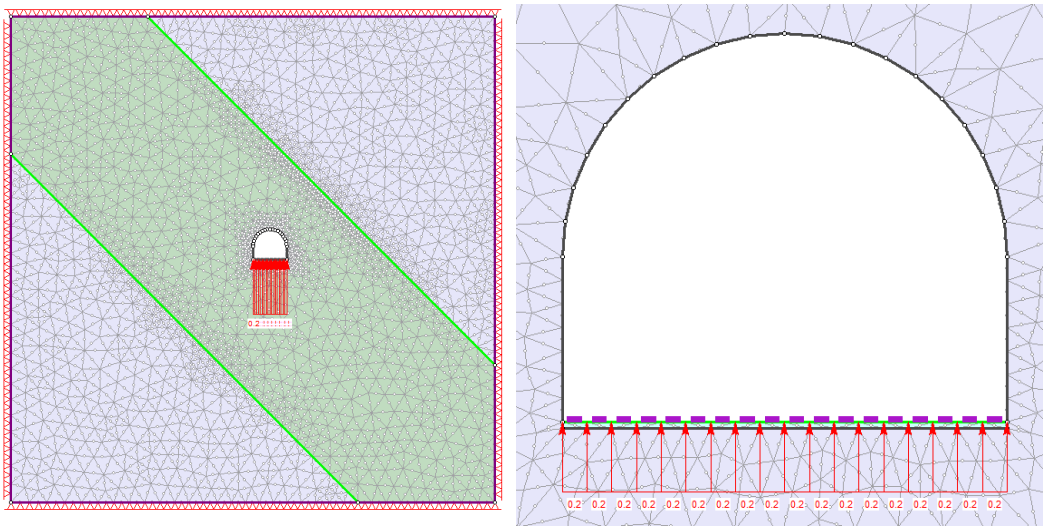

Figure 43 – (wright) Establishing model with insert of pressure under asphalt layer in RS2.

Figure 44 – (left) Establishing model of case 3 in RS2.

Filed stresses are applied. For weak rock mass condition, weakness zone of other material properties is addressed, see Figure 44. In the last part of the establishing, excavation of the tunnel is done. Aggregate and asphalt lining is applied.

Moving to stage two, where pressure under asphalt lining is applied (Figure 43). Using load distribution of 0.2 MN/m^2, as this is for Roskrepp at normal situation. A load distribution of 0.4 MN/m^2 is used in case three, to see worst case scenario of asphalt displacement.

5.2 RESULTS

Yielded elements of shear and tension, stress situation of σ_1, total – and vertical displacement are presented in the results for each case. In case of gneiss of weak rock condition, a larger pressure is presented as well to see if max pressure makes a different regarding the stability of the asphalt lining.

5.2.1 Granite of Good Rock Condition with Asphalt Lining

Yielded elements: 42 yielded elements. Most shear, but yielded elements of tension showed at the floor area.

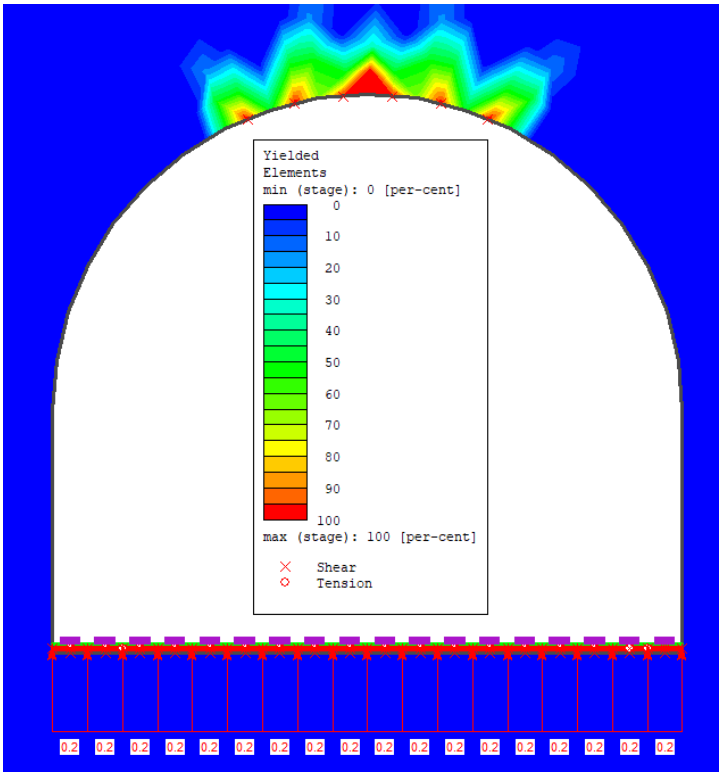

Stress Situation: Stress concentrated at ceiling and floor corners. Maximum stress situation is for case of pressure under lining, with a sigma one of 39 MPa at the corners. No big difference for the two cases.

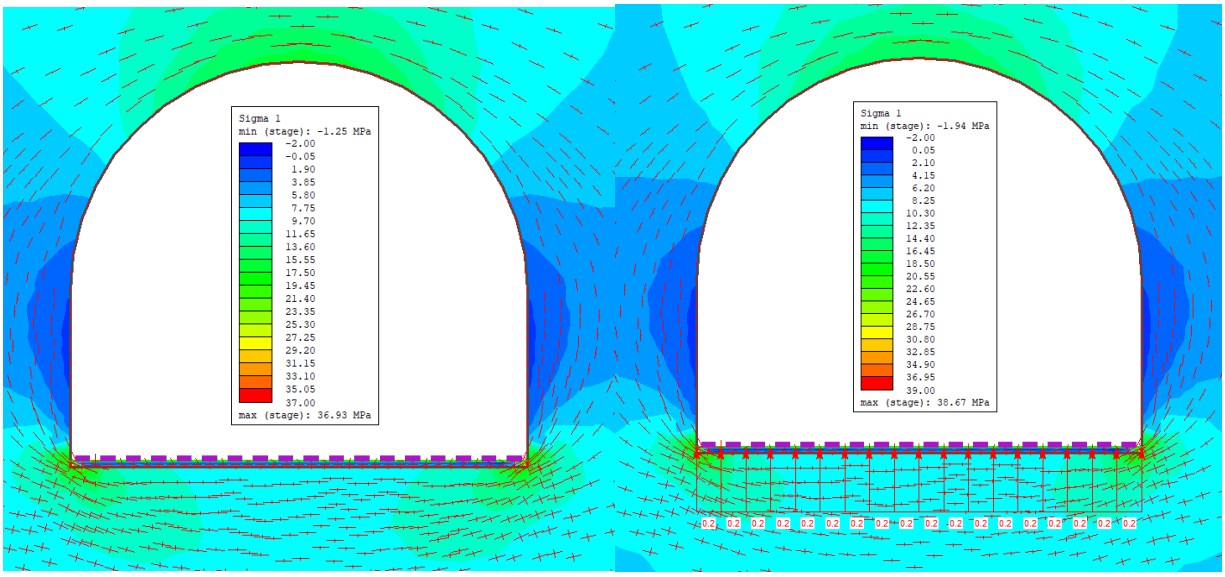

Total displacement: Most displacement at the walls, 0.6 mm, for both cases. Displacement at floor are are minimal, but there are some increace in displacement for case of pressure under apshalt lining. Looking into this case by looking at vertical displacement only.

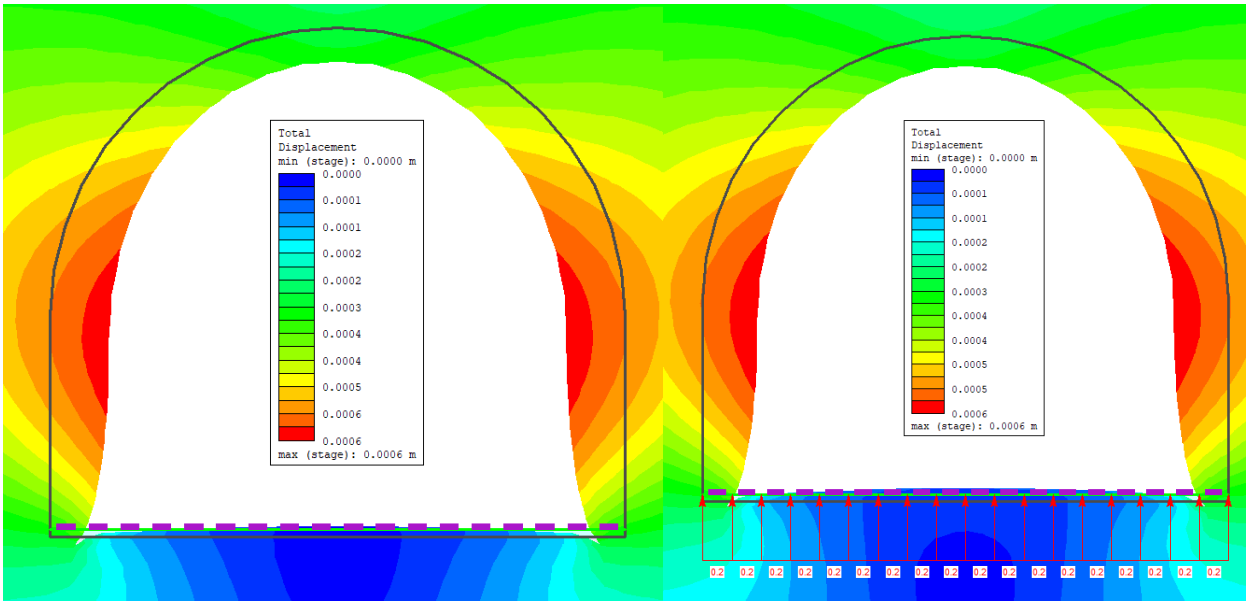

Vertical displacement: For case of no pressure under asphalt lining, total vertical displacement is approximately 0.02mm. For case of pressure under asphalt lining, total vertical displacement is approximately 0.06 mm.

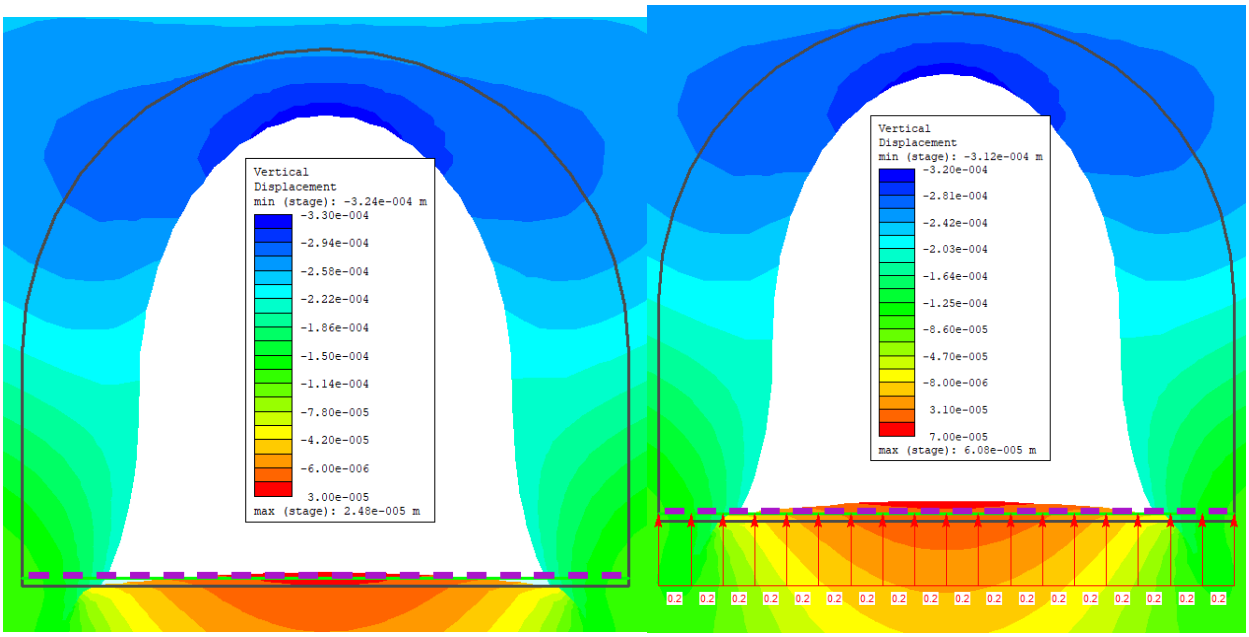

5.2.2 Gneiss of Good Rock Condition with Asphalt Lining

Yielded elements of 24, where 17 elements are tension and are concentrated at floor area.

Stress situation: No big difference with and without pressure under lining. Stress concentration at ceiling and floor corners. Max stress in case of pressure under asphalt lining, is recorded to be 43 MPa at the floor corners.

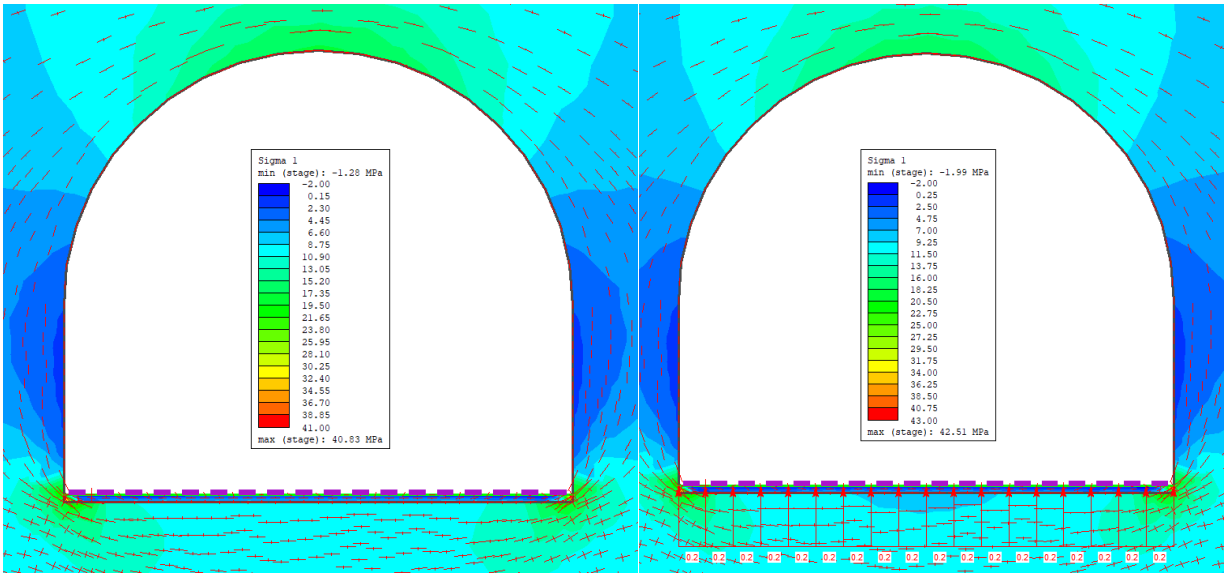

Total Displacement: Most displacement at the walls, with a maximum of 0.7 mm with and without pressure under asphalt lining. Some displacement differences at floor. Looking into displacement situation at floor area by changing from total displacement to vertical displacement.

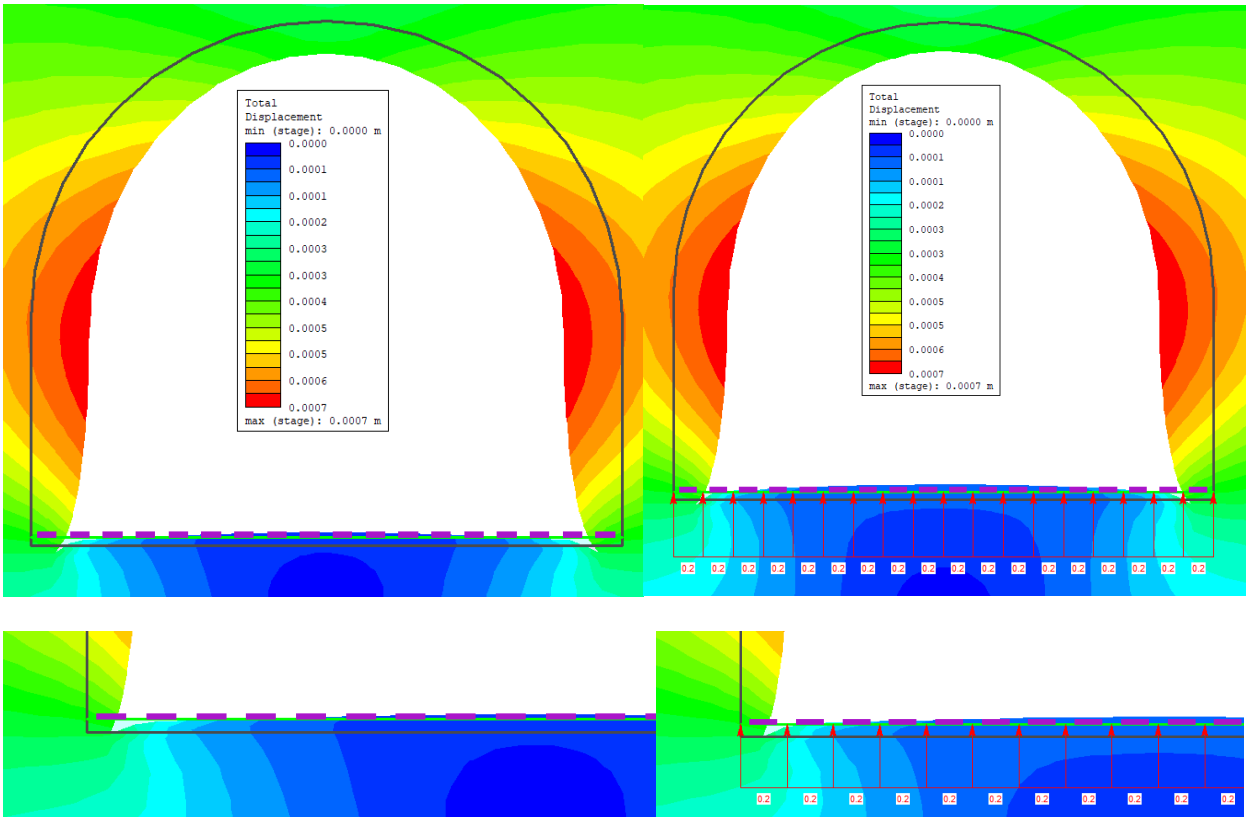

Vertical displacement: 0.05 mm for no pressure under, 0.09 mm for pressure under asphalt lining.

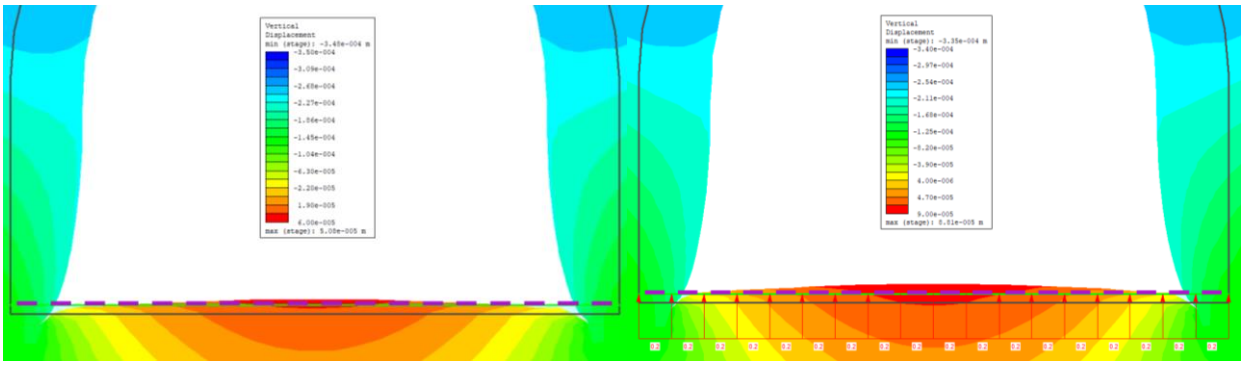

5.2.3 Gneiss of Weak Rock Condition with Asphalt Lining

Looking into three different scenarios; no pressure under lining, pressure of 0.2 MN/m^2 under asphalt lining and pressure of 0.4 MN/m^2 under asphalt lining. 0.4 MN/m^2 under asphalt lining is seen as worse case scenario.

85 yielded elements where most of them are of shear. Yielded elements of tension are present at the floor area.

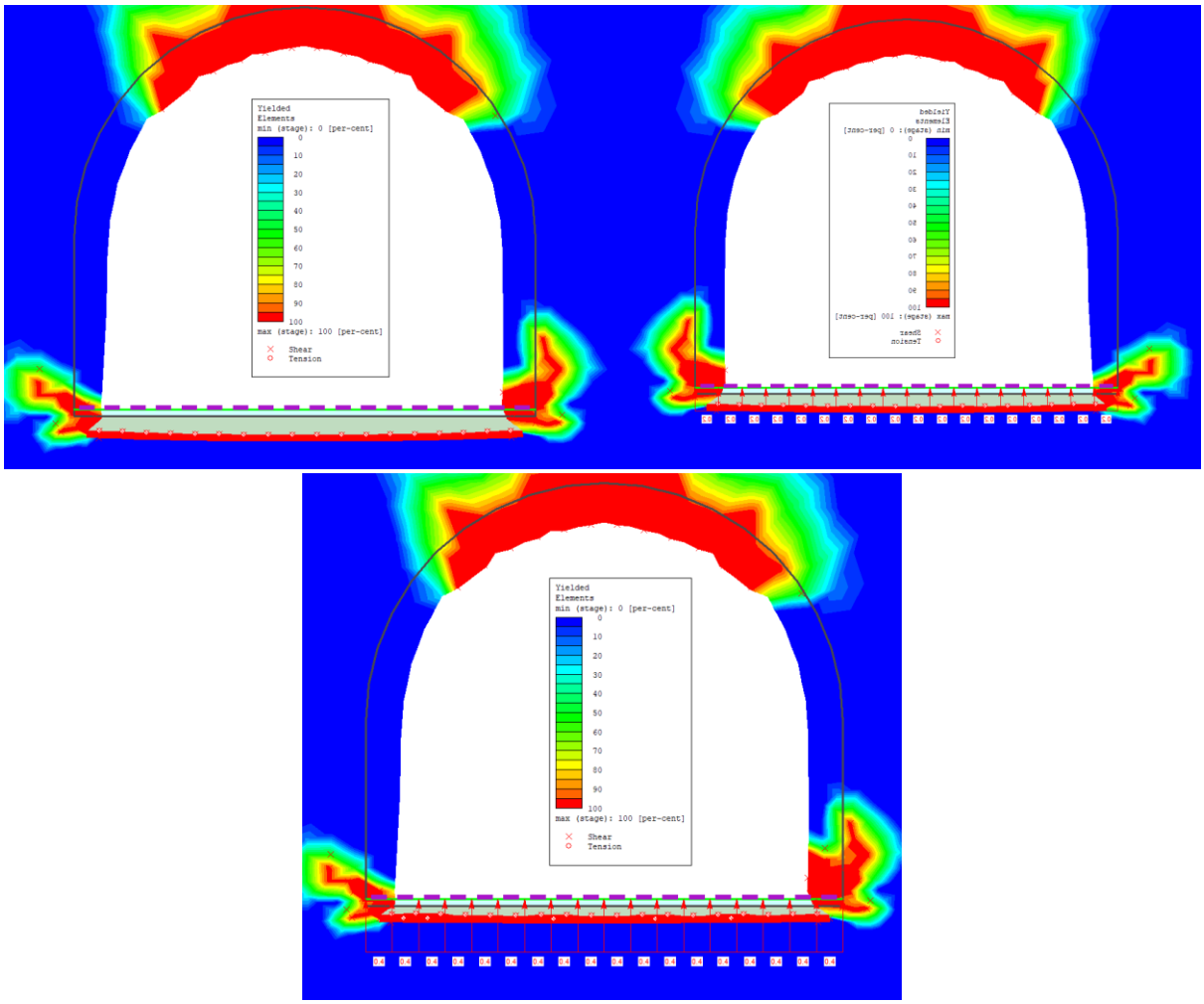

Stress Situation: Largest stress situation for case of 0.4 MN/m^2 pressure under asphalt lining, but maximum stress not recorded for this situation. Max stress is recorded for 0.2 MN/m^2 pressure under asphalt lining. For all scenarios, stress concentrated at ceiling and floor. Maximum stress concentrations at floor corners of approximately 7MPa.

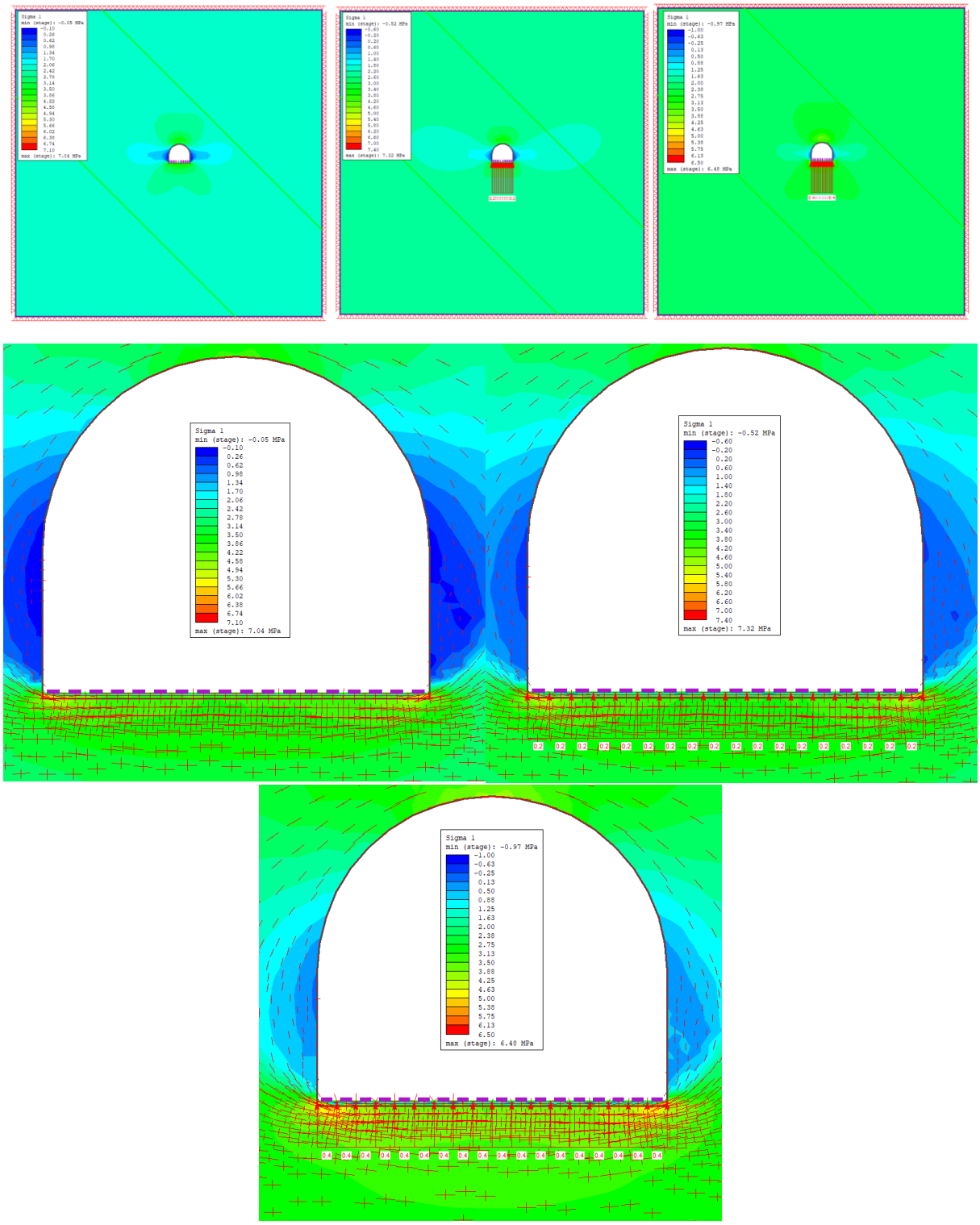

Displacement: For all scenarios the ceiling and the walls are the areas with most total displacement, and has a displacement of 0.3 mm. There is some insignificant displacement at the

floor area. Looking into the floor area by changing from total displacement to vertical displacement.

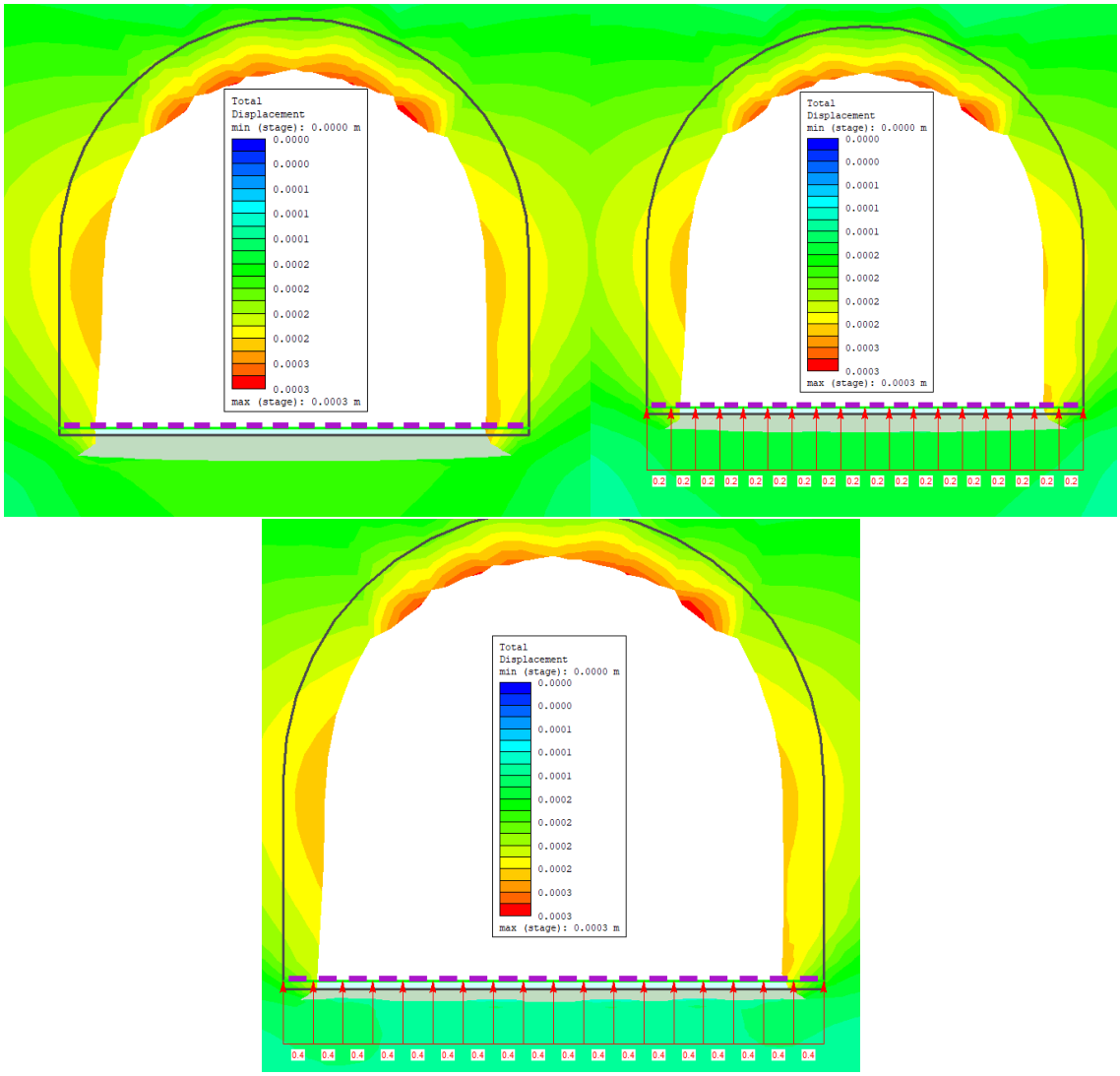

Vertical displacement: Increase of vertical displacement of asphalt lining with increase of pressure under asphalt lining. 0.07 mm of vertical displacement with 0 MN/m^2 under asphalt lining. 0.09 mm for 0.2 MN/m^2 under asphalt lining and 0.10 mm for 0.4 MN/m^2 under asphalt lining.

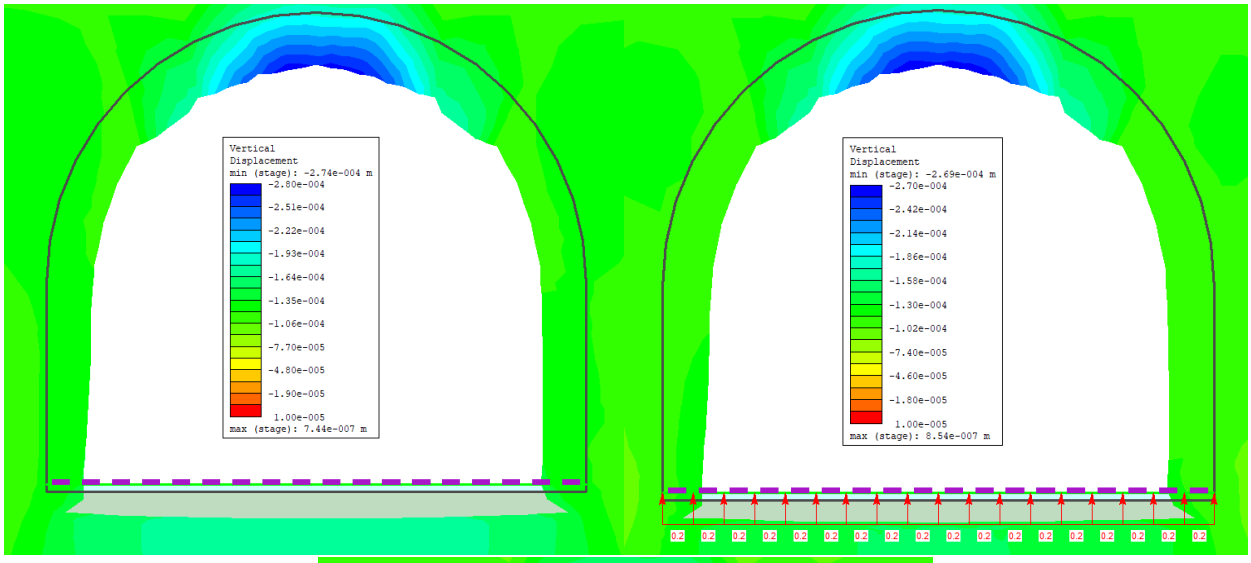
Vertical
Displacement
min (stage): -2.74e-004 m
-2.80e-004
-2.51e-004
-2.22e-004
-1.93e-004
-1.64e-004
-1.35e-004
-1.06e-004
-7.70e-005
-4.80e-005
-1.90e-005
1.00e-005
max (stage): 7.44e-007 m
Vertical
Displacement
min (stage): -2.69e-004 m
-2.70e-004
-2.42e-004
-2.14e-004
-1.86e-004
-1.58e-004
-1.30e-004
-1.02e-004
-7.40e-005
-4.60e-005
-1.80e-005
1.00e-005
max (stage): 8.54e-007 m
0.2

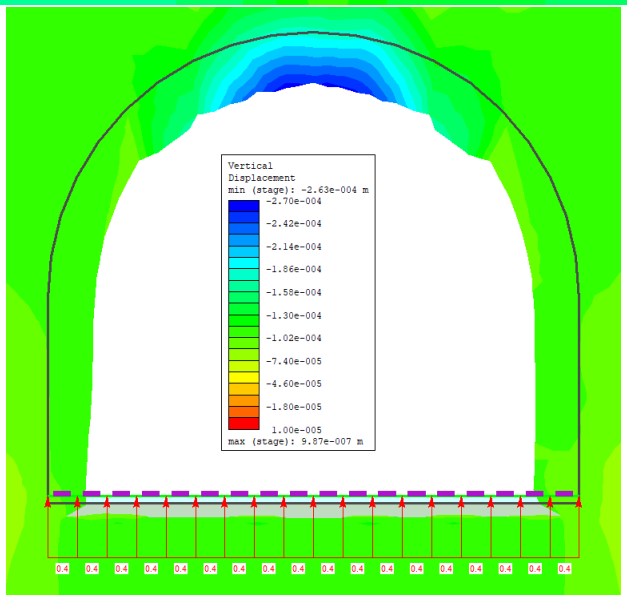
Vertical
Displacement
min (stage): -2.63e-004 m
-2.70e-004
-2.42e-004
-2.14e-004
-1.86e-004
-1.58e-004
-1.30e-004
-1.02e-004
-7.40e-005
-4.60e-005
-1.80e-005
1.00e-005
max (stage): 9.87e-007 m
0.4

5.3 SUMMARY ON NUMERICAL MODELING

Table 17 - Summary of numerical analysis results.

	Granite, good rock conditions	Gneiss, good rock conditions	Gneiss, weak rock conditions	Pressure under asphalt lining
Yielded elements	42, most shear	42, most shear	85, most shear	
Maximum stress [MPa]	36.93 – floor corners	40.83 – floor corners	7.04 – floor corners	0.0 MN/m^2
	38.67 – floor corners	42.51 – floor corners	7.32 – floor corners	0.2 MN/m^2
	-	-	6.48 – floor corners	0.4 MN/m^2
Maximum total deformation [mm]	0.6 - walls	0.7 – walls	0.3 – ceiling	0.0 MN/m^2
	0.6 – walls	0.7 – walls	0.3 – ceiling	0.2 MN/m^2
	-	-	0.3 – ceiling	0.4 MN/m^2
Maximum vertical deformation of asphalt lining [mm]	0.02	0.05	0.07	0.0 MN/m^2
	0.06	0.09	0.09	0.2 MN/m^2
	-	-	0.10	0.4 MN/m^2

For a better overview of the results from numerical analysis, the results are presented in Table 17.

- Most yielded elements for the weakness zone. Yielded elements of shear is dominating, but yielded elements of tension are present at the asphalt lining area for all cases.
- Highest stress for the case of gneiss of good rock conditions, lowest for the case of the weakness zone. Maximum stress concentration at the floor corners for all cases, but also high stress concentration at ceiling.
- Maximum total displacement at the wall area for both cases of good rock conditions, ceiling area of maximum total displacement for weakness zone. Insignificant displacement for all cases, excluding floor area, regarding stability assessment of rock mass.
- Increase of vertical displacement with increase of pressure under asphalt for all cases. Most vertical displacement for gneiss of both weak and good rock conditions.

Regarding stability of rock mass, the ceiling area are the most critical part for all cases. Too high stress concentration can cause rock fall, most critical for gneiss of good rock conditions. High stress concentration at the floor corners can also cause joints/cracks, which can lead to seeping of

water into the joint and under the asphalt lining. Total displacement for all cases are insignificant and will most likely not influence the stability of the rock mass.

Combining results of yielded elements and vertical displacement to investigate the stability of asphalt lining with different pressure under it. Present yielded elements at the asphalt lining, which indicates a possibility of destruction. Vertical deformation increases with increase of pressure under asphalt lining. Even though the analysis shows a possibility of uplift with increase of pressure under asphalt, it does not show how the asphalt reacts to repeatedly pressure differences and the dynamic movement of the headrace tunnel.

To get a better understanding of the interaction between water flow and the stability of the asphalt lining and gravel layer, a physical modeling can be conducted. This physical model is presented in the next chapter.

6 HYDRAULIC MODEL: SET-UP

To get a better understanding of the interaction between water flow and asphalt- and aggregate layer, a physical model is approached. This model is supposed to indicate the same situation for a potential pumped-storage plant at Roskrepp in the headrace tunnel. Investigation of pressure differences under and over asphalt layer with different discharge and discharge direction. Observation of movement of asphalt layer is interesting but was not tested in this thesis. To accomplish similar possible results as for Roskrepp headrace tunnel, scaling of model is necessary. This chapter presents the idea of the hydraulic model, theory and method for scaling and the establishment of the model.

6.1 Idea of Hydraulic Model Test

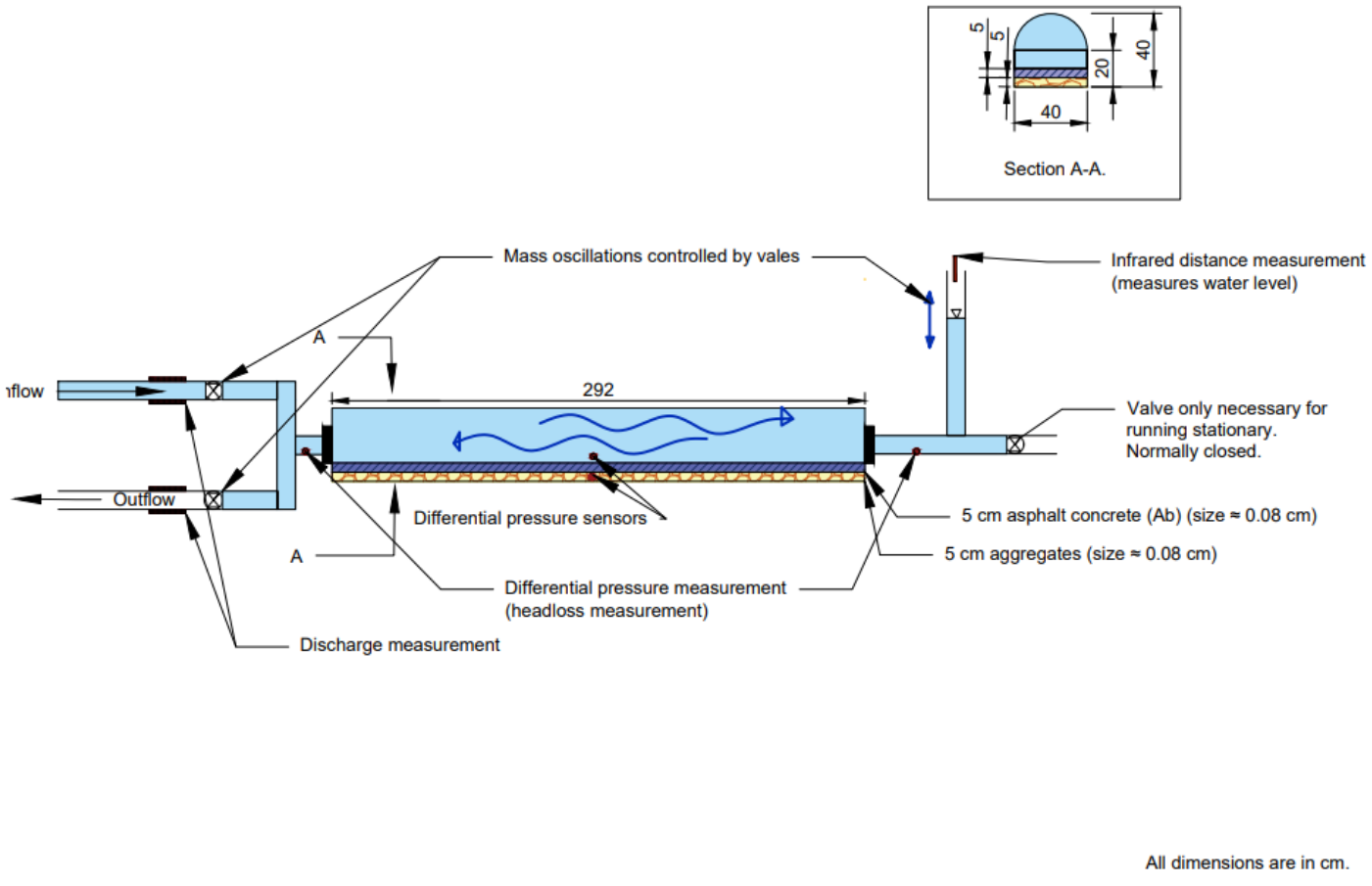

Figure 45 - Hydraulic scale modeling of mass oscillations in a hydropower tunnel with asphalt lining.

The idea behind this test is to make observation on the reaction to the asphalt to a potential pumped-storage plant. What is being interested to investigate is how asphalt reacts to:

- Water flow in two different directions.
- Water flow at different velocities.

Figure 45 presents a simple sketch of the hydraulic model. Description is included in the sketch as well.

Inflow and outflow pipes are installed with simple valves that manually opens/closes. Between these pipes and the tunnel, a discharge measurement is installed (this is not illustrated in the figure). A layer of aggregates (under) and asphalt concrete is being placed in the tunnel. Pressure sensors are placed over and under the asphalt layer to measure the differences in pressure. The illustration of the testing above includes additional pressure sensors and infrared distance measurement, but they were not used in this test.

Inflow of water runs in the tunnel till a wanted height in the “surge shaft” (the vertical pipe to the left. Measurement tape of distance is attached to the “surge shaft”. Inflow valve close and outflow valve open and water flows out of the tunnel. Pressure is being measured during the whole process.

6.2 Scaling

6.2.1 Theory

Hydraulic investigations performed in lab are, in many cases, different in scaling compared to the potential prototype in “real life”, often scaled in a smaller format. Dimensional analysis is therefore an important part of a hydraulic investigation in research work for design and for conducting model tests. According to Siddique, dimensional analysis can be defined as use of study of dimensions by mathematical techniques. It deals with the physical parameters that will influence the flow. These parameters are predicted at first, and then, they are grouped in

dimensionless combinations for a better understanding of the flow phenomenon (Siddique, 2018).

There are two types of dimensions;

1) Fundamental Dimensions or Fundamental Quantities (basic quantities such as time, length force) (MLT).
2) Secondary Dimensions or Derived Quantities (quantities that possess more than one fundamental dimensions such as velocity (unit per time), acceleration, density).

For a better understanding, the two types of dimensions are presented below in Table 18.

Table 18 – Dimension MLT and FLT.

CHARACTERISTICS		UNITS	DIMENSION (MLT)	DIMENSION (FLT)
GEOMETRY	Length	m	L	
	Area	m^2	L^2	
	Volume	m^3	L^3	
KINEMATIC	Time	s	T	
	Velocity	m/s	L/T	
	Acceleration	m/s^2	L/T^2	
	Discharge	m^3/s	L^3/T	
DYNAMIC	Mass	kg	M	$(F*T^2)/L$
	Force	$N=(kg*m)/s^2$	$(M*L)/T^2$	F
	Pressure	$Pa=N/m^2$	$M/(L*T^2)$	F/L^2
	Energy	J=N*m	$(M*L^2)/T^2$	F*L
	Power	Watt=(N*m)/s	$(M*L^3)/T^3$	(F*L)/T

When dealing with dimensional analysis, dimensions of each terms in an equation on both sides are equal. This is called dimensional homogeneity.

The relation among the variables can be determined by two methods if the number of variables involved in a physical phenomenon are known. These methods are:

- Rayleigh's Method

- Determines expression for a variable (dependent) which depends upon maximum three to four variable (independent) only.

- Buckingham's π- Theorem
  - Determines expressions if there are *n* variables (Independent and Dependent) in a physical phenomenon and if these variables contain *m* fundamental dimensions. The variables are then arranged into *(n-m)* dimensionless terms which are called π-terms.

As mentioned earlier, experiments are often performed on small scale models, called model analysis. Model analysis is an experimental method of finding solutions of complex flow problems. The model analysis tries to imitate the actual structure or machine, the so-called prototype. There should be similarity between the model and prototype in every respect, which means model and prototype have similar properties or model and prototype are completely similar.

Between model and prototype, three types of similarities must exist:

1) Geometric Similarity
2) Kinematic Similarity
3) Dynamic Similarity

1)Geometric Similarity = the similarity of shape

If ratio of all the corresponding linear dimensions in the model and prototype are equal, geometric similarity will exist between model and prototype.

$$\frac{L_p}{L_m} = \frac{B_p}{B_m} = \frac{D_p}{D_m} = L_r \qquad [6.1]$$

L_p, B_p, D_p are the length, breadth, and diameter of the prototype, while the ones with m's are for the model analysis. Lr = scale ratio

2)Kinematic Similarity = similarity of motion

If ratio of velocities and acceleration at the corresponding points in the model and prototype are equal.

$$\frac{V_{p1}}{V_{m1}} = \frac{V_{p2}}{V_{m1}} = V_r \quad ; \quad \frac{a_{p1}}{a_{m1}} = \frac{a_{p2}}{a_{m2}} = a_r \qquad [6.2]$$

3)Dynamic Similarity = similarity of forces

If ratio of forces at the corresponding points in the model and prototype are equal.

$$\frac{(F_i)_p}{(F_i)_m} = \frac{(F_v)_p}{(F_v)_m} = \frac{(F_g)_p}{(F_g)_m} = F_r \qquad [6.3]$$

$(F_i)_p$, $(F_v)_p$, $(F_g)_p$ are inertia, viscous and gravitational forces in prototype the others in model.

Fr is the Force ratio.

In fluid phenomenon there are different types of forces that should be included. These forces are presented below in Table 19.

Table 19 - Types of forces.

Force		Includes
Fi	Inertia Force	Mass and acceleration in the flowing fluid
Fv	Viscous Force	Shear stress due to viscosity and surface area of flow
Fg	Gravity Force	Mass and acceleration due to gravity
Fp	Pressure Force	Pressure intensity and cross-sectional area of flowing fluid.
Fs	Surface Tension Force	Surface tension and length of surface of flowing fluid
Fe	Elastic Force	Elastic stress and area of flowing fluid.

The numbers which are obtained by dividing the inertia force by viscous-, gravity-, pressure-, surface tension- or elastic force, are called dimensionless numbers. The most important dimensionless numbers are listed below in Table 20.

Table 20 - Important dimensionless numbers.

Dimensionless numbers:		Defined as:	Formulas:
Reynold's Number	Re	The ratio of the inertia force to the viscous force of flowing fluid.	$Re = \frac{Fi}{Fv} = \cdots = \frac{volume * length}{velocity} = \frac{VL}{v}$
Froude's Number	Fe	The ratio of inertia force to the gravity force of flowing fluid.	$Fe = \sqrt{\frac{Fi}{Fg}} = \cdots = \frac{volume}{\sqrt{gravitational\ acceleration * length}} = \frac{V}{\sqrt{gL}}$
Euler's Number	Eu	The ratio force to the pressure force of flowing fluid.	$E_u = \sqrt{\frac{Fi}{Fp}} = \cdots = \frac{volume}{\sqrt{\frac{pressure}{density}}} = \frac{V}{\sqrt{P/\rho}}$
Weber's Number	We	The ratio of inertia force to the surface tension force of flowing fluid.	$We = \sqrt{\frac{Fi}{Fs}} = \cdots = \frac{volume}{\sqrt{\frac{surface\ tension}{density * length}}} = \frac{V}{\sqrt{\frac{\sigma}{\rho L}}}$
Mach's Number	Ma	The ratio of inertia to the elastic force of flowing fluid.	$Ma = \sqrt{\frac{Fi}{Fe}} = \cdots = \frac{volume}{\sqrt{\frac{elastic\ stress}{density}}} = \frac{V}{\sqrt{K/\rho}}$

The Predominant force is the most significant force compared to other forces. For practical problems this significant force is considered for dynamic similarity. On the other hand, the models are designed on the basis of ratio force, which is the dominating in the phenomenon.

The laws on which models are designed for dynamic similarity are called model laws or laws of similarity. The following are the different types of model laws:

- Reynold's Model Law
- Froude's Model Law
- Euler's Model Law
- Weber's Model Law
- Mach's Model Law

The models can be classified as True Models of Undistorted Models. A True Model can be defined as a model that has a scale ratio of linear dimensions the same as its prototype. On the other hand, a distorted model uses different scale ratios for linear dimensions (Siddique, 2018).

6.2.2 Method

For this physical test the Buckingham's π- Theorem is used as the method to determine the relation among the variables that are included in this physical phenomenon. There are nine variables (=n) and six variables that are arranged into dimensionless terms (n-m).

Parameter included in this test are presented below in Table 21.

Table 21 - Parameters included in this test.

PARAMETERS		SI-UNITS	MLT	
Density of water	ρ	kg/ m^3	M/ L^3	Independent
Diameter tunnel	Dt	m	L	Independent
Velocity	Ve	m/s	L/T	Independent
Pressure	P	$Pa=N/m^2$	$M/(LT^2)$	ρVe^2
Volume	Vo	m^3	L^3	Dt^3
Dynamic viscosity	μ	kg/(sm)	M/(TL)	ρVeDt
Gravity	g	m/s^2	L/T^2	Ve^2/Dt
Amplitude of mass oscillation	Hmax	m	L	Dt
Discharge	Q	m^3/s	L^3/T	$VeDt^2$

Different model laws were evaluated for the decision of which model law that should be used in this test. The evaluated model laws are presented below in Table 22.

Table 22 - The evaluated model laws.

			Comments, notes
π_1	$P/(\rho Ve^2)$	Euler	Pressure.
π_2	Vo/ Dt^3		-
π_3	μ /(ρVeDt)	Reynold	Excluding this law, since both Re(proto) and Re(model) >2600, and then the dynamic viscosity will not affect the results.
π_4	L/Dt		Amplitude of the mass oscillation.
π_5	gDt/ Ve^2	Froude	The gravity - not that important
π_6	Hmax/Dt		-

- π_1, Euler's Model law, represents the relation to the pressure force of flowing fluid. Pressure sensors are being attached to the test and are playing a big role in the testing.

- π_2 represents the relation of the volume. The volume of the model compared to the prototype will not be the most influencing factor of pressure changes.
- Evaluating π_3, Reynold's Model Law, the Reynold's number was calculated for model and prototype.
    - $Re = \frac{VeDt\rho}{\mu}$
    - $\mu = 0{,}001$, $\rho = 1000$ kg /m^3
    - $Re_m = \frac{0{,}34*0{,}4*1000}{0{,}001} = 136000 > 2600$
    - $Re_p = \frac{1{,}42*7*1000}{0{,}001} = 99940000 > 2600$
    - Calculations for the velocity for prototype and model are shown in Table 24.
    - The flow of the prototype and model can both be considered as turbulent since $Re_p > Re_m > 2600$. Hence, Re will not influence changes during testing the hydraulic model. This law can therefore be excluded as the predominant force affecting the testing.
- π_4, represents the relation of the amplitude of the mass oscillation. As pressure seems to be the most predominant force for now, π_4 is excluded.
- π_5, Froude's Model Law, represents the relation between the inertia forces and the gravitational forces. Gravitation is relevant when dewatering tunnel. This test will not focus on dewatering tunnel.

Choosing Euler's Model law because the pressure seems to have the most impact of influencing the result on the test.

Assumed the model to be a true model, where all the linear dimensions for prototype and model had the same scale ratio. The parameters and their values for prototype and model are listed below in Table 23.

*Table 23 - The parameters and their values for prototype and model.*Already known dimension for prototype and model (width of the tunnel, Dt).*

Parameter		Prototype		Model		Ratio	
Diameter	Dt	Dtp	7	Dtm	0.4	Lr*	17.5
Height of tunnel	H	Hp	6.2	Hm	0.4	Hr*	15.5
Area	A	Ap	38.1	Am	0.428	Ar*	266.8067

Choosing scale ratio, Lr =17.5, the ratio of the tunnel diameter, for further calculations of other parameters. Perfect scaled model was not possible because of time. Table 24 presents scaled values for a perfect scaled model for Roskrepp headrace tunnel.

Table 24 - Scaling of parameters for physical model.

Parameters		Ratio		Prototype [SI]		Model [SI]	
Height of tunnel	H	Lr	17.5	H_p	6.2 m	H_m	0.3548 m
Area	A	Lr^2	306.25	A_p	38.1 m^2	A_m	0.3543 m^2
Volume	Vo	L^3	5359.375	Vo_p	343 m^3	Vo_m	0.064 m^3
Dynamic viscosity	μ	-	1	μ	0.001 kg/ms	μ	0.001 kg/ms
Discharge	Q	$Lr^{2.5}$	1 281.136	Q_p	54.22 m^3/s	Q_m	0.04231 m^3/s
Velocity	**Ve**	**$Lr^{0.5}$**	**4.18**	**Ve_p**	**1.42 m/s**	**Ve_m**	**0.34 m/s**
Asphalt thickness	As	Lr	17.5	As_p	0.1 m	As_m	0.006 m
Aggregate thickness	Ag	Lr	17.5	Ag_p	0.1 m	Ag_m	0.006 m
Amplitude of the mass oscillations	**Hmax**	**Lr**	**17.5**	**$Hmax_p$**	**60 m**	**$Hmax_m$**	**3.43 m**
Pressure over asphalt	Po	Lr	17.5	Po_p	Calculations from model testing	Po_m	Will be measured
Pressure under asphalt	Pu	Lr	17.5	Pu_p	Calculations from model testing	Pu_m	Will be measured

As the maximum height of water in the air chamber are 935 m and the minimum height of water in the air chamber is 875, the amplitude of this mass oscillation will be 60 m.

$Qp = 54.22\ m^3/s$ is found in papers from Roskrepp. $Ap = 31.8\ m^2$ is found in papers from Roskrepp. Velocity is found through the equation Ve = Q/A. Dynamic viscosity is forced into value of 1. Testing velcoties:

- Ve_m = normal = 0.34 m/s
- Ve_m = high = 0.50 m/s

Two pressure sensors will be applied to the model, one over and one under the tunnel to measure the difference of the pressures with different discharge and flow directions.

6.3 Establishment

Building and testing was done in Vassdragslaboratoriet. An already existing tunnel model is being used for this test, with dimensions:

Table 25 - Fixed dimension for model.

Dt_m	0.4 m
Ag_m*	0.05 m
As_m*	0.05m
A_m*	0.14 m^2
Length of layer	2.3 m
Length of model	2.92 m
Height of surge shaft	2.5 m

Installation of pipes in wanted positions and installation of two valves are done, see Figure 46.

Figure 46 - Hydraulic model test. All elements in wanted position.

To get wanted dimensions on asphalt and aggregate layer, cases of wood are made for layering of aggregate and asphalt. Peab Asfalt Norge AS contributed with distribution of aggregate and asphalt and layering process (Figure 47). Sealing of gravel with use of court membrane between asphalt and wooden board.

Figure 47 - Layering of asphalt done by Peap Asfalt Norge AS.

Discharge measurement is installed between the valves and the tunnel to measure the discharge. Pressure sensors are attached to the model; one that is positioned at a height over asphalt layer and one at a height under asphalt layer (Figure 48). Asphalt layer inserted in tunnel with help of truck, and last pressure sensor under asphalt layer inserted by boring hole at the floor area.

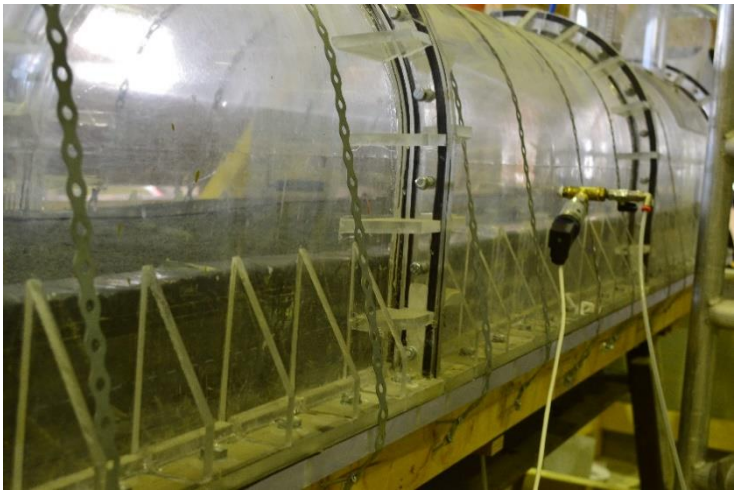

Figure 48 - Differential pressure sensor attached to the hydraulic model.

Pressure and discharge is connected to a software program, called Keysight, that records the pressure.

Attaching measuring tape that measures the height, with markings of 0.34 m intervals (blue markings) and 0.5 meter (white markings). Placing camera at a point to give a good overview of the testing.

Procedure of testing:

1) Have small opening of outflow valve, and open inflow valve. Fill the tunnel until the tunnel is full - level of water at the surge shaft is at height of 0 meter. Now the water is at a stable position.
2) Second counter with sound and camera is on for control of wanted velocity.
3) Starting software program.
4) Stopping waterflow to get stable condition when reached wanted height at surge shaft.
5) Open outflow valve for decrease in water height at surge shaft with controlled velocity.
6) Stop the velocity at 0 m.
7) Stop the running at the software program.

8) Repeating the test 20 times for normal velocity situation and 10 times for maximum velocity situation.
9) Data is exported and treated in excel.
10) Graphs can be made to get a better overview of how the pressures and discharge corresponds to the tests.

Figure 49 - The hydraulic model, ready for testing.

7 HYDRAULIC MODEL: TEST RESULTS

This chapter presents the results in form of the change in pressure regarding the differential pressure results.

7.1 Testing with normal velocity, Ve_m = 0.34 m/s

Table 26 presents results from testing with normal velocity, Ve_m = 0.34 m/s. Results in table are roughly presented. A more thorough presentation can be found in appendix I.

Table 26 - Differential pressure results with velocity 0.34 m/s.

Test #	Direction D1 = 0-1.75 [m] D2 = 1.75-0 [m]	Ve_m [m/s]	$\Delta P_m = Pu_m - Po_m$ [KPa]	$\Delta P_m = Pu_p - Po_p$ (calc.) [KPa]
1	**D1**	**0.34**	**-1**	**-17.5**
	D2	**0.34**	**2**	**35**
2	D1	0.34	-0.5	-8.8
	D2	0.34	0.5	8.8
3	D1	0.34	-0.7	-12.3
	D2	0.34	0.2	3.5
4	D1	0.34	-0.1	-1.8
	D2	0.34	0.5	8.8
5	D1	0.34	-0.3	5.3
	D2	0.34	0.7	12.3
6	D1	0.34	-0.4	-7
	D2	0.34	0.5	8.8
7	D1	0.34	-0.3	-5.3
	D2	0.34	0.1	1.8
8	D1	0.34	-0.5	-8.8
	D2	0.34	0.3	5.3
9	D1	0.34	0.1	1.8
	D2	0.34	0.6	10.5
10	D1	0.34	-0.2	3.5
	D2	0.34	0.8	14

Test #	Direction D1 = 0-1.75 [m] D2 = 1.75-0 [m]	Ve_m [m/s]	$\Delta P_m = Pu_m - Po_m$ [KPa]	$\Delta P_m = Pu_p - Po_p$ (calc.) [KPa]
11	D1	0.34	-0.1	-1.8
	D2	0.34	0.1	1.8
12	D1	0.34	-0.1	-1.8
	D2	0.34	0.4	7
13	D1	0.34	-0.1	-1.8
	D2	0.34	0.3	5.3
14	D1	0.34	0	0
	D2	0.34	0	0
15	D1	0.34	-0.2	-3.5
	D2	0.34	0.6	10.5
16	D1	0.34	-0.2	-3.5
	D2	0.34	0.6	10.5
17	D1	0.34	-0.2	-3.5
	D2	0.34	0.6	10.5
18	D1	0.34	-0.3	-5.3
	D2	0.34	0.7	12.3
19	D1	0.34	-0.1	1.8
	D2	0.34	0.5	8.8
20	D1	0.34	-0.2	3.5
	D2	0.34	0.3	5.3

Most of the results shows that there are some changes of the differential pressure measurement when the water increases/decreases from stable state to movement with height in the “surge shaft”.

Figure 50 presents Test1. This test had most change in differential pressure out of the 20 tests performed with Ve_m = 0.34 m/s. The graph shows how pressure corresponds in time when the height of water increases/decreases between 0 meter to 1.75 meters with the normal velocity. Total pressure line (blue) corresponds to the water height, and it is therefore possible to observe the change in water height in the surge shaft. The orange line represents the differential pressure. Observing that the differential pressure decreases as the water height increases, which means that the pressure under asphalt lining is lower than the pressure over the asphalt lining in this situation. The differential pressure stabilizes as the velocity stops. This shows that the pressure under the asphalt lining is delayed comparing to the pressure over the asphalt lining. Similar reaction of the differential pressure when decreasing the water height with normal velocity. Delay in the pressure under the asphalt lining. In this case the pressure under the asphalt lining is higher than the pressure over the asphalt lining.

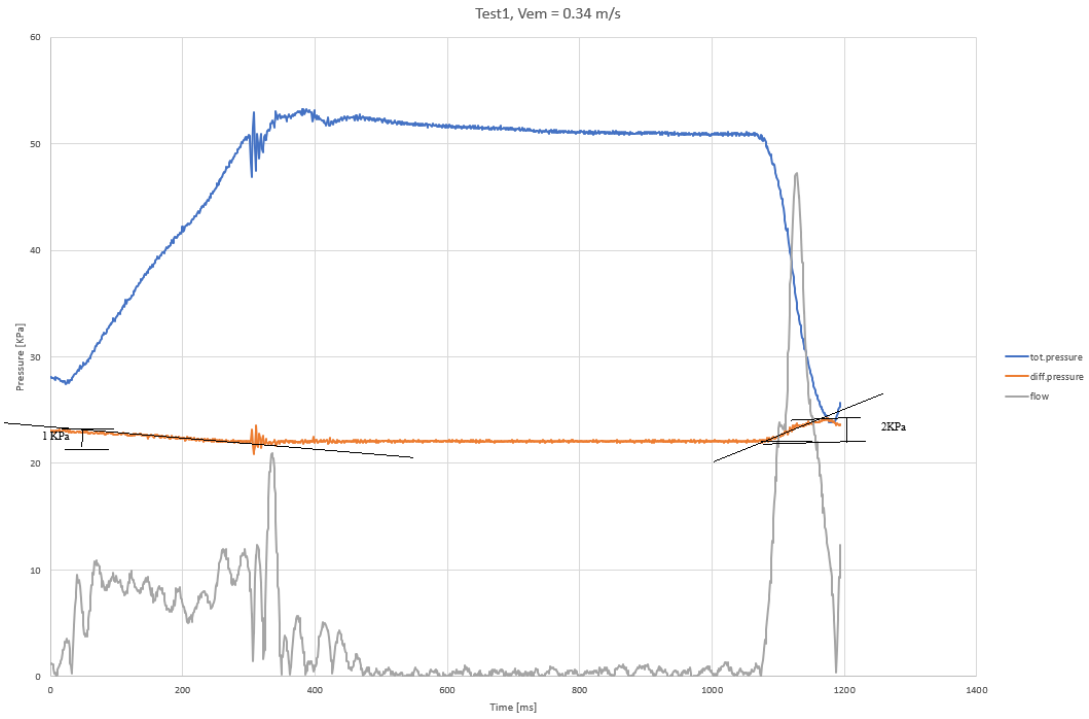

Figure 50 - Test 1. Graph presenting differential pressure, total pressure and flow rate versus time.

Figure 50 shows that there is difference in pressure change regarding the two directions. Since the velocity is regulated manually, it is difficult to achieve perfect wanted velocity. In this case it seems like the velocity in "D2" is faster than for "D1", this could maybe impact the magnitude of the pressure values. Testing with maximum velocity to see if the magnitude of change in pressure will increase with increase of velocity.

7.2 Testing with maximum velocity, Ve_m = 0.50 m/s

Maximum height in the model is 2.5 meters. Wanted maximum height is 3.5 meters, which is the correct scaled maximum height that correlates to Roskrepp situation.

Table 27 - Differential pressure results with velocity 0.50 m/s.

Test #	Direction D1 = 0-2.5 [m] D2 = 2.5-0 [m]	Ve_m [m/s]	$\Delta P_m = Pu_m - Po_m$ [KPa]	$\Delta P_m = Pu_p - Po_p$ (calc.) [KPa]
21	D1	0,50	-0.3	5.3
	D2	0,50	0.2	3.5
22	D1	0,50	-0.3	5.3
	D2	0,50	0.2	3.5
23	**D1**	**0,50**	**-0.2**	**3.5**
	D2	**0,50**	**0.9**	**15.8**
24	**D1**	**0,50**	**-0.1**	**1.8**
	D2	**0,50**	**0.9**	**15.8**
25	D1	0,50	-0.3	5.3
	D2	0,50	0.2	3.5

Test #	Direction D1 = 0-1.75 [m] D2 = 1.75-0 [m]	Ve_m [m/s]	$\Delta P_m = Pu_m - Po_m$ [KPa]	$\Delta P_m = Pu_p - Po_p$ (calc.) [KPa]
26	**D1**	**0,50**	**-0.1**	**1.8**
	D2	**0,50**	**0.9**	**15.8**
27	D1	0,50	-0.3	5.3
	D2	0,50	0.3	5.3
28	D1	0,50	-0.1	1.8
	D2	0,50	0.5	8.8
29	D1	0,50	-0.1	1.8
	D2	0,50	0.5	8.8
30	D1	0,50	-0.1	1.8
	D2	0,50	0.3	5.3

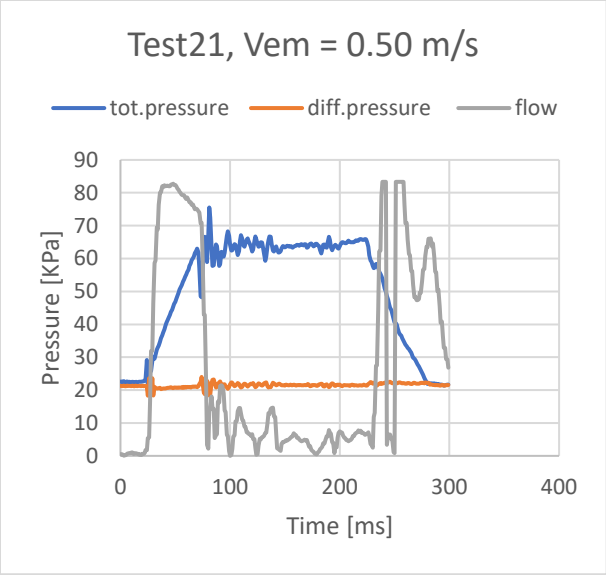

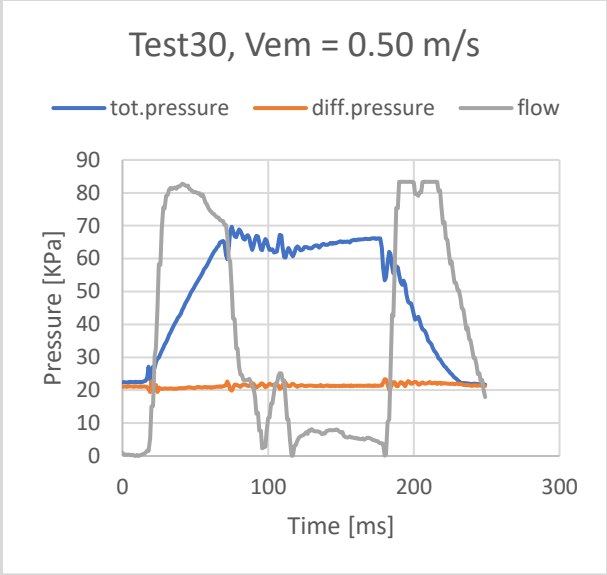

Figure 51 – (Wright) Results of Test21 in graph time versus pressure.

Figure 52 –(Left) Results of Test30 in graph time versus pressure.

Observing a trend in the results, see Figure 51 and Figure 52. The differential pressure seems to be highest in D2, which can indicate the direction of upper reservoir to lower reservoir in Roskrepp headrace tunnel.

7.3 Summary of testing

Change in velocity does not seem to have a great impact on the magnitude of the differential pressure. Results of the differential pressure are minor when change of discharge. The thickness of the asphalt layer compared to the size of the tunnel in the model can be a crucial reason for the small values. Although there is tendency of larger differential pressure when decrease of height in surge shaft compared to increase of height in surge shaft, which indicates that there are delay in pressure under asphalt lining.

8 DISCUSSION

An indication and an evaluation on what can happen if Roskrepp hydropower plant turns into a pumped-storage station will be discussed based on literature studies, field investigation, laboratory testing, numerical analysis a physical model testing. Changing to opposite direction of water flow will cause mass oscillation in form of a big wave, see Figure 53. This will result in high pressure in the headrace tunnel that can challenge the stability of the rock mass and the asphalt lining.

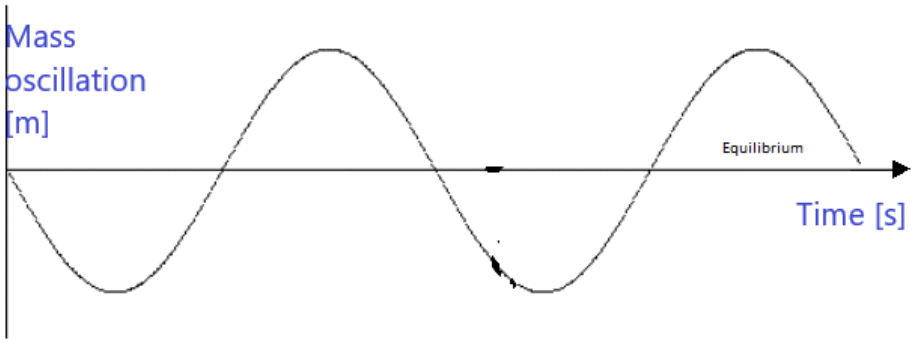

Figure 53 - Mass oscillation.

Even though the tunnel might be stable for a hydropower plant, there are uncertainties regarding the stability when dealing with change of discharge direction and rapidly pressure changes. Different scenarios on what tunnel instability can lead to if the plant changes to a pumped-storage plant, is taken care of in this chapter. The discussion part is focusing on worst case scenarios.

8.1 Rock mass stability

8.1.1 Caving

Explained in chapter 2.4.6, weakness zones can cause instabilities in a tunnel. If the potential weakness zones contain of large amount of crushed rock material, there will be a possibility of caving problems. With rapidly change of water pressure and discharge direction, such for a potential pumped-storage station, can cause extra pressure to the weakness zone and cause crushed rock to “fall out” of its position. This can result in large amount of crushed rock material flowing down to the turbines and destroying them. The amount of the crushed rock material might be a crucial factor regarding the destruction. It can also be problematic if the rock materials are big. If the crushed rock materials are big and heavy enough, it might touch the asphalt and develop cracks. This can lead to pressure under the asphalt and then tear the asphalt from the floor.

Weakness zone number four, Ramsdalen, is considered as the largest and possibly, the most crucial weakness zone crossing the headrace tunnel in Roskrepp. It was easily discovered from flight photo before doing any field investigations. The zone is considered to have a width of approximately 40 meters and have the same orientation as the foliation. Possibilities of same width at the location of tunnel crossing is present. If the water pressure is changing, and wave occurs, it can give the ceiling and the walls an extra pressure and cause crushed material to fall (Figure 54).

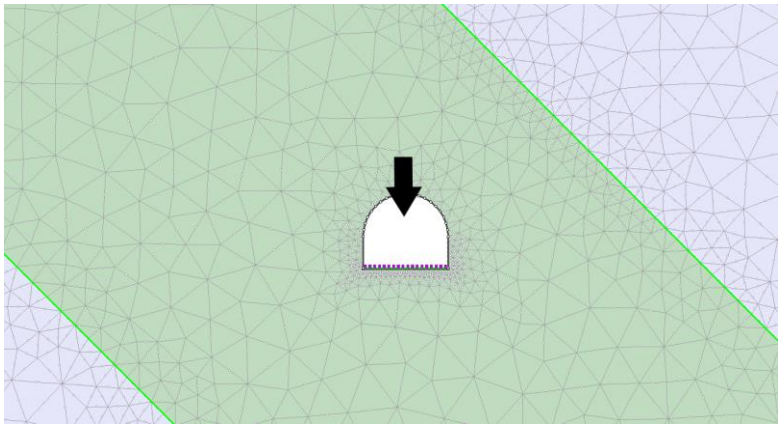

Figure 54 - Illustration of caving.

Another scenario of caving is places where jointing is very concentrate with unfortunate orientations. The joint rosette from field mapping is showing that one of the main joint sets is oriented in the same direction as tunnel directions. This main joint set is labeled as “Joint set 2” and has an unfortunate orientation. The combination of the three main joint sets can cause rock fall, but it is not for sure. Investigation inside the tunnel should be done when possible.

When building a tunnel, it is of interest to avoid main joint sets in the same direction as the tunnel itself. Because of gravity and orientations on joint sets that crosses each other, rock fall can occur, especially in the ceiling. In this case we are dealing with water in the tunnel, so the effect from gravity might not be as big as in a highway tunnel. On the other hand, the extra water pressure can cause extra pressure on already loose rock blocks in the tunnel, in form of hydraulic jacking. If rock blocks were to fall or loosen off the walls or ceiling, these blocks can end up streaming down to the turbines and destroy them. There is also a chance that rock blocks can crash in the concrete asphalt and create cracks in the asphalt.

Numerical analysis of the three cases presented in chapter 5.2 showed some stress concentration at the ceiling area. If the stress concentration exceeds UCS value, rock failure can occur. Approximately 85 yielded elements in the ceiling of shear was analyzed in RS2 of the weakness zone of gneiss. Compared to the two other scenarios, this scenario seems to be more crucial when it comes to having/getting caving problems in the tunnel.

8.2 Stability of Asphalt layer

8.2.1 Erosion of Rock Mass

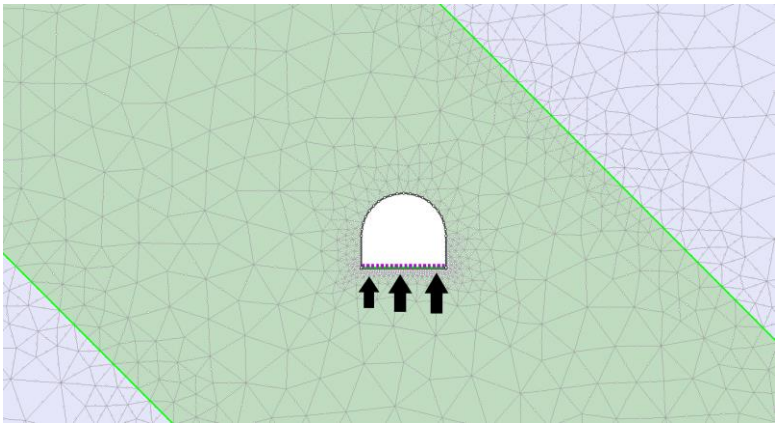

Figure 55 – Illustration of dig up of rock mass from weakness zone.

Dewatering headrace tunnel or downwards discharge direction can cause the water under the asphalt lining to dig-up possible loose rock masses with help of gravity. This can cause loose rock masses to build up under the asphalt lining and cause large pressure under and eventually tear up asphalt lining. Pieces of asphalt and rock masses can then flow down to the turbines and destroy them.

Zones of crushed rock material are possibly the most crucial areas for this scenario. Weakness zone four might be of crushed rock material and is therefore of interest for erosion problem under the asphalt lining.

The rock mass quality closer to the turbines, has lower q-values than the rock mass close to the Roskrepp dam. Even though this area is not covered with asphalt, a variation in water pressure can still make damage to the turbines. With or without asphalt, there is a chance that weak rock materials can erode. If the schistosity of the granitic gneiss is very high, flakes and parts of the rock can easily break from the rock mass if extra pressure is applied.

8.2.2 Uplift caused by pressure differences

Results from hydraulic testing shows that there is a delay in the pressure under asphalt compared to the pressure over it when mass oscillation at surge shaft is present. Figure 56, also shown in chapter 7.1, illustrates the situation. The results show a trend of larger differential pressure in direction two, when mass oscillation is on its way down. This is seen as the most critical situation, since the pressure under asphalt lining is still pointing upwards as the water pressure in the headrace tunnel is decreasing. With rapidly change of discharge and discharge direction, the differential pressure can cause an uplift to the asphalt lining and eventually tear it up. Parts of the asphalt might stream down to the turbines and destroy them.

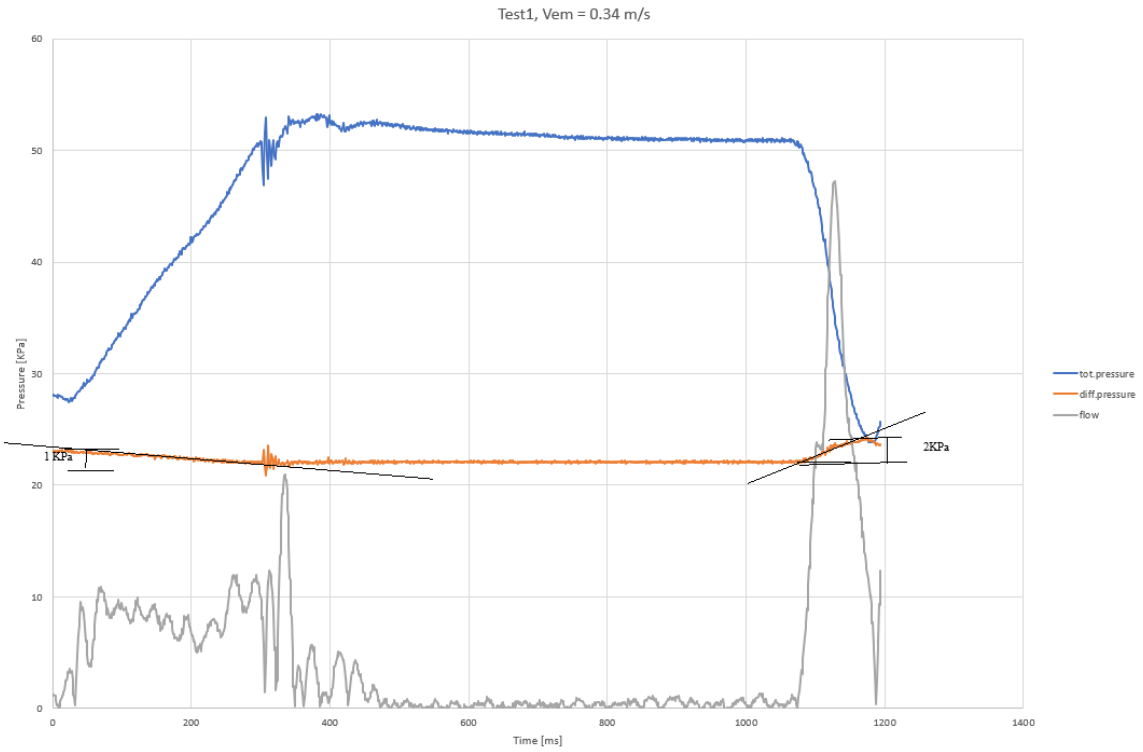

Figure 56 - Result from Test1 of hyrauloc model test.

The first tests performed in the physical model testing has most distinct results. Later tests showed less differential pressure. One reason for this cause, can be the observed sealing being less sealed after running several tests. This can have caused an increase of access for the water to stream under asphalt lining. It seems like the issue of uplifting caused by differential pressure depends on a fine balance of the amount of access for water to stream through the asphalt lining.

Too much access can maybe correspond to the same as high permeability in the asphalt layer. Cracks/joints in the asphalt or at rock wall connecting the area under the lining, will most likely impact the instability when mass oscillation is present, because Roskrepp situation is in much larger scaled than model type.

In combination of literature study and results from hydraulic model testing, there is delay in pressure under asphalt lining when change of discharge in the headrace tunnel. This can cause instabilities, and especially when the changes are rapidly.

8.2.3 Uplift caused by rock condition

The rock mass itself can also cause uplifting of the asphalt lining. Low stress concentration at the floor can some deformation, see Figure 57. Results from numerical modeling shows that there is a possibility of 0.06 mm deformation at the floor for granite, and 0.09 for the gneiss in both good and bad rock conditions. Already established deformation might indicate high stresses in the middle of the asphalt lining. Hight stress concentration at the middle of the lining plus extra pressure from water or other materials might cause cracks in the middle.

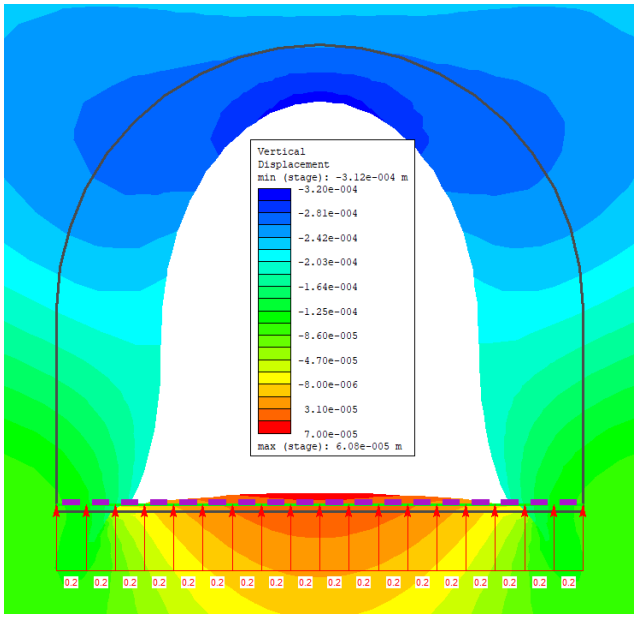

Figure 57 - Analysis of good rock condition of granite in RS2.

9 CONCLUSION AND FURTHER WORK

If the asphalt is fully sealed, no cracks are developed, and the rock quality is good, there will most likely not be any problems turning Roskrepp hydropower plant into a pumped-storage plant. On the other hand, bad rock quality at certain areas along the headrace alignment is discovered. Assumptions that asphalt lining is fully sealed can be risky as well. Results from field investigation, lab testing and numerical analysis shows that there are some crucial areas along the headrace alignment that need to be further investigated:

- the area around weakness zone 4
- the area close to the power station
- asphalt lining area and maybe already developed cracks in it

All the scenarios mentioned in the discussion leads to avoid destroying the turbines. The results of the rock conditions from field mapping can be realistic in the tunnel. To collect safer and more reliable data, more time in field would probably help. There was spent two days field mapping in rain which slowed down the work.

A more thorough physical model should be carried out for more reliable data regarding how the pressure under asphalt reacts. It was the first time this hydraulic test was carried out, and because of lack of time, already existing tunnel model was used. This caused some mistakes in scaling.

- More sensitive valves next time for a more controlled discharger.
- Higher surge shaft for simulating max mass oscillation.
- More time for testing at different asphalt layers.

Delaying of important elements for the set-up of the physical test, caused short time for testing. This lead to testing one asphalt layer only. To gain more reliable data, several layers of asphalt should be tested with different extent of sealing to see if the magnitude of water under asphalt

layer influence the asphalt stability at un-stationary scenarios. A student with more hydrological background should carry out this kind of test for further investigations.

If a pumped-storage system is to be built in Roskrepp, water pressure in the headrace tunnel will rapidly change. This rapidly pressure change can cause destruction of asphalt layer and rock mass over time and can destroy the turbines. Even though destruction will not happen right after installation, destruction can occur after a long period of time. This can result in large economical losses. Thorough and further investigations should be performed.

Further studies:

- a physical model that can give indications on how the asphalt will react when variation of water pressure is applied.
- literature research on the permeability of asphalt concrete.
- further investigations of the permeability to the asphalt concrete of Roskrepp headrace tunnel.
- engineering geological field investigations inside the headrace tunnel.
- perfect scaled model of hydraulic test, with similar asphalt liner. Many tests results, to collect more reliable data.

BIBLIOGRAPHY

AKSU, I., BAZILEVSKAYA, E. & KARPYN, Z. T. 2015. Swelling of clay minerals in unconsolidated porous media and its impact on permeability. *GeoResJ,* vol. 7**,** pp. 1-13.

APEAGYEI, A. K., DIEFENDERFER, B. K. & DIEFENDERFER, S. D. 2012. Development of dynamic modulus master curves for hot-mix asphalt with abbreviated testing temperatures. *International Journal of Pavement Engineering,* vol. 13**,** pp. 98-109.

ARNGRIMSSON, H. O., GUNNARSSON, T. B., FOGED, F. N. & ERLINGSSON, S. (eds.) 2010. *Numerical analysis of rock support strategy for the Budarhals tunnel* Authors

BENSON, R. 1989. Design of unlined and lined pressure tunnels. *TUNNELLING UNDERGROUND SPACE TECHNOL,* vol. 4**,** pp. 155-170.

BROX, D. 2011. Design, construction, and operation of unlined pressure tunnels: Suggestions for good industry practice. *Proceedings - Rapid Excavation and Tunneling Conference* pp. 87-101.

BRUHNI, I. 2017. *Dypbergart* [Online]. Store norske leksikon. Available: https://snl.no/dypbergart [Accessed 07.12 2017].

BRYHNI, I. 2017. *Kaledonske fjellkjede* [Online]. Store norske leksikon Available: https://snl.no/Kaledonske_fjellkjede [Accessed 19.12 2017].

ENTREPRENØRFORENINGEN - BYGG OG, A. 1999. *Vegdekker,* Oslo, BA forl. Universitetsforl.

FERJERSKOV, M. 1996. Determination of in-situ Rock Stresses Related to Petroleum Activities on the Norwegian Continetial Shelf *Department of Geology and Mineral Resources Enginnering NTNU***,** pp. "Apendix B.3 Overcoring Database ".

FORNYBAR. 2016. *Teknologi* [Online]. Available: http://www.fornybar.no/vannkraft/teknologi [Accessed 24.11 2017].

GUTTORMSEN, O. 2014. Vassgragsteknikk II. *(Kompendium)***,** pp. 144-177.

HINO, T. & LEJEUNE, A. 2012. 6.15 - Pumped Storage Hydropower Developments A2 - Sayigh, Ali. *Comprehensive Renewable Energy.* Oxford: Elsevier.

HOEK, E. 2007. Practical Rock Engineering *In:* ROCSCIENCE (ed.).

HOEK, E. & BROWN, E. T. 1980 Underground Excavations in Rock . *London: Institution of Mining and Metallurgy*

HOEK, E., KAISER, P. K. & BAWDEN, W. F. 1995. *Support of underground excavations in hard rock,* Rotterdam, Balkema.

HOEK, E. & MARINO, P. 2000. Predicting tunnel squeezing problems in weak heterogenous rock masses. . *Tunnels and Tunneling International* pp. 1-21.

HOFSTAD, K. 2017. *Energiressurs* [Online]. Available: https://snl.no/energiressurs [Accessed].

HYDROCEN. 2017. *HydroCen* [Online]. NTNU. Available: https://www.ntnu.no/hydrocen [Accessed 2017].

ISRM 1979. Suggested methods for determining the uniaxial compressive strength and deformability of rock materials. . *International Journal of Rock Mechanics and Mining Sciences,* vol. 16:138–140.

LI, C. C. 2015. Applied Rock Mechanics. *(Kompendium).*

LIA, L. 2017. Vannvegar - utforming of prinsipp. *Vannkraftverk og Vassdragsteknikk (Power Point).*

MAMLOUK, M. S. & ZANIEWSKI, J. P. 2011. Materials for civil and construction engineers. pp. 375-411.

MYRVANG, A. 2001. *Bergmekanikk,* Trondheim, Institutt for geologi og bergteknikk. NTNU.

NESSE, W. D. 2000. Introduction to mineralogy. *New York: Oxford University Press.*

NGI. 2015. *Q-system Quick Reference 2015* [Online]. Available: https://www.ngi.no/eng/Publications-and-library/Books/Q-system [Accessed 09.10 2017].

NIELSEN, T. K. Dynamic Dimensioning of Hydro Power Plants (Komdendium). *Vannkraftlaboratoriet NTNU***,** pp. 29-31. .

NILSEN, B. & BROCH, E. 2010. *Ingeniørgeologi - berg : grunnkurskompendium,* Trondheim, Tapir akademisk forlag, Kompendieforlaget.

NILSEN, B. & PALMSTRÖM, A. 2000. Engineering Geology and Rock Engineering - Handbook No 2. . *Norwegian Group of Rock Mechanics*

PALMSTRÖM, A. & STILLE, H. 2010. Geology in Rock Engineering *Rock Engineering.* ICE Publishing.

PANTHI, K. K. 2006. Analysis of engineering geological uncertainties related to tunnelling in Himalayan rock mass conditions. vol. 2006:41.

PANTHI, K. K. 2017a. Review on the prevailing methods for the prediction of potential rock burst / rock spalling in tunnels.

PANTHI, K. K. 2017b. Rock burst prediction methods and their applicability. . *Elsevier,* Chapter 11.2 of the book to be published in 2018 with title "Rock Burst - Mechanism, Monitoring, Warning and Mitigation" edited by Xia-Ting Feng. .

RAADE, G. 2016. *Granitt* [Online]. Store norske leksikon. Available: https://snl.no/granitt [Accessed 07.12 2017].

RAMBERG, I. B., BRYHNI, I., NØTTVEDT, A. & RANGNES, K. 2007. *Landet blir til - Norges geologi* Trondheim Norsk Geologisk Forening

RAST, N. & CRIMES, T. P. 1969. Caledonian orogenic episodes in the British Isles and North-Western France and their tectonic and chronological interpretation. *Tectonophysics,* vol. 7**,** pp. 277-307.

ROCSCIENCE. 2018a. *Triaxial Tests on Sand* [Online]. Available: https://www.rocscience.com/help/phase2/webhelp9/pdf_files/tutorials/Tutorial_37_Triaxial_Tests_on_Sand.pdf [Accessed 23.04 2018].

ROCSCIENCE. 2018b. *Tutorial 27, Drawdown Analyisis for Tunnel* [Online]. Available: https://www.rocscience.com/help/phase2/webhelp9/pdf_files/tutorials/Tutorial_27_Drawdown_Analysis_for_Tunnel.pdf [Accessed 05.05 2018].

SEO, J.-W., PARK, D.-W. & LE, T. H. M. 2017. Development of an asphalt concrete mixture for Asphalt Core Rockfill Dam. *Construction and Building Materials,* vol. 140**,** pp. 301-309.

SHRESTHA, P. K. & PANTHI, K. K. 2014. Analysis of the plastic deformation behavior of schist and schistose mica gneiss at Khimti headrace tunnel, Nepal. *Bulletin of Engineering Geology and the Environment,* vol 73**,** pp. 759-773.

SIDDIQUE, D. M. 2018. Dimensional analysis, similtude and model analysis. . *Power Point*

SIRA-KVINA 2017a. *Oppgradering av Roskrepp Karftverk* Oppgraderingskonferansen 08.06.2017.

SIRA-KVINA. 2017b. *Sira-Kvina Kraftselskap* [Online]. Available: https://www.sirakvina.no/ [Accessed 2017].

SOLVIK, Ø. 1992. *Design criteria for asphalt and concrete pavement in unlined tunnels,* Rotterdam, A. A. Balkema.

SOLVIK, Ø. & TESAKER, E. 1997. Floor paving in unlined hydropower tunnels

STATENS VEGVESEN. 2017. *Asfalt* [Online]. Available: https://www.vegvesen.no/fag/teknologi/Vegteknologi/Vegbyggingsmaterialer/Asfalt [Accessed 11.09 2017].

STATKRAFT. 2017. *Vannkraft* [Online]. Available: https://www.statkraft.no/Energikilder/Vannkraft/ [Accessed 24.11 2017].

THE EDITORS OF ENCYCLOPÆDIA BRITANNICA. 2006. *Schistosity* [Online]. Enclopædia Britannica Available: https://www.britannica.com/science/schistosity [Accessed 19.12 2017].

TRINH, Q. N. & HOLMØY, K. 2012. Nummerisk modellering i bergteknikk: Hva det og kan brukes til, fordeler og ulenper, programvare og begrensninger. I. *Oslo, Fjellsprengningsteknikk, Bergmekanikk/Geoteknikk.* .

VARDANEGA, P. & WATERS, T. 2011. Analysis of Asphalt Concrete Permeability Data Using Representative Pore Size. *J. Mater. Civ. Eng.,* 23**,** 169-176.

VEGVESEN, S. 2014. *Håndbok N200 Vegbygging* [Online]. Available: https://www.vegvesen.no/_attachment/188382/binary/980128?fast_title=H%C3%A5ndbok+N200+Vegbygging+%2821+MB%29.pdf [Accessed 11.09 2017].

ZHANG, Y., GU, F., BIRGISSON, B. & LYTTON, R. L. 2018. Modelling cracking damage of asphalt mixtures under compressive monotonic and repeated loads using pseudo J-integral Paris' law. *Road Materials and Pavement Design,* vol. 19**,** pp. 525-535.

ZHANG, Y., LUO, R. & LYTTON, R. L. 2013. Characterization of viscoplastic yielding of asphalt concrete. *Construction and Building Materials,* vol. 47**,** pp. 671-679.

ZIARI, H., AMERI, M. & KHABIRI, M. M. 2007. Resilient behaviour of hot mixed and crack sealed asphalt concrete under repeated loading. *Technological and Economic Development of Economy,* vol. 13**,** pp. 56-60.

APENDICIES

A) Asphalt properties from Handbook N200, Stavens Vegvesen

Krav til hulrom ved proporsjonering[1)]	ÅDT	
	≤ 5000	> 5000
Slitelag		
- minste hulrominnhold, %	2,0	2,5
- største hulrominnhold, %	5,5	5,5
- minste bitumenfylt hulrom, %	72	72
- største bitumenfylt hulrom, %	89	86
Bindlag		
- minste hulrominnhold, %	2,5	2,5
- største hulrominnhold, %	7,0	7,0
- minste bitumenfylt hulrom, %	65	65
- største bitumenfylt hulrom, %	86	86

1) Prøvens densitet skal bestemmes vha hydrostatisk overflatetørr metode.

Figur 632.4 Krav til hulrom ved proporsjonering, Ab

ÅDT	≤ 300	301 - 1500	1501 - 3000	3001 - 5000	5001 - 15000	> 15000
Overflatebehandling						
Eo og Do	≤ 25	≤ 25	≤ 25			
Eog og Dog	≤ 30	≤ 25				
Varmproduserte asfaltdekker						
Agb	≤ 30	≤ 30	≤ 30			
Ab	≤ 30	≤ 30	≤ 30	≤ 30	≤ 25	≤ 25
Ska				≤ 30	≤ 25	≤ 25
Ma	≤ 35	≤ 30	≤ 25			
Sta		≤ 30[1)]	≤ 30[1)]	≤ 30[1)]	≤ 25	≤ 25
Top		≤ 30[1)]	≤ 30[1)]	≤ 30[1)]	≤ 25	≤ 25
Da	≤ 30	≤ 30	≤ 30	≤ 25	≤ 25	
T			≤ 25	≤ 25	≤ 25	≤ 25
Kaldproduserte asfaltdekker						
Egt	≤ 35	≤ 30	≤ 25			
Asg	≤ 35	≤ 30				

1) Kravet gjelder også for fuktmembran på bruer

Figur 622.5 Krav til flisighetsindeks for steinmaterialer i asfaltdekker

ÅDT	≤ 300	301 - 1500	1501 - 3000	3001 - 5000	5001 - 15000	> 15000
Overflatebehandling						
Eo og Do	≤ 40	≤ 30	≤ 30			
Eog og Dog	≤ 40	≤ 30				
Varmproduserte asfaltdekker						
Agb	≤ 40	≤ 30	≤ 30			
Ab	≤ 40	≤ 30	≤ 30	≤ 30	≤ 25	≤ 15
Ska				≤ 25	≤ 25	≤ 15
Ma	≤ 40	≤ 30	≤ 30			
Sta		≤ 30[1)]	≤ 30[1)]	≤ 25[1)]	≤ 25	≤ 15
Top		≤ 30[1)]	≤ 30[1)]	≤ 25[1)]	≤ 25	≤ 15
Da	≤ 40	≤ 30	≤ 30	≤ 25	≤ 25	
T			≤ 25	≤ 15	≤ 15	≤ 15
Kaldproduserte asfaltdekker						
Egt	≤ 40	≤ 30	≤ 30			
Asg	≤ 40	≤ 30				

1) Kravet gjelder også for fuktmembran på bruer

Figur 622.6 Krav til Los Angeles-verdi for steinmaterialer i asfaltdekker

ÅDT	≤ 300	301 - 1500	1501 - 3000	3001 - 5000	5001 - 15000	> 15000
Overflatebehandling						
Eo og Do	≤ 19	≤ 19	≤ 14			
Eog og Dog	≤ 19	≤ 19				
Varmproduserte asfaltdekker						
Agb	≤ 19	≤ 19	≤ 14			
Ab	≤ 19	≤ 19	≤ 14	≤ 10	≤ 10	≤ 7
Ska				≤ 10	≤ 10	≤ 7
Ma	≤ 19	≤ 19	≤ 14			
Sta					≤ 10	≤ 7
Top					≤ 10	≤ 7
Da	≤ 19	≤ 19	≤ 14	≤ 10	≤ 10	
T			≤ 10	≤ 7	≤ 7	≤ 7
Kaldproduserte asfaltdekker						
Egt	≤ 19	≤ 19	≤ 14			
Asg	≤ 19	≤ 19				

Figur 622.7 Krav til mølleverdi for steinmaterialer i asfaltdekker

ÅDT	≤ 300	301 - 1500	1501 – 3000	3001 - 5000	5001 - 15000	> 15000
Overflatebehandling						
Eo og Do	$C_{90/1}$	$C_{90/1}$	$C_{90/1}$			
Eog og Dog	-	-				
Varmproduserte asfaltdekker						
Agb	$C_{20/70}$	$C_{20/70}$	$C_{20/70}$			
Ab	$C_{50/30}$	$C_{50/30}$	$C_{50/30}$	$C_{50/30}$	$C_{50/30}$	$C_{50/20}$
Ska				$C_{50/20}$	$C_{100/0}$	$C_{100/0}$
Ma	$C_{20/70}$	$C_{20/70}$	$C_{30/60}$			
Sta		$C_{90/1}$[1)]	$C_{90/1}$[1)]	$C_{90/1}$[1)]	$C_{100/0}$	$C_{100/0}$
Top		$C_{90/1}$[1)]	$C_{90/1}$[1)]	$C_{90/1}$[1)]	$C_{100/0}$	$C_{100/0}$
Da	$C_{50/20}$	$C_{50/20}$	$C_{50/20}$	$C_{100/0}$	$C_{100/0}$	
T			$C_{50/20}$	$C_{100/0}$	$C_{100/0}$	$C_{100/0}$
Kaldproduserte asfaltdekker						
Egt	$C_{20/70}$	$C_{20/70}$	$C_{20/70}$			
Asg						

1) Kravet gjelder også for fuktmembran på bruer

Figur 622.8 Krav til knusningsgrad for steinmaterialer til asfaltdekker

B) Q-system, with property description, NGI Handbook.

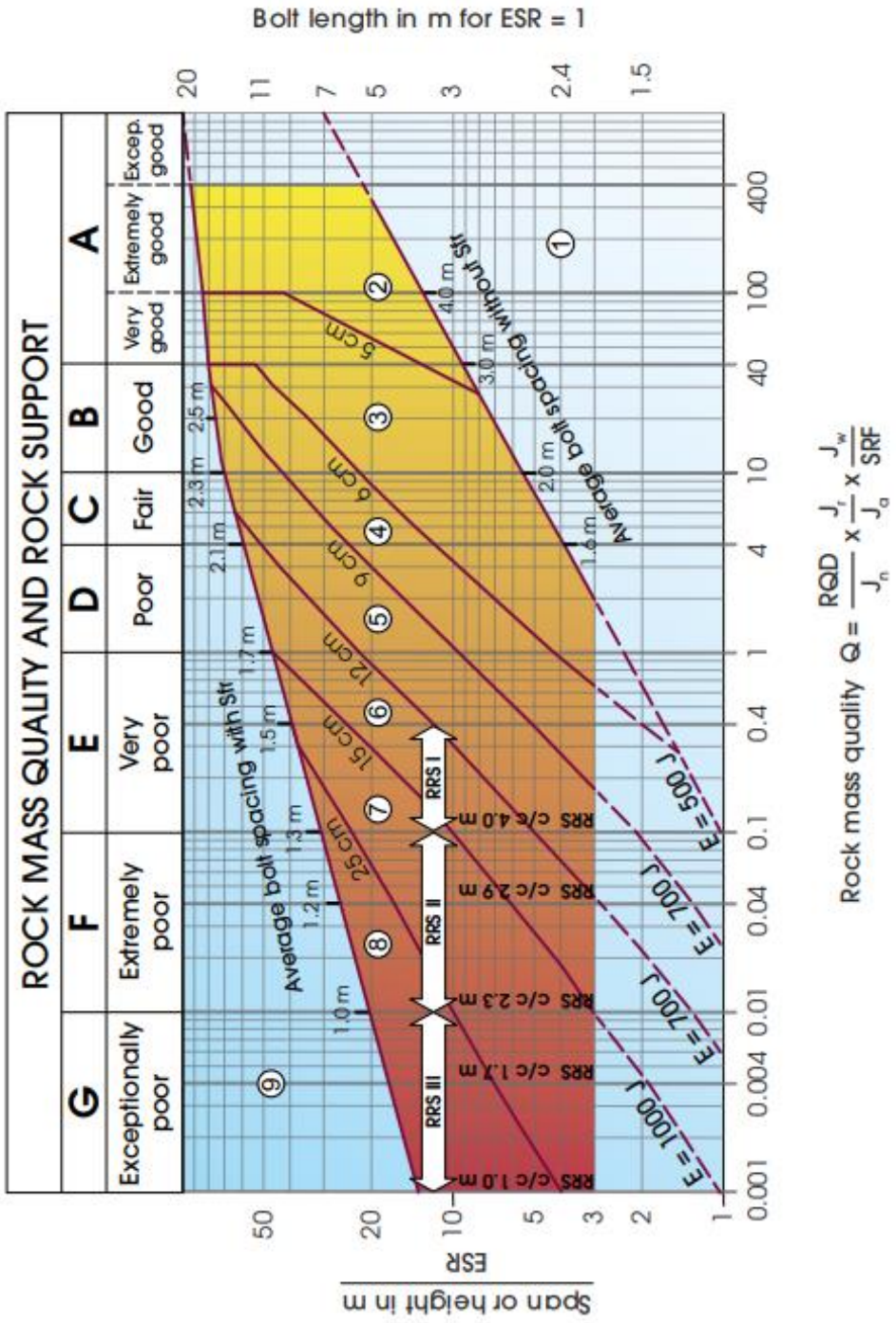

Table 1 RQD-values and volumetric jointing.

1 RQD (Rock Quality Designation)			RQD
A	Very poor	(> 27 joints per m^3)	0-25
B	Poor	(20-27 joints per m^3)	25-50
C	Fair	(13-19 joints per m^3)	50-75
D	Good	(8-12 joints per m^3)	75-90
E	Excellent	(0-7 joints per m^3)	90-100
Note: i) Where RQD is reported or measured as ≤ 10 (including 0) the value 10 is used to evaluate the Q-value ii) RQD-intervals of 5, i.e. 100, 95, 90, etc., are sufficiently accurate			

Table 2 J_n – values.

2 Joint set number		J_n
A	Massive, no or few joints	0.5-1.0
B	One joint set	2
C	One joint set plus random joints	3
D	Two joint sets	4
E	Two joint sets plus random joints	6
F	Three joint sets	9
G	Three joint sets plus random joints	12
H	Four or more joint sets, random heavily jointed "sugar cube", etc	15
J	Crushed rock, earth like	20
Note: i) For tunnel intersections, use 3 x J_n ii) For portals, use 2 x J_n		

Table 3 J_r – values.

3 Joint Roughness Number		J_r
a) *Rock-wall contact, and* ***b)*** *Rock-wall contact before 10 cm of shear movement*		
A	Discontinuous joints	4
B	Rough or irregular, undulating	3
C	Smooth, undulating	2
D	Slickensided, undulating	1.5
E	Rough, irregular, planar	1.5
F	Smooth, planar	1
G	Slickensided, planar	0.5
Note: i) Description refers to small scale features and intermediate scale features, in that order		
c) *No rock-wall contact when sheared*		
H	Zone containing clay minerals thick enough to prevent rock-wall contact when sheared	1
Note: ii) Add 1 if the mean spacing of the relevant joint set is greater than 3 m (dependent on the size of the underground opening) iii) J_r = 0.5 can be used for planar slickensided joints having lineations, provided the lineations are oriented in the estimated sliding direction		

Table 4 J_a – values.

4	Joint Alteration Number	Φ_r approx.	J_a
a) *Rock-wall contact (no mineral fillings, only coatings)*			
A	Tightly healed, hard, non-softening, impermeable filling, i.e., quartz or epidote.		0.75
B	Unaltered joint walls, surface staining only.	25-35°	1
C	Slightly altered joint walls. Non-softening mineral coatings; sandy particles, clay-free disintegrated rock, etc.	25-30°	2
D	Silty or sandy clay coatings, small clay fraction (non-softening).	20-25°	3
E	Softening or low friction clay mineral coatings, i.e., kaolinite or mica. Also chlorite, talc gypsum, graphite, etc., and small quantities of swelling clays.	8-16°	4
b) *Rock-wall contact before 10 cm shear (thin mineral fillings)*			
F	Sandy particles, clay-free disintegrated rock, etc.	25-30°	4
G	Strongly over-consolidated, non-softening, clay mineral fillings (continuous, but <5 mm thickness).	16-24°	6
H	Medium or low over-consolidation, softening, clay mineral fillings (continuous, but <5 mm thickness).	12-16°	8
J	Swelling-clay fillings, i.e., montmorillonite (continuous, but <5 mm thickness). Value of J_a depends on percent of swelling clay-size particles.	6-12°	8-12
c) *No rock-wall contact when sheared (thick mineral fillings)*			
K	Zones or bands of disintegrated or crushed rock. Strongly over-consolidated.	16-24°	6
L	Zones or bands of clay, disintegrated or crushed rock. Medium or low over-consolidation or softening fillings.	12-16°	8
M	Zones or bands of clay, disintegrated or crushed rock. Swelling clay. J_a depends on percent of swelling clay-size particles.	6-12°	8-12
N	Thick continuous zones or bands of clay. Strongly over-consolidated.	12-16°	10
O	Thick, continuous zones or bands of clay. Medium to low over-consolidation.	12-16°	13
P	Thick, continuous zones or bands with clay. Swelling clay. J_a depends on percent of swelling clay-size particles.	6-12°	13-20

Table 5 J_w – values.

5	Joint Water Reduction Factor	J_w
A	Dry excavations or minor inflow (humid or a few drips)	1.0
B	Medium inflow, occasional outwash of joint fillings (many drips/"rain")	0.66
C	Jet inflow or high pressure in competent rock with unfilled joints	0.5
D	Large inflow or high pressure, considerable outwash of joint fillings	0.33
E	Exceptionally high inflow or water pressure decaying with time. Causes outwash of material and perhaps cave in	0.2-0.1
F	Exceptionally high inflow or water pressure continuing without noticeable decay. Causes outwash of material and perhaps cave in	0.1-0.05

Note: i) Factors C to F are crude estimates. Increase J_w if the rock is drained or grouting is carried out

ii) Special problems caused by ice formation are not considered

Table 6 SRF-values.

6 Stress Reduction Factor				SRF
a) *Weak zones intersecting the underground opening, which may cause loosening of rock mass*				
A	Multiple occurrences of weak zones within a short section containing clay or chemically disintegrated, very loose surrounding rock (any depth), or long sections with incompetent (weak) rock (any depth). For squeezing, see 6L and 6M			10
B	Multiple shear zones within a short section in competent clay-free rock with loose surrounding rock (any depth)			7.5
C	Single weak zones with or without clay or chemical disintegrated rock (depth ≤ 50m)			5
D	Loose, open joints, heavily jointed or "sugar cube", etc. (any depth)			5
E	Single weak zones with or without clay or chemical disintegrated rock (depth > 50m)			2.5
Note: i) Reduce these values of SRF by 25-50% if the weak zones only influence but do not intersect the underground opening				
b) *Competent, mainly massive rock, stress problems*		σ_c / σ_1	σ_θ / σ_c	SRF
F	Low stress, near surface, open joints	>200	<0.01	2.5
G	Medium stress, favourable stress condition	200-10	0.01-0.3	1
H	High stress, very tight structure. Usually favourable to stability. May also be unfavourable to stability dependent on the orientation of stresses compared to jointing/weakness planes*	10-5	0.3-0.4	0.5-2 2-5*
J	Moderate spalling and/or slabbing after > 1 hour in massive rock	5-3	0.5-0.65	5-50
K	Spalling or rock burst after a few minutes in massive rock	3-2	0.65-1	50-200
L	Heavy rock burst and immediate dynamic deformation in massive rock	<2	>1	200-400
Note: ii) For strongly anisotropic virgin stress field (if measured): when $5 \leq \sigma_1 / \sigma_3 \leq 10$, reduce σ_c to $0.75\ \sigma_c$. When $\sigma_1 / \sigma_3 > 10$, reduce σ_c to $0.5\ \sigma_c$, where σ_c = unconfined compression strength, σ_1 and σ_3 are the major and minor principal stresses, and σ_θ = maximum tangential stress (estimated from elastic theory) iii) When the depth of the crown below the surface is less than the span; suggest SRF increase from 2.5 to 5 for such cases (see F)				
c) *Squeezing rock: plastic deformation in incompetent rock under the influence of high pressure*			σ_θ / σ_c	SRF
M	Mild squeezing rock pressure		1-5	5-10
N	Heavy squeezing rock pressure		>5	10-20
Note: iv) Determination of squeezing rock conditions must be made according to relevant literature (i.e. Singh et al., 1992 and Bhasin and Grimstad, 1996)				
d) *Swelling rock: chemical swelling activity depending on the presence of water*				SRF
O	Mild swelling rock pressure			5-10
P	Heavy swelling rock pressure			10-15

Table 7 ESR-values.

7	Type of excavation	ESR
A	Temporary mine openings, etc.	*ca.* 3-5
B	Vertical shafts*: i) circular sections ii) rectangular/square section * Dependant of purpose. May be lower than given values.	*ca.* 2.5 *ca.* 2.0
C	Permanent mine openings, water tunnels for hydro power (exclude high pressure penstocks) water supply tunnels, pilot tunnels, drifts and headings for large openings.	1.6
D	Minor road and railway tunnels, surge chambers, access tunnels, sewage tunnels, etc.	1.3
E	Power houses, storage rooms, water treatment plants, major road and railway tunnels, civil defence chambers, portals, intersections, etc.	1.0
F	Underground nuclear power stations, railways stations, sports and public facilitates, factories, etc.	0.8
G	Very important caverns and underground openings with a long lifetime, ≈ 100 years, or without access for maintenance.	0.5

Table 8 Conversion from actual Q-values to adjusted Q-values for design of wall support.

In rock masses of good quality	$Q > 10$	Multiply Q-values by a factor of 5.
For rock masses of intermediate quality	$0.1 < Q < 10$	Multiply Q-values by a factor of 2.5. In cases of high rock stresses, use the actual Q-value.
For rock masses of poor quality	$Q < 0.1$	Use actual Q-value.

C) Geological map of Roskrepp from field mapping, week 38 (2017)

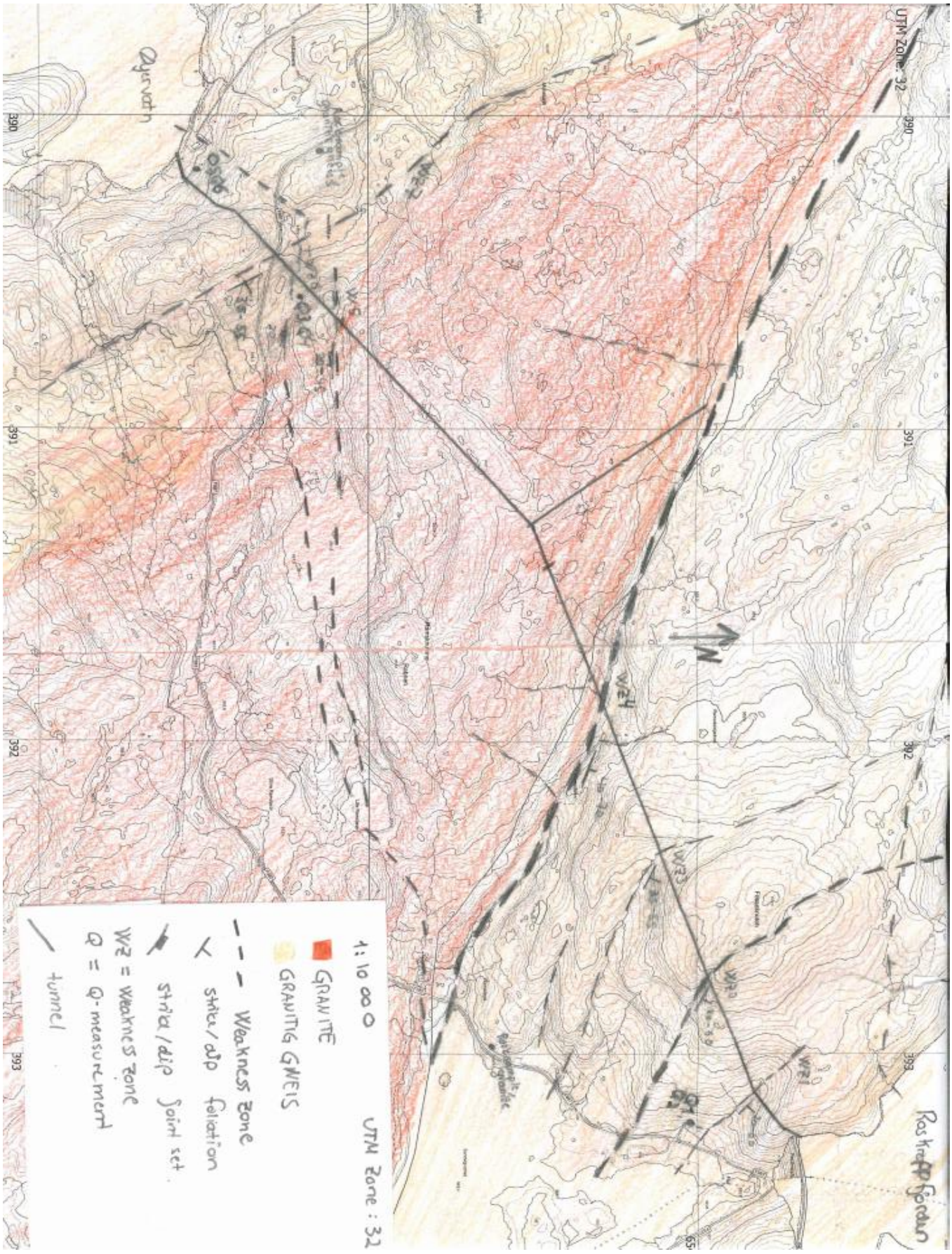

D) Joint rosette from field mapping of Roskrepp, week 38 (2017)

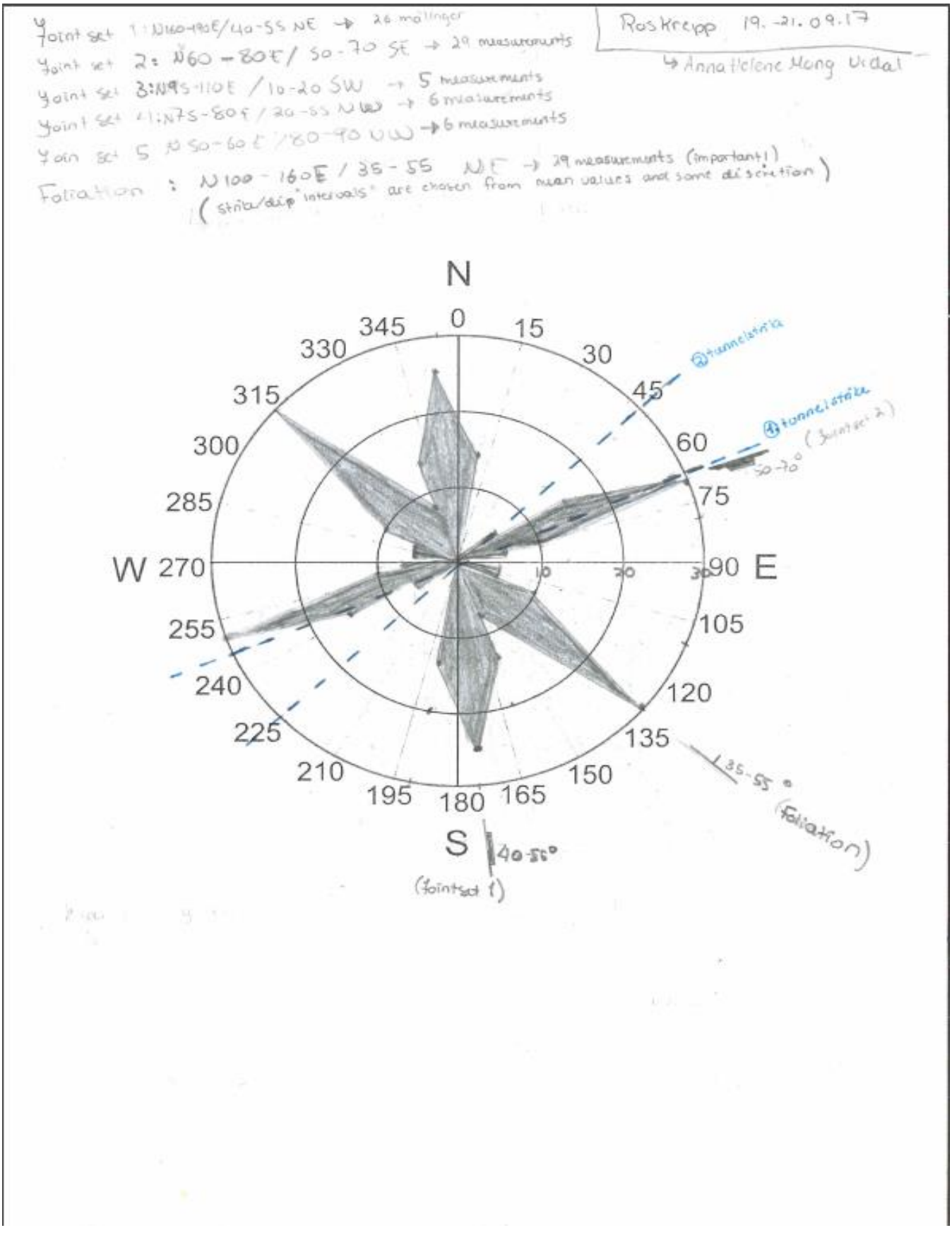

E) Joint measurement from field mapping field mappin, week 38 (2017)

Foliation

90	62	NE	a t	
92	42	NE		2
96	70	NE		10
100	20	NE		19
110	65	NE		18
112	60	NE	a t	
112	40	NE	a t	
115	50	NE		2
115	40	NE		17
116	46	NE	a t	
116	36	NE (F)	adt	
120	60	NE	adt	
120	48	NE	a t	
122	52	NE	a t	
128	56	NE	a t	
130	30	NE		2
130	60	NE		18
132	42	NE		14
134	55	NE		14
140	70	NE		7
145	32	NE	a t	
146	40	NE	a t	
148	35	NE	adt	
155	70	NE		16
156	54	NE	a t	
160	50	NE		2
160	20	NE		11
160	20	NE	adt	
178	50	NE	a t	
126,9595	44,81515	NE (F)	geo mean	
130	45	NE (F)		
128,8966	47,41379	NE (F)	vanlig gj.snitt	
130	**45**	**NE (F)**		
120-140	40-50			

Joint set 1 - deep dipping towards west

150	78	SW	a t	
158	70	SW	adt	
160	88	SW		4
160	75	SW		5
160	80	SW		6
168	50	SW	a t	
175	75	SW		5
175	70	SW	a t	
178	75	SW	adt	
180	60	SW		14
182	70	NW	a t	
180	70	W		6
180	89	W		19
180	70	W		19
175	80	W		20
180	85	W		20
185	80	W		20
184	72	NW	a t	
185	80	NW		15
185	62	NW	adt	
186	68	NW	a t	
190	75	NW	adt	
190	80	NW		12
192	66	NW	adt	
192	50	NW	adt	
192	50	NW	adt	
177,3819	71,00436		geo mean	
175	70	SW		
180	70	W		
177,7692	**71,84615**			
180	**70**	**W**	**vanlig gj.snitt**	
170-10	60-80	W		

joint set 2				
55	50	SE		9
50	60	SE		9
75	50	SE		1
60	80	SE		3
50	80	SE		5
45	90	SE		6
50	75	SE		7

joint set 3				
95	30	SW		15
98	35	SW		10
100	55	SW	adt	
104	38	SW	adt	
110	20	SW		17
101,2687	33,76549	SW	geo mean	
100	35	SW		

75	80	SE		14
74	48	SE		14
82	68	SE		16
70	74	SE	a t	
60	84	SE	a t	
58	55	SE	a t	
60	30	SE	a t	
88	68	SE	adt	
78	70	SE	adt	
66	80	SE	adt	
58	60	SE	adt	
58	60	SE	adt	
72	72	SE	adt	
75	70	SE	adt	
75	70	SE	adt	
82	58	SE	adt	
70	50	SE	adt	
86	52	SE	adt	
80	92	SE	adt	
66	60	SE	adt	
68	62	SE	adt	
94	38	SE	adt	
67,12021	63,17822	SE	geo mean	
70	65	SE		
68,27586	**65,03448**	**SE**	**vanlig gj.snitt**	
70	**65**	**SE**		

joint set 4				
60	45	NW		19
75	55	NW		11
78	28	NW	adt	
80	30	NW		19

80	20	NW		19
100	20	NW		19
77,96766	30,66567		geo mean	
80	30	NW		

joint set 5				
40	88	NW		6
45	85	NW		17
50	80	NW		5
55	85	NW		15
60	90	NW		5
80	75	NW		18
53,61765	83,67949			
55	85	NW		

F) Longitudinal map of Roskrepp headrace tunnel

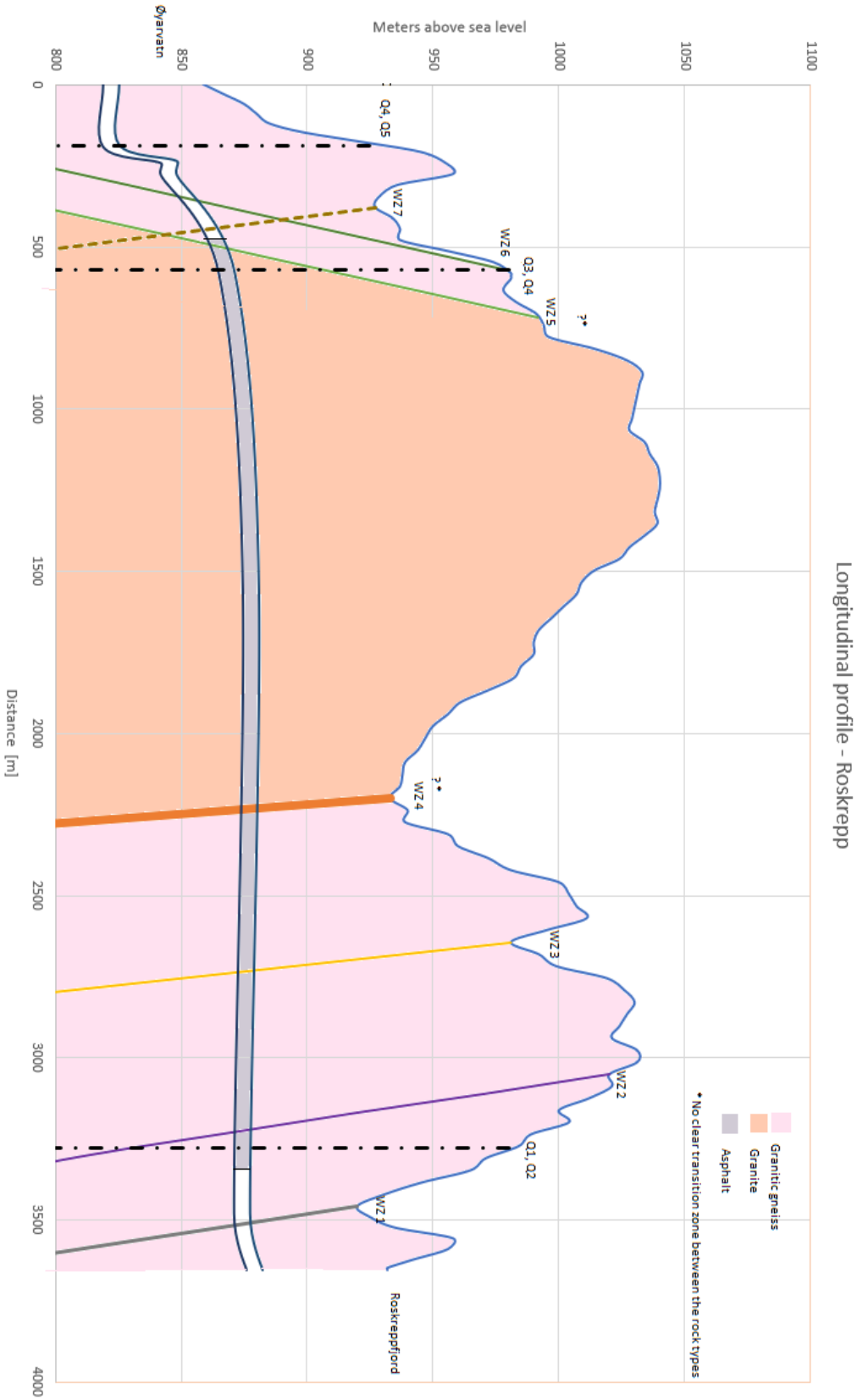

G) Scanned information from Sira-Kvina Kraftverk

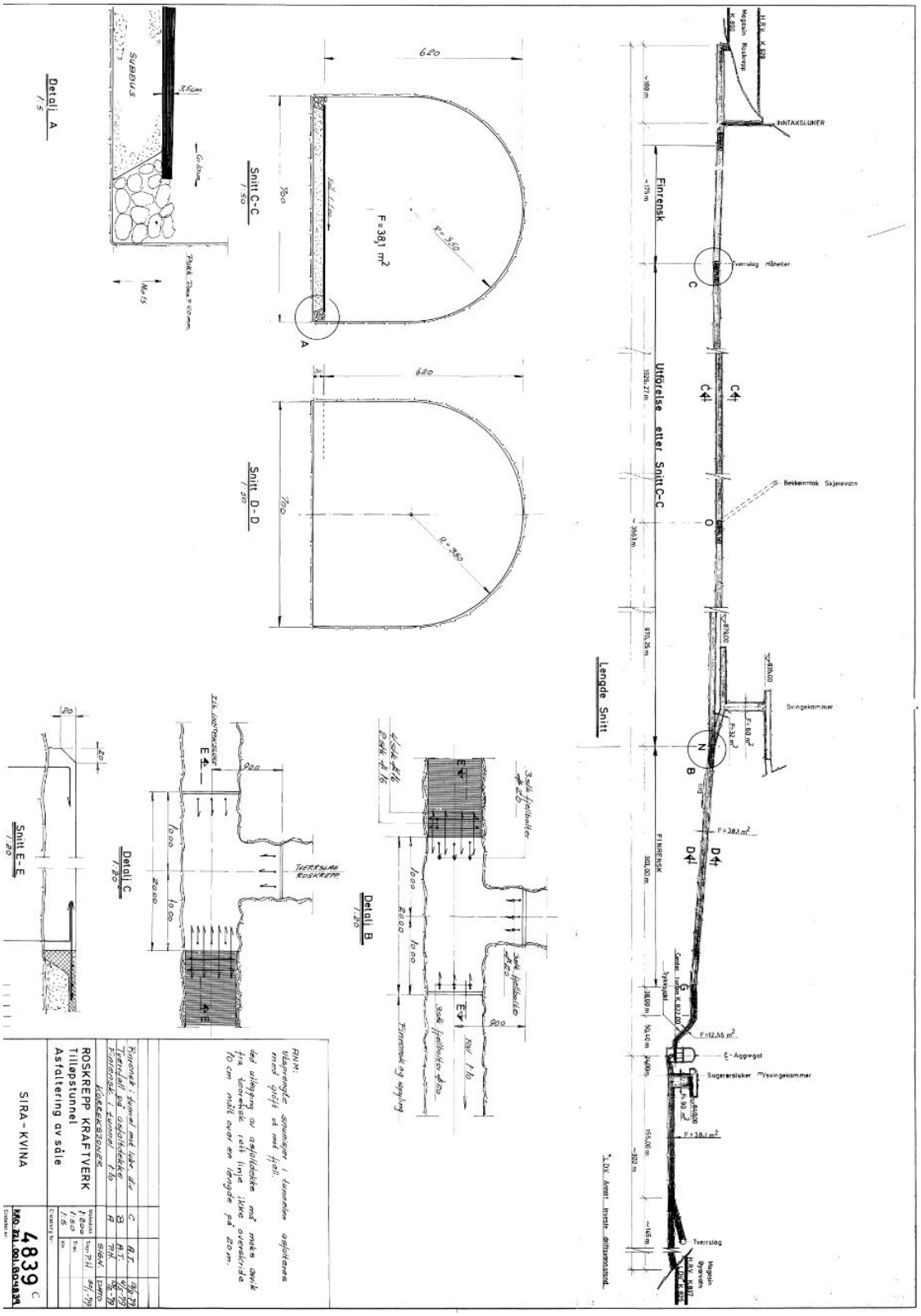

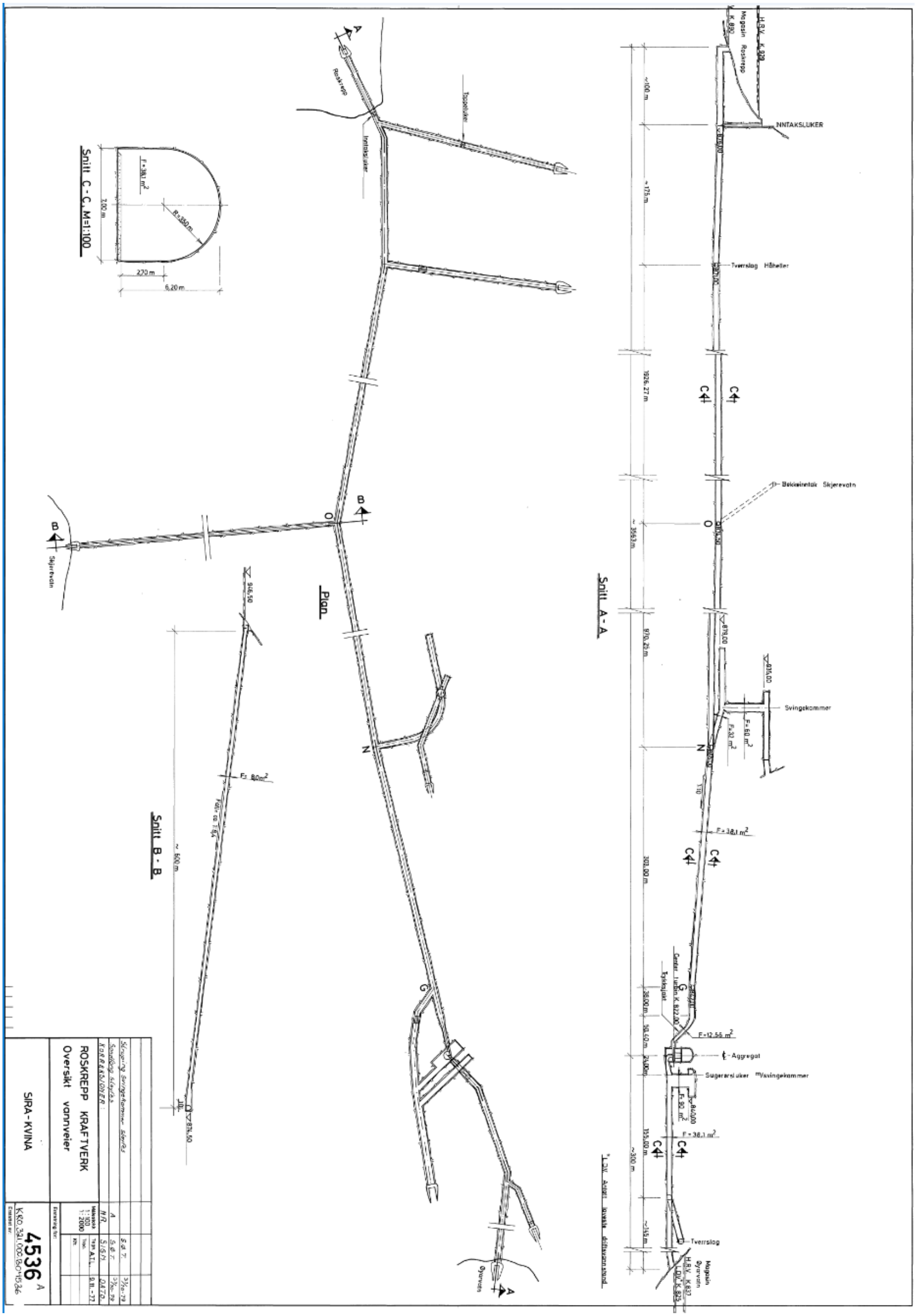
Snitt A - A
Plan
Snitt B - B
Snitt C - C, M=1:100
INNTAKSLUKER
Svingekammer
Aggregat
Tverrslag
ROSKREPP KRAFTVERK
Oversikt vannveier
SIRA-KVINA
4536

ROSKREPP KRAFTVERK, Avløpstunell

Befart den 15.6.

I avløpstunellen er man nå kommet inn i noe dårlig fjell i bergfjellsonen. Det opplyses at man har kun 3-4 m overdekning, og man er kommet inn i et parti hvor båndgneisen viser en sterk oppsprekkning parallelt foliasjonen. Man har våte, glatte sprekker/sprekker etter foliasjonen sammen med en (kompleks?) leirsone som følger samme retning i en overgangssone mellom migmatitt/båndgneis og en mer massiv granodioritisk gneis som ligger i en ca 20 bred bue. Dette forhold kan iakttas ved påhugg til adkomst avløpstunellen, - ventelig er det samme forhold som gjør seg gjeldende begge steder. Man er, så vidt vites, enda ikke kommet inn i den bedre, granodioritiske gneisen i selve avløpstunellen.

Oppsprekkningen i det dårlige partiet synes å følge retninge

I 120-140° / 40-45°N, sprekkavst. 0,1-0,5m, glatt, utholdende (=foli
II ~20°-40° / ~40°Ø, sprekkavst. ~0,75m i gj.snitt, maks 1m, ml. like ut
III ~100° / 80°N, sprekkavst gj.snitt 0,5m, like utholdende

I er hovedoppsprekkingen (etter bergartsgrensen)
II er den svakest utviklede oppsprekkning

Den grovfragmenterte oppknusningssonen/Elvpa følger I

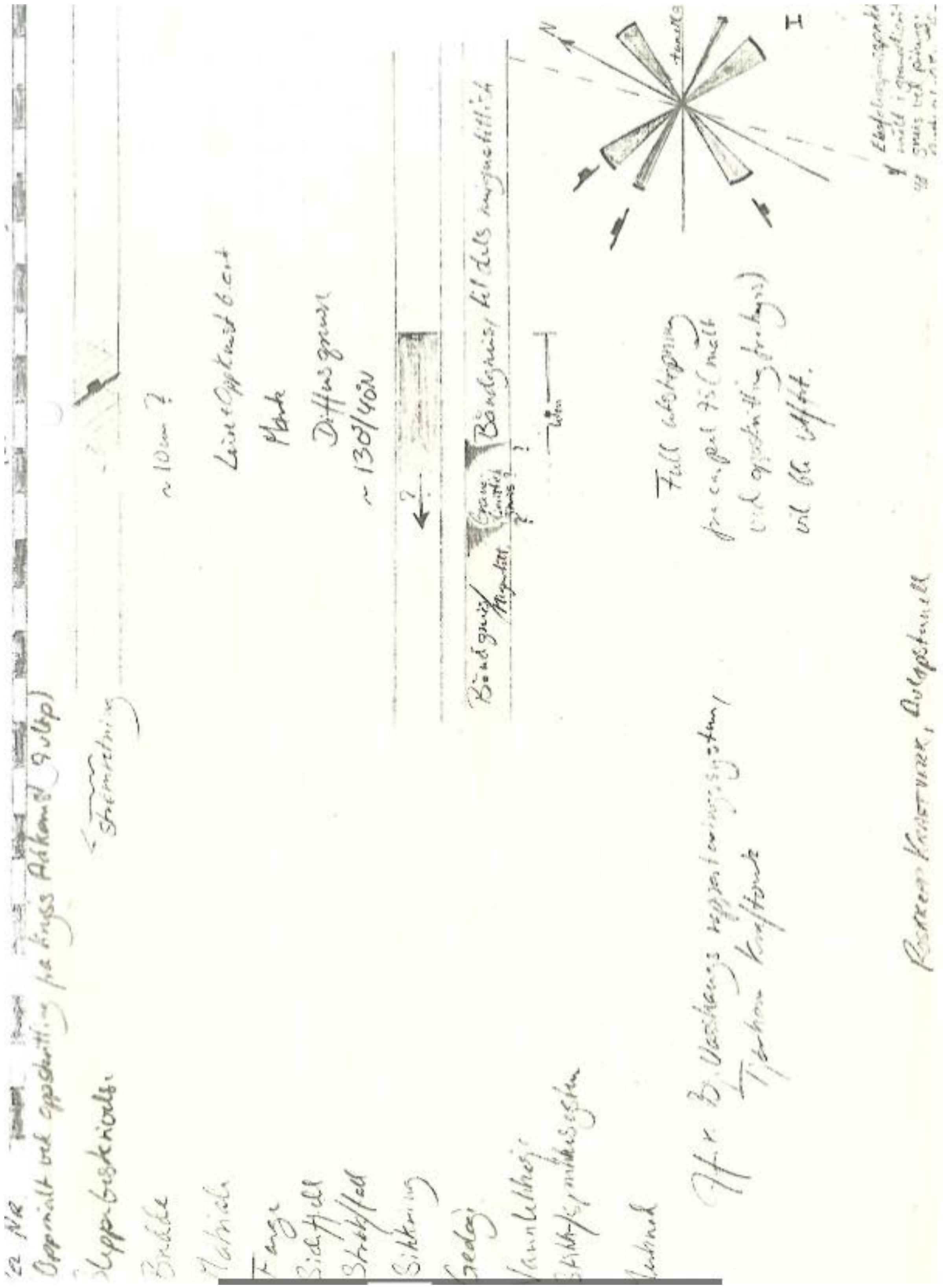

Befart den 15.6.

Svingekammeret skjæres av ei leirslepp. Denne sleppa synes å tilsvare svakhetssone nr. 6 i Bjørn Vasshaug rapport "ROSKREPP KRAFTVERK, ingeniørgeologisk forundersøkelse". Muligens er det også den samme sleppa en kan se ved pel 70 i tverrslaget til svingekammeret, dette tverrslaget munner ut i tilløpstunnellen ved pel 300.

Sleppa ligger i grensesone mellom en overliggende, grovkornet granitt og underliggende, mørk, biotittrik gneis (el. biotittisert amfibolitt?)
Granitten er massiv og homogen, mens den mørke gneisen har et markert, ca rettvinklet oppsprekkingsmønster i sprekkeavstand ned til ca 0,5 m. Gneisen gir følgelig et blokkrikt, ustabilt parti, hvor den mest markerte sprekkeretning ligger parallelt sleppa.

Ved et par meter under sleppa, synes gneisen å gå over i granitt igjen.

Skisse av situasjonen:

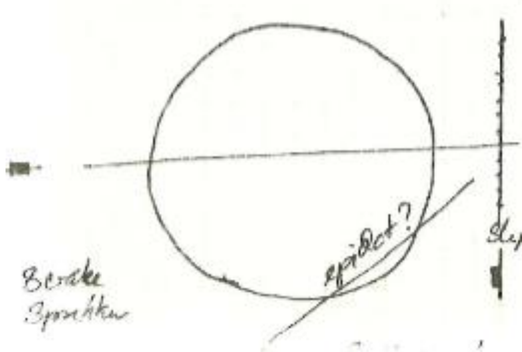

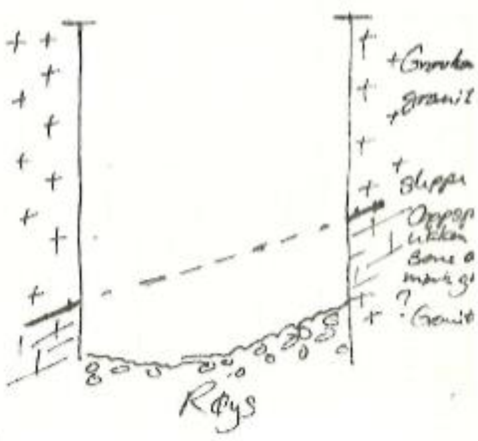

Sett fra siden (SV)

ROSKREPP KRAFTV., Rom 8 - kammer fase. 2

Bedømming av sleppa:

Bredde: Maks 10 cm (?)
Material: Leire (under 20%?) + oppknust bergart
Farge: Mørk (svart?)
Sidefjell: Relativt tydelig overgang
Strøk/fall: N60Ø, 25°N (?)
Vannforhold: Liten vannlekkasje

Sikring:

Det ble vurdert som å forsegle leirsleppa med sprøytebetong (etter forutgående spyling). Det ustabile parti under boltes systematisk med 3m innstøpte bolter og fjellbånd.

T.S. Dahl
19/6-79

Cand. Real.
Rolf Selmer-Olsen
Amanuensis

Trondheim, den 30. okt. 1961

Sira-Kvina.

Ingeniørgeologiske forundersøkelser

for

Tonstad kraftverk.

Generelt.

Det undersøkte området omfatter tunneltraceen fra Tonstad til Tjørhom på østsiden av Sirdalen. Dessuten traceen Ljosdal-Homstølvann. Geologisk sett ligger dette området i det sydnorske grunnfjellsområdet. Bergartene i dette området er nokså ensartet og består vesentlig av granitt, gneis-granitt og granittiske gneiser med enkelte drag av amfibolitt. (Se vedlagte tegning).

Anleggsteknisk er det stort sett gunstige bergarter. Enkelte partier vil by på visse mindre stabilitetsproblemer, nemlig der hvor bergartens strøk og fall står uheldig i forhold til tunnelretningen og der hvor bergarten er særlig grovkornig og oppsprukket. Oppsprekkingen er stort sett kubisk og med det mest markante sprekkesystem parallelt bergartenes skifrighet. Bergartene virker imidlertid forholdsvis massive (liten sprekketetthet) bortsett fra knusningssonene og i nærheten av disse.

Knusningssonene som er av noen størrelse har alle strøk tilnærmet øst-vest og fallet er steilt. Isens bevegelsesretning under siste istid er tvers på disse knusningssonene så en må regne med at de er heller lite markert i terrenget i forhold til oppknusningsgraden. Knusningssonenes bredde og karakter er vanskelig å si noe sikkert om bare ved observasjoner i dagen, men de er inndelt etter antatt bredde i tre grupper som da samtidig gir uttrykk for de sikringstiltak en kan regne med (se vedlagte tegning). En har undersøkt materialet

H) Tilt test results

Test		Repetition	Angle [°]	Mean repitition [°]	Mean core [°]	Mean total [°]
A2 - AA	A	1	35,9			
		2	35,0			
		3	36,3	35,7		
	B	1	34,4			
		2	35,3			
		3	35,7	35,1		
	C	1	33,9			
		2	33,4			
		3	33,8	33,7		
	D	1	33,6		34,5	
		2	33,1			
		3	34,0	33,6		
A3 - BB	A	1	33,0			
		2	35,0			
		3	34,8	34,3		
	B	1	31,5			
		2	32,3			
		3	30,2	31,3		
	C	1	35,9			
		2	34,9			
		3	34,1	35,0		
	D	1	34,7		33,8	
		2	34,4			
		3	35,2	34,8		
A4 - CC	A	1	34,6			
		2	35,6			
		3	35,8	35,3		
	B	1	34,7			
		2	33,7			
		3	34,3	34,2		
	C	1	33,6			
		2	33,6			
		3	33,8	33,7		
	D	1	34,6		34,3	
		2	32,7			34,2
		3	34,3	33,9		

Test		Repetition	Angle [°]	Mean repitition [°]	Mean core [°]	Mean total [°]
B2 - AA	A	1	29,3			
		2	30,6			
		3	33,6	31,2		
	B	1	30,8			
		2	31,5			
		3	33,3	31,9		
	C	1	31,8			
		2	31,3			
		3	31,9	31,7		
	D	1	30,2		31,3	
		2	31,4			
		3	29,5	30,4		
B3 - BB	A	1	33,1			
		2	31,4			
		3	34,5	33,0		
	B	1	31,2			
		2	31,1			
		3	30,9	31,1		
	C	1	28,9	29,8		
		2	29,8			
		3	30,8			
	D	1	29,7		31,3	
		2	30,7			
		3	33,8	29,8		
B4 - CC	A	1	31,5			
		2	31,7			
		3	30,9	31,4		
	B	1	29,5			
		2	30,2			
		3	29,5	29,7		
	C	1	28,8			
		2	28,0			
		3	29,1	28,8		
	D	1	28,8		29,6	
		2	29,3			
		3	27,4	28,5		30,7

I) Hydraulic test results

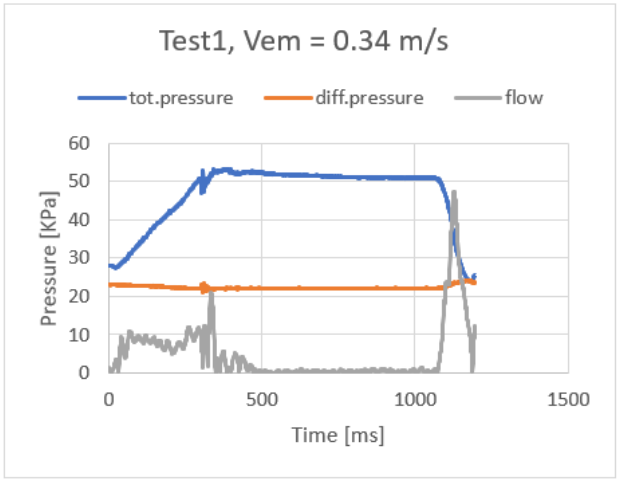

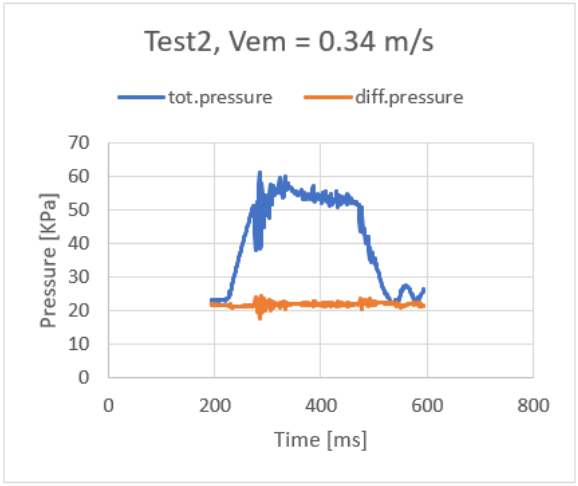

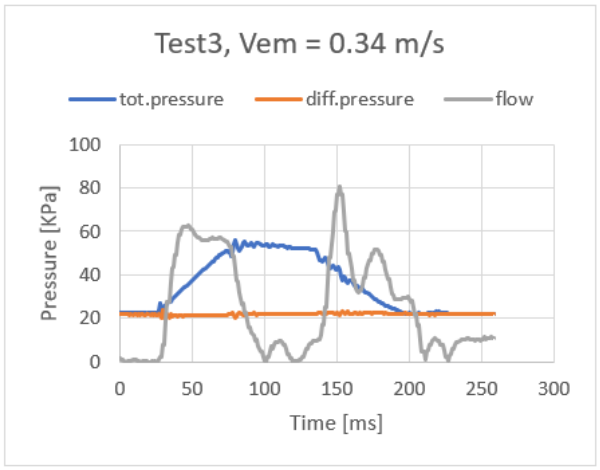

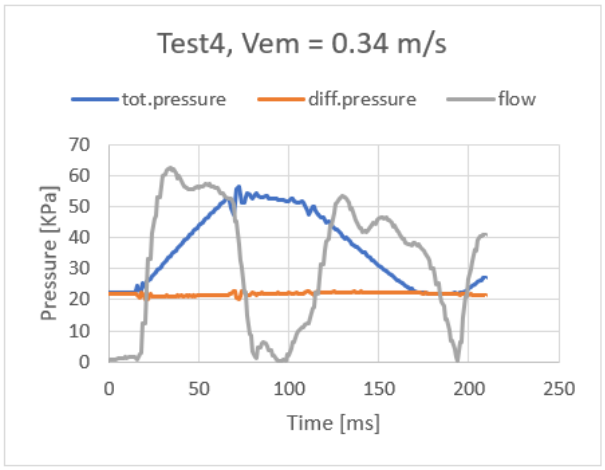

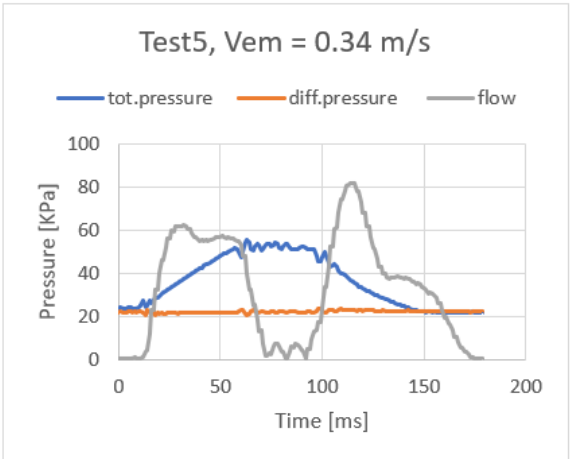

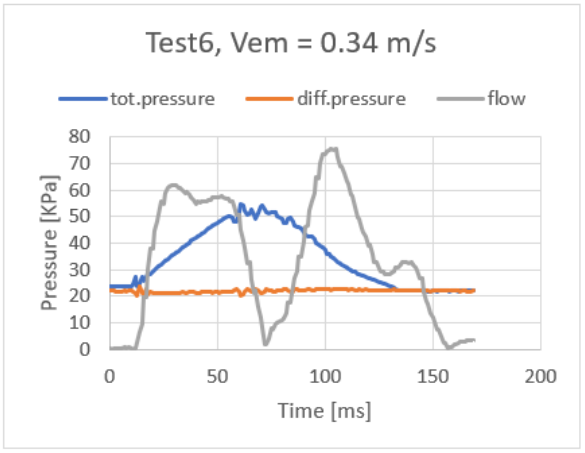

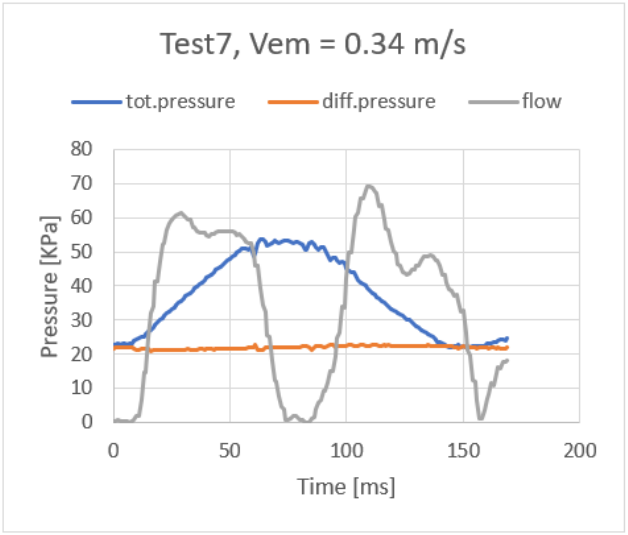
Test7, Vem = 0.34 m/s
tot.pressure
diff.pressure
flow
Pressure [KPa]
Time [ms]

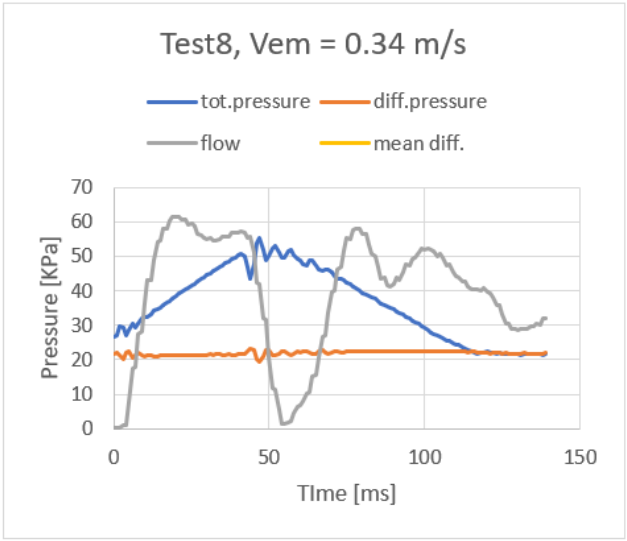
Test8, Vem = 0.34 m/s
tot.pressure
diff.pressure
flow
mean diff.
Pressure [KPa]
TIme [ms]

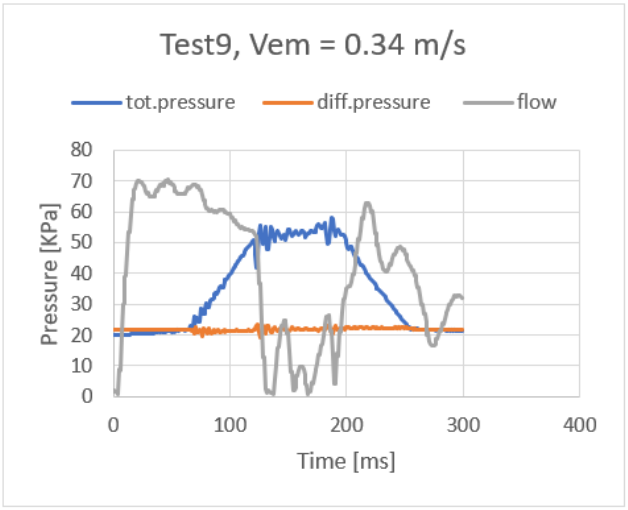
Test9, Vem = 0.34 m/s
tot.pressure
diff.pressure
flow
Pressure [KPa]
Time [ms]

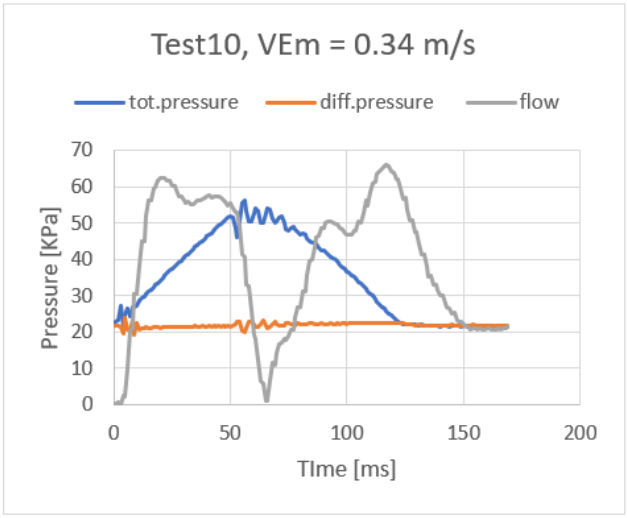
Test10, VEm = 0.34 m/s
tot.pressure
diff.pressure
flow
Pressure [KPa]
TIme [ms]

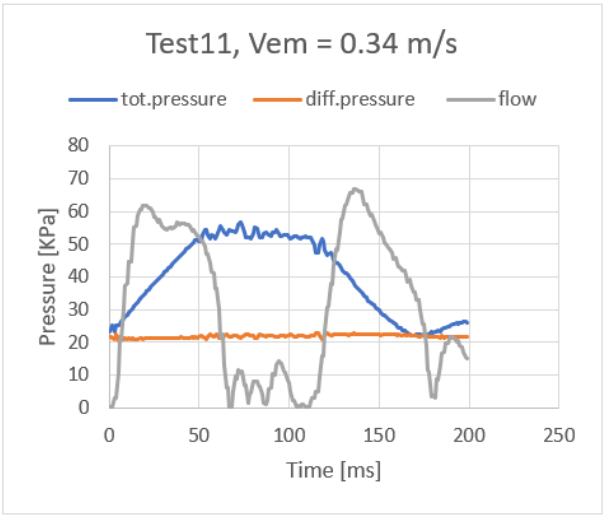
Test11, Vem = 0.34 m/s
tot.pressure
diff.pressure
flow
Pressure [KPa]
Time [ms]

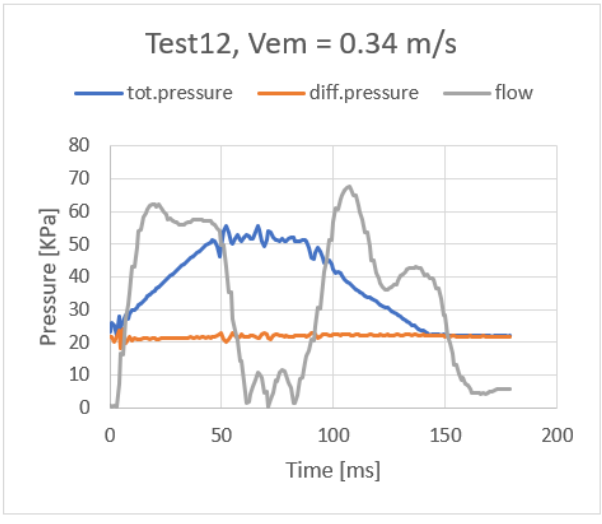
Test12, Vem = 0.34 m/s
tot.pressure
diff.pressure
flow
Pressure [KPa]
Time [ms]

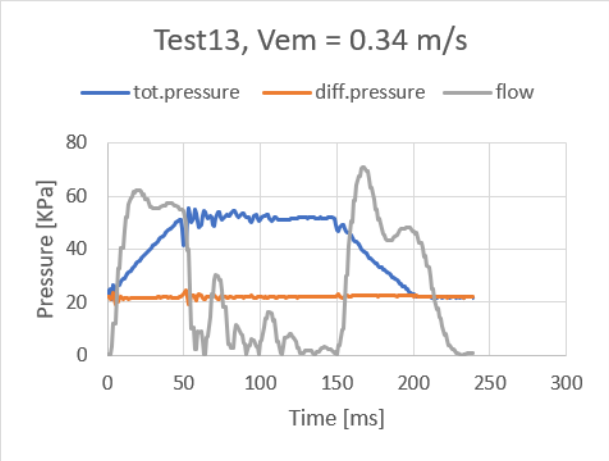
Test13, Vem = 0.34 m/s
tot.pressure
diff.pressure
flow
Pressure [KPa]
Time [ms]

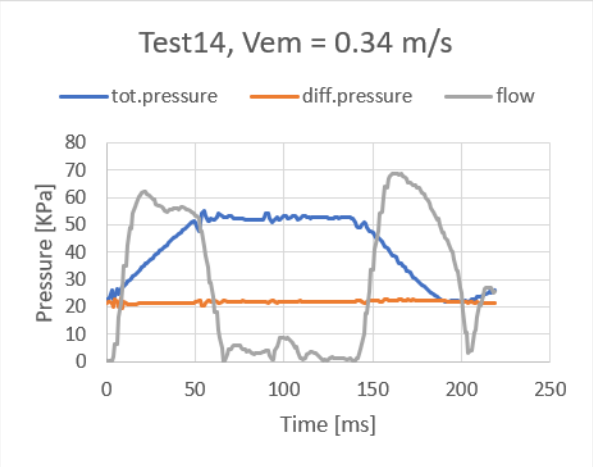
Test14, Vem = 0.34 m/s
tot.pressure
diff.pressure
flow
Pressure [KPa]
Time [ms]

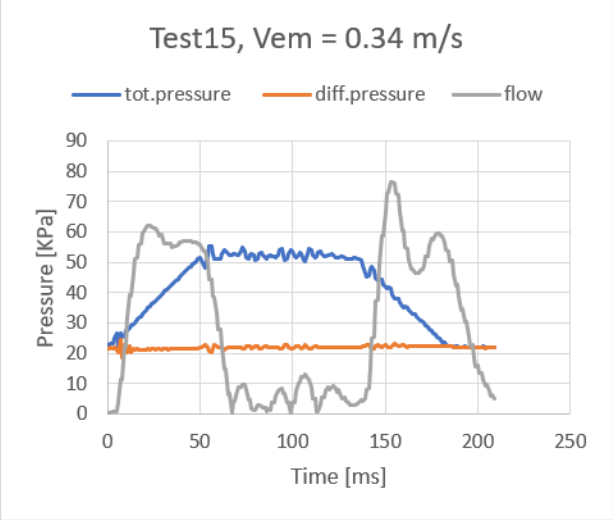
Test15, Vem = 0.34 m/s
tot.pressure
diff.pressure
flow
Pressure [KPa]
Time [ms]

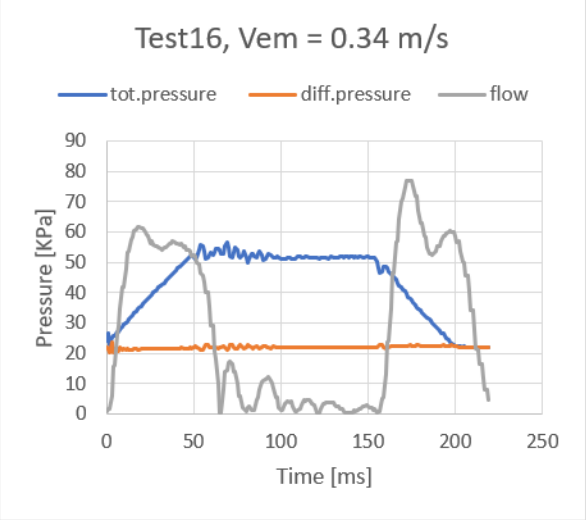
Test16, Vem = 0.34 m/s
tot.pressure
diff.pressure
flow
Pressure [KPa]
Time [ms]

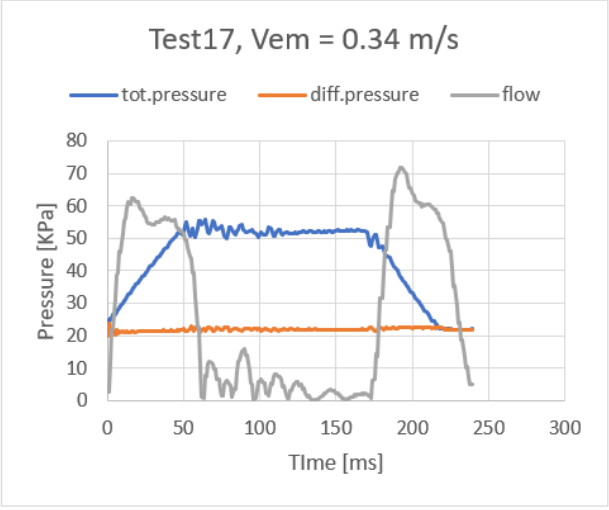
Test17, Vem = 0.34 m/s
tot.pressure
diff.pressure
flow
Pressure [KPa]
TIme [ms]

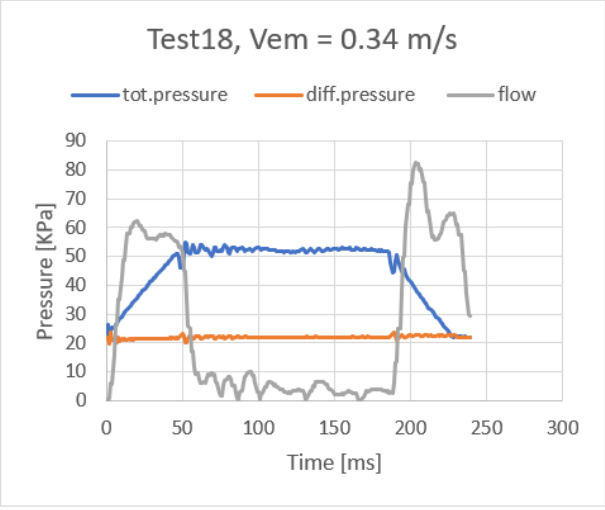
Test18, Vem = 0.34 m/s
tot.pressure
diff.pressure
flow
Pressure [KPa]
Time [ms]

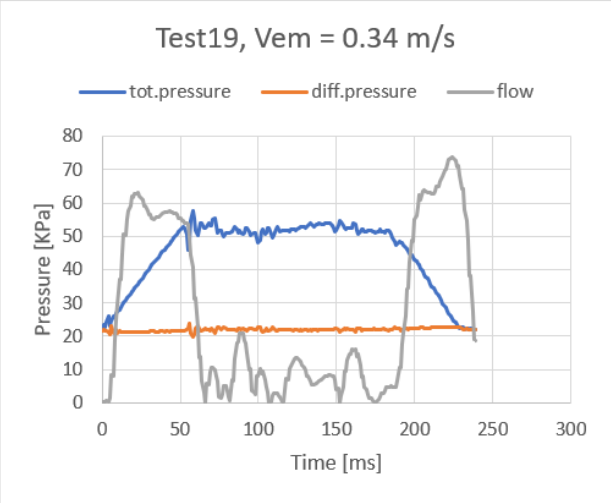
Test19, Vem = 0.34 m/s
tot.pressure
diff.pressure
flow
Pressure [KPa]
Time [ms]

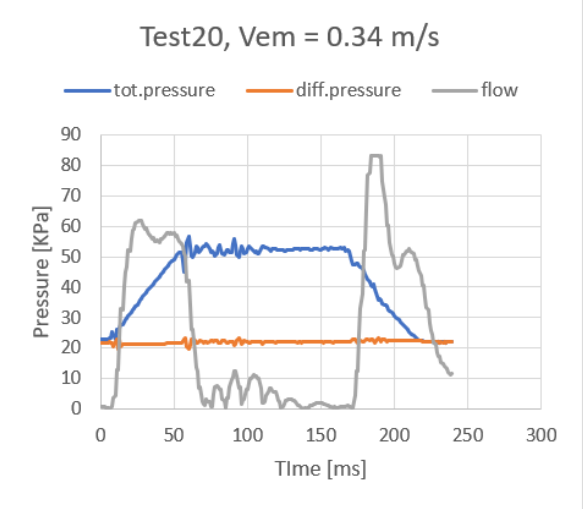
Test20, Vem = 0.34 m/s
tot.pressure
diff.pressure
flow
Pressure [KPa]
TIme [ms]

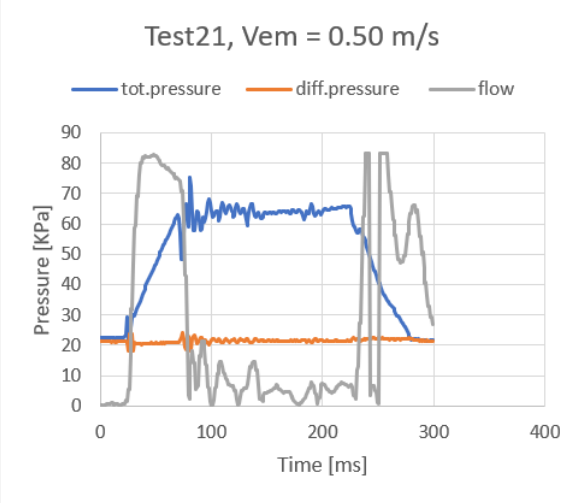
Test21, Vem = 0.50 m/s
tot.pressure
diff.pressure
flow
Pressure [KPa]
Time [ms]

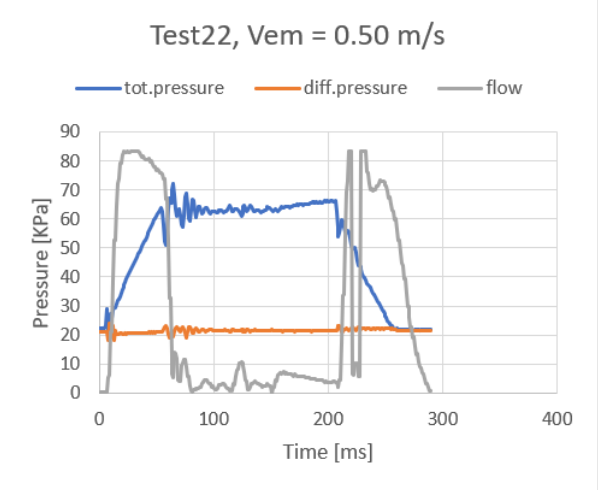
Test22, Vem = 0.50 m/s
tot.pressure
diff.pressure
flow
Pressure [KPa]
Time [ms]

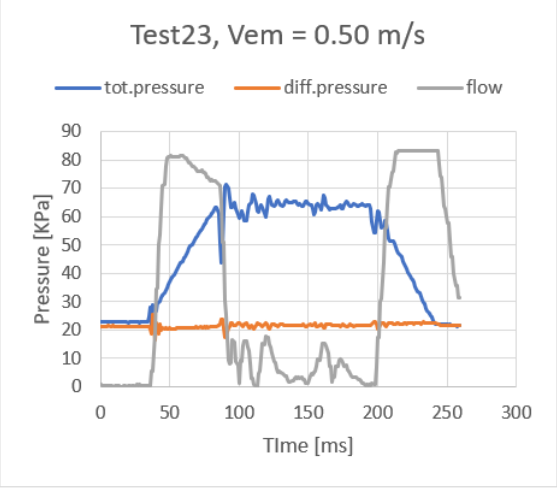
Test23, Vem = 0.50 m/s
tot.pressure
diff.pressure
flow
Pressure [KPa]
TIme [ms]

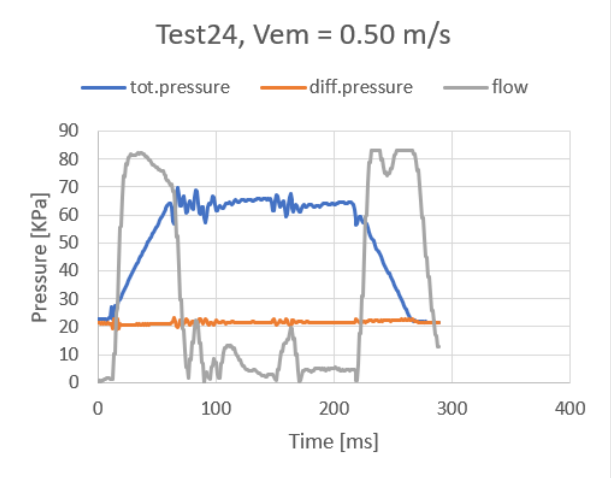
Test24, Vem = 0.50 m/s
tot.pressure
diff.pressure
flow
Pressure [KPa]
Time [ms]

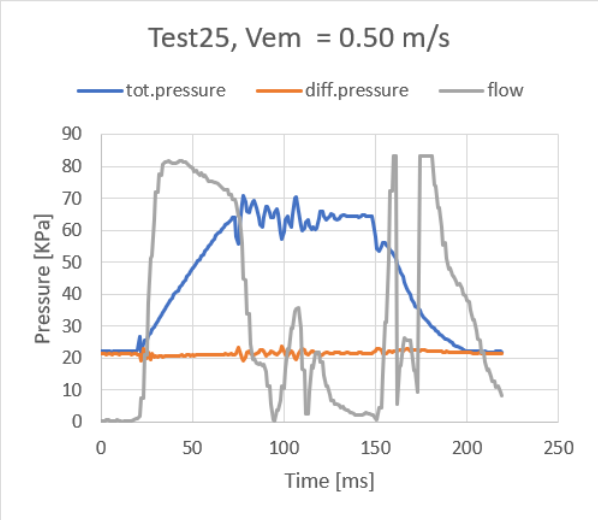
Test25, Vem = 0.50 m/s
tot.pressure
diff.pressure
flow
Pressure [KPa]
Time [ms]

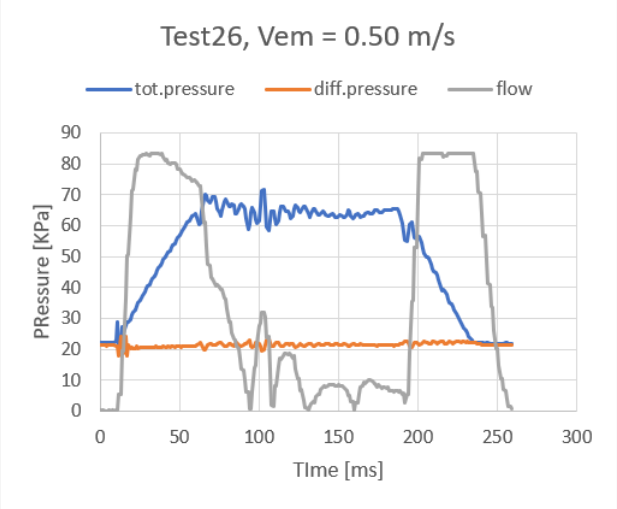
Test26, Vem = 0.50 m/s
tot.pressure
diff.pressure
flow
PRessure [KPa]
TIme [ms]

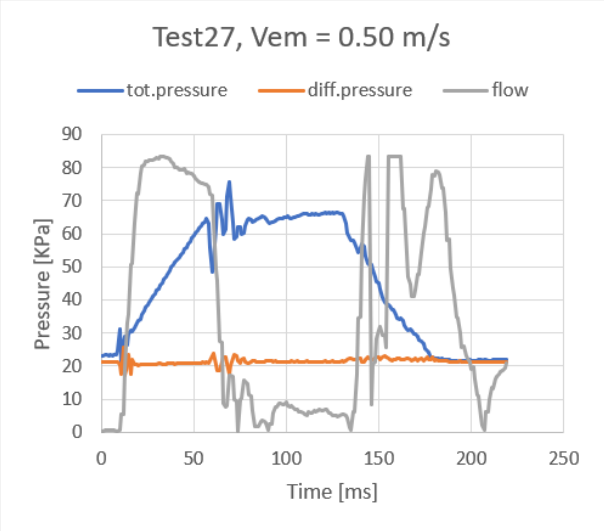
Test27, Vem = 0.50 m/s
tot.pressure
diff.pressure
flow
Pressure [KPa]
Time [ms]

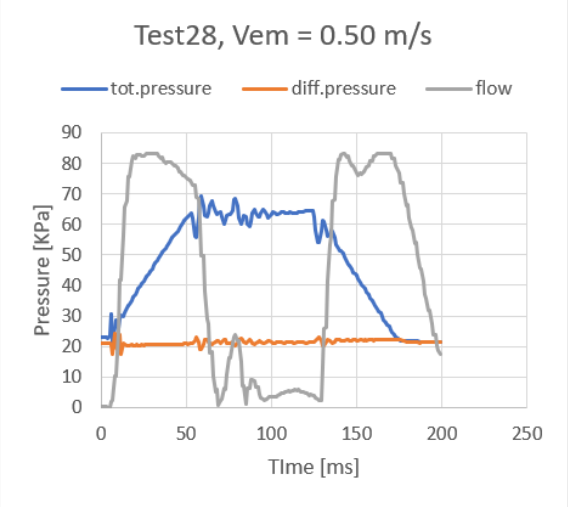
Test28, Vem = 0.50 m/s
tot.pressure
diff.pressure
flow
Pressure [KPa]
TIme [ms]

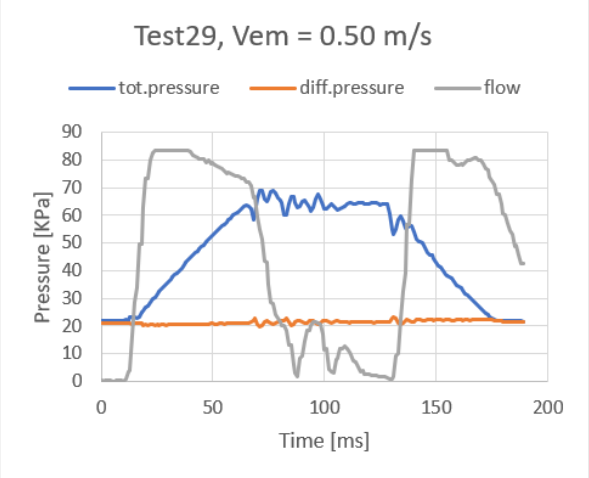
Test29, Vem = 0.50 m/s
tot.pressure
diff.pressure
flow
Pressure [KPa]
Time [ms]

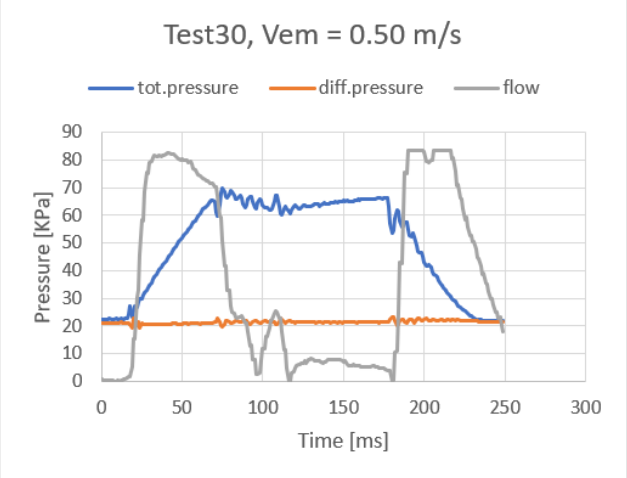
Test30, Vem = 0.50 m/s
tot.pressure
diff.pressure
flow
Pressure [KPa]
Time [ms]

J) XRD test results

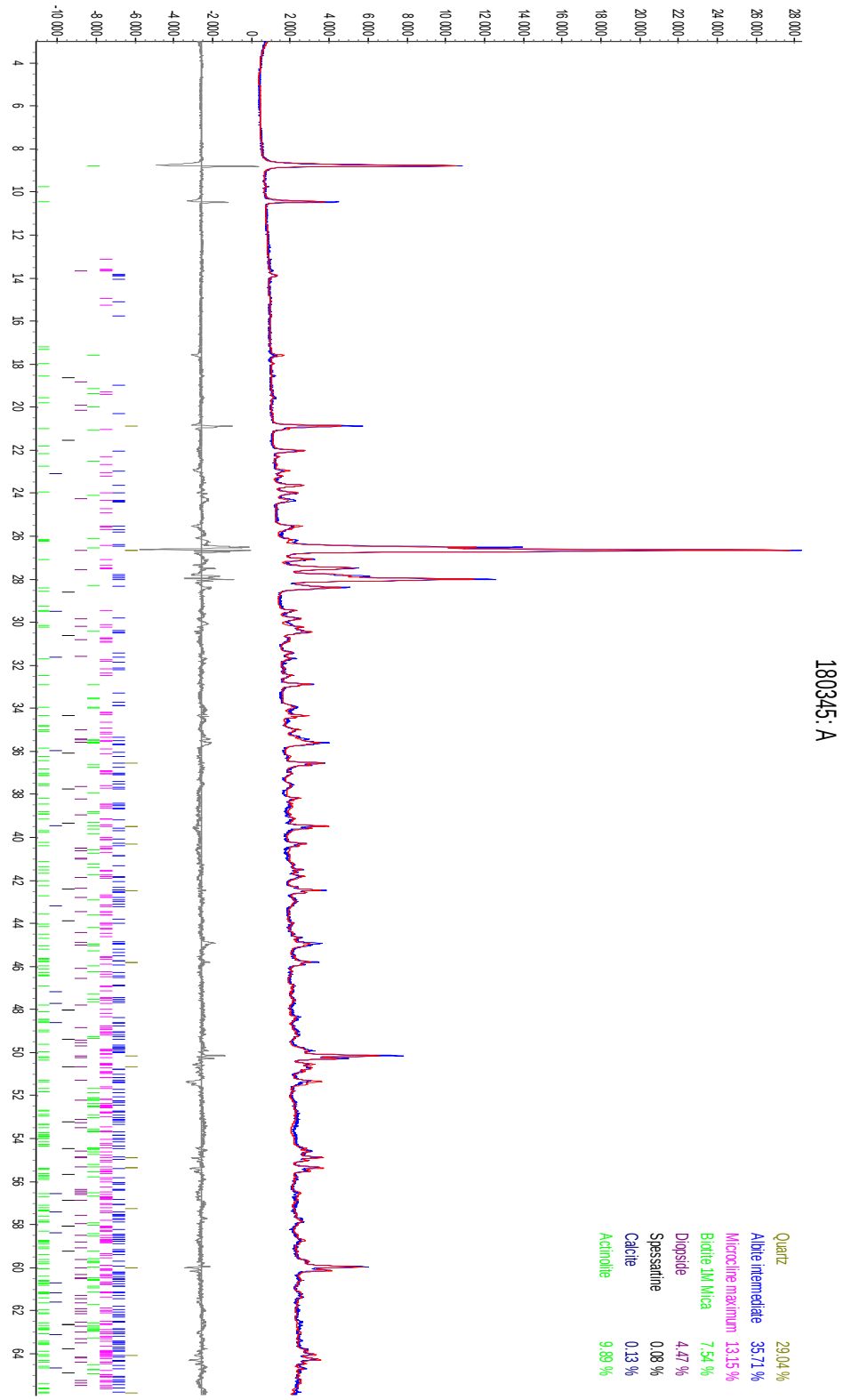

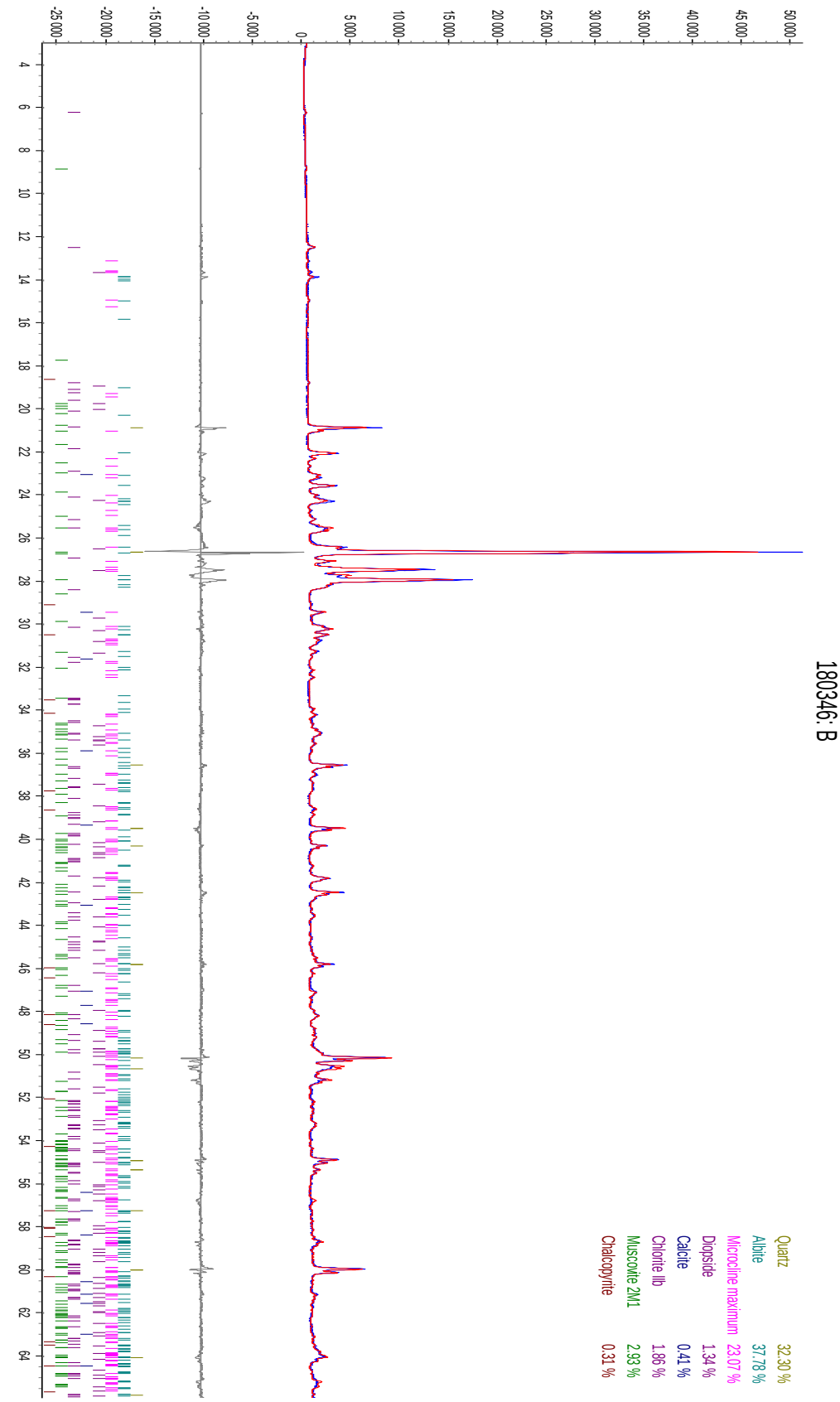
180346: B
Quartz 32.30 %
Albite 37.78 %
Microcline maximum 23.07 %
Diopside 1.34 %
Calcite 0.41 %
Chlorite IIb 1.86 %
Muscovite 2M1 2.93 %
Chalcopyrite 0.31 %